GEOLOGICAL SURVEY OF CANADA
COMMISSION GÉOLOGIQUE DU CANADA

PAPER/ÉTUDE
90-1A

CURRENT RESEARCH, PART A
NATIONAL AND GENERAL PROGRAMS

RECHERCHES EN COURS, PARTIE A
PROGRAMMES NATIONAUX ET GÉNÉRAUX

Energy, Mines and Resources Canada
Énergie, Mines et Ressources Canada

Canada

THE ENERGY OF OUR RESOURCES
THE POWER OF OUR IDEAS

NOTICE TO LIBRARIANS AND INDEXERS

The Geological Survey's Current Research series contains many reports comparable in scope and subject matter to those appearing in scientific journals and other serials. Most contributions to Current Research include an abstract and bibliographic citation. It is hoped that these will assist you in cataloguing and indexing these reports and that this will result in a still wider dissemination of the results of the Geological Survey's research activities.

AVIS AUX BIBLIOTHÉCAIRES ET PRÉPARATEURS D'INDEX

La série Recherches en cours de la Commission géologique paraît une fois par année; elle contient plusieurs rapports dont la portée et la nature sont comparables à ceux qui paraissent dans les revues scientifiques et autres périodiques. La plupart des articles publiés dans Recherches en cours sont accompagnés d'un résumé et d'une bibliographie, ce qui vous permettra, nous l'espérons, de cataloguer et d'indexer ces rapports, d'ou une meilleure diffusion des résultats de recherche de la Commission géologique.

GEOLOGICAL SURVEY OF CANADA
COMMISSION GÉOLOGIQUE DU CANADA
PAPER/ÉTUDE 90-1A

CURRENT RESEARCH, PART A
NATIONAL AND GENERAL PROGRAMS

RECHERCHES EN COURS, PARTIE A
PROGRAMMES NATIONAUX ET GÉNÉRAUX

1990

Available in Canada through

authorized bookstore agents and other bookstores

or by mail from

Canadian Government Publishing Centre
Supply and Services Canada
Ottawa, Canada K1A 0S9

and from

Geological Survey of Canada offices:

601 Booth Street
Ottawa, Canada K1A 0E8

3303-33rd Street N.W.
Calgary, Alberta T2L 2A7

100 West Pender Street
Vancouver, British Columbia V6B 1R8

A deposit copy of this publication is also available
for reference in public libraries across Canada

Cat. No. M44-90/1A
ISBN 0-660-55680-4

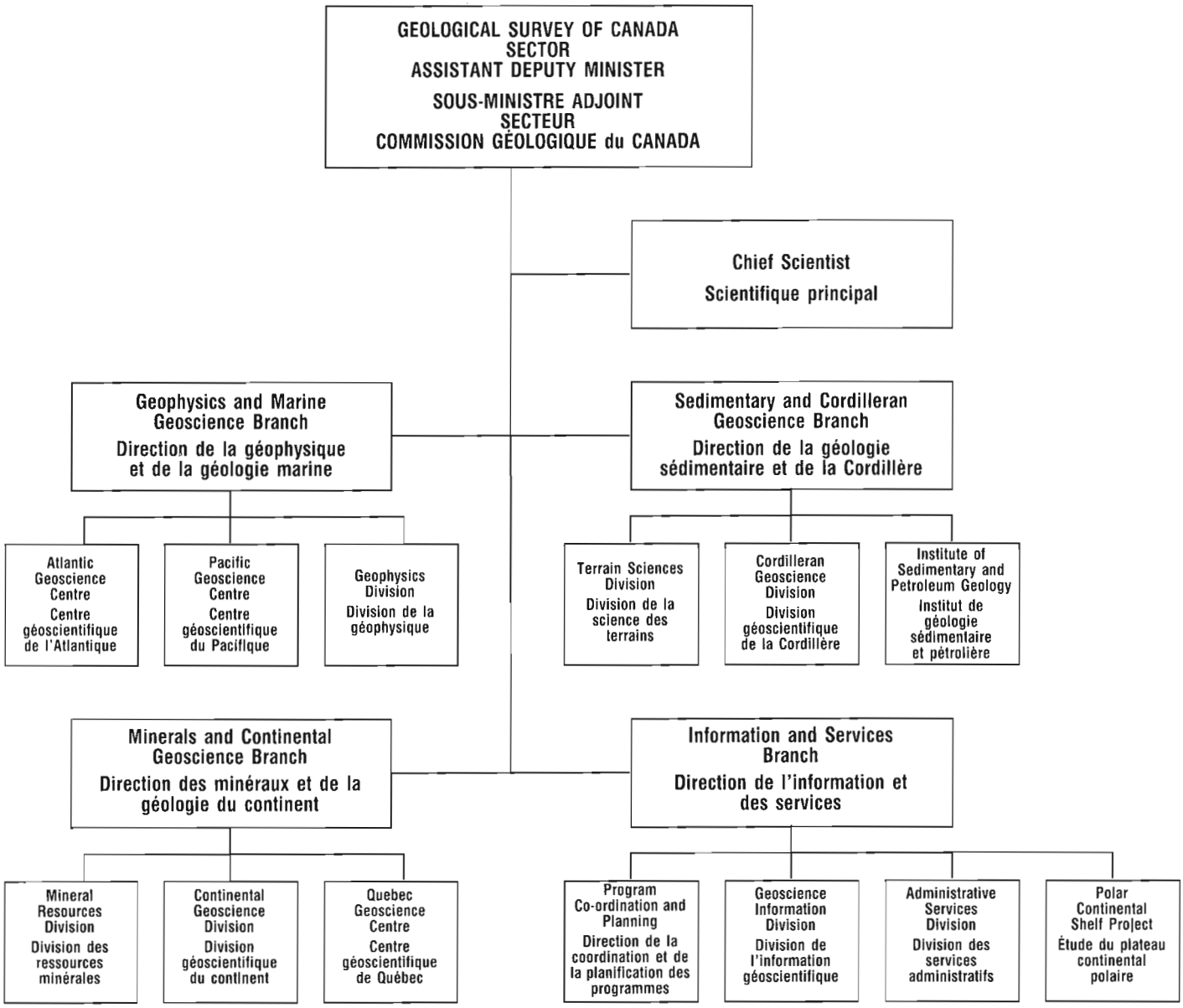
GEOLOGICAL SURVEY OF CANADA
SECTOR
ASSISTANT DEPUTY MINISTER
SOUS-MINISTRE ADJOINT
SECTEUR
COMMISSION GÉOLOGIQUE du CANADA
Chief Scientist
Scientifique principal
Geophysics and Marine Geoscience Branch
Direction de la géophysique et de la géologie marine
Sedimentary and Cordilleran Geoscience Branch
Direction de la géologie sédimentaire et de la Cordillère
Atlantic Geoscience Centre
Centre géoscientifique de l'Atlantique
Pacific Geoscience Centre
Centre géoscientifique du Pacifique
Geophysics Division
Division de la géophysique
Terrain Sciences Division
Division de la science des terrains
Cordilleran Geoscience Division
Division géoscientifique de la Cordillère
Institute of Sedimentary and Petroleum Geology
Institut de géologie sédimentaire et pétrolière
Minerals and Continental Geoscience Branch
Direction des minéraux et de la géologie du continent
Information and Services Branch
Direction de l'information et des services
Mineral Resources Division
Division des ressources minérales
Continental Geoscience Division
Division géoscientifique du continent
Quebec Geoscience Centre
Centre géoscientifique de Québec
Program Co-ordination and Planning
Direction de la coordination et de la planification des programmes
Geoscience Information Division
Division de l'information géoscientifique
Administrative Services Division
Division des services administratifs
Polar Continental Shelf Project
Étude du plateau continental polaire

Separates

A limited number of separates of the papers that appear in this volume are available by direct request to the individual authors. The addresses of the Geological Survey of Canada offices follow:

601 Booth Street,
OTTAWA, Ontario
K1A 0E8
(FAX: 613-996-9990)

Institute of Sedimentary and Petroleum Geology,
3303-33rd Street N.W.,
CALGARY, Alberta
T2L 2A7
(FAX: 403-292-5377)

Cordilleran Division,
100 West Pender Street,
VANCOUVER, B.C.
V6B 1R8
(FAX: 604-666-1124)

Pacific Geoscience Centre
P.O. Box 6000,
9860 Saanich Road
SIDNEY, B.C.
V8L 4B2
(FAX: 604-356-6565)

Atlantic Geoscience Centre
Bedford Institute of Oceanography,
P.O. Box 1006,
DARTMOUTH, N.S.
B2Y 4A2
(FAX: 902-426-2256)

Québec Geoscience Centre
2700, rue Einstein
C.P. 7500
Ste-Foy, Quebec
G1V 4C7
(FAX: 418-654-2615)

When no location accompanies an author's name in the title of a paper, the Ottawa address should be used.

Tirés à part

On peut obtenir un nombre limité de «tirés à part» des articles qui paraissent dans cette publication en s'adressant directement à chaque auteur. Les adresses des différents bureaux de la Commission géologique du Canada sont les suivantes:

601, rue Booth
OTTAWA (Ontario)
K1A 0E8
(facsimilé: 613-996-9990)

Institut de géologie sédimentaire et pétrolière
3303-33rd St. N.W.,
CALGARY (Alberta)
T2L 2A7
(facsimilé: 403-292-5277)

Division de la Cordillère
100 West Pender Street,
VANCOUVER (Colombie-Britannique)
V6B 1R8
(facsimilé: 604-666-1124)

Centre géoscientifique du Pacifique
B.P. 6000,
9860 Saanich Road
SIDNEY (Colombie-Britannique)
V8L 4B2
(facsimilé: 604-356-6565)

Centre géoscientifique de l'Atlantique
Institut océanographique de Bedford
B.P. 1006
DARTMOUTH (Nouvelle-Écosse)
B2Y 4A2
(facsimilé: 902-426-2256)

Centre géoscientifique de Québec
2700, rue Einstein
C.P. 7500
Ste-Foy (Québec)
G1V 4C7
(facsimilé: 418-654-2615)

Lorsque l'adresse de l'auteur ne figure pas sous le titre d'un document, on doit alors utiliser l'adresse d'Ottawa.

CONTENTS

Aeromagnetic survey program of the Geological Survey of Canada, 1989-90

D.J. Teskey, E.E. Ready, P.E. Stone, B. Ellis, J. Tod, F. Kiss, and R.A. Gibb
Geophysics Division

Teskey, D.J., Ready, E.E., Stone, P.E., Ellis, B., Tod, J., Kiss, F., and Gibb, R.A., Aeromagnetic survey program of the Geological Survey of Canada, 1989-90; in Current Research, Part A, Geological Survey of Canada, Paper 90-1A, p. 1-3, 1990.

Abstract

During 1989-90, the GSC collected 87 000 line kilometres of aeromagnetic data. Of these, 30 000 line kilometres were flown in Nova Scotia under the Canada-Nova Scotia Mineral Development Agreement, 46 000 line kilometres in the Yukon and British Columbia as part of the GSC's ongoing aeromagnetic survey program, and 11 000 line kilometres in the Lincoln Sea as part of a joint National Aeronautical Establishment/Defence Research Establishment Pacific/Geological Survey of Canada project. Approximately 25 000 line kilometres of detailed total field/gradiometer/VLF data collected in 1988 in the Northwest Territories, Manitoba, and New Brunswick and 13 500 km collected in 1987 in New Brunswick were processed by the contractors.

Résumé

En 1989-1990, la CGC a recueilli des données aéromagnétiques sur 87 000 kilomètres linéaires dont 30 000 ont été levés en Nouvelle-Écosse dans le cadre de l'Entente Canada-Nouvelle-Écosse d'exploitation minérale, 46 000 au Yukon et en Colombie-Britannique dans le cadre d'un programme continu de levés aéromagnétiques de la CGC et 11 000 dans la mer de Lincoln dans le cadre d'un projet commun de l'Établissement aéronautique national, du Centre de recherche pour la défense (Pacifique) et de la Commission géologique du Canada. Les données détaillées du champ total/gradiométriques/et de très basse fréquence, recueillies en 1988 sur environ 25 000 kilomètres linéaires dans les Territoires du Nord-Ouest, au Manitoba et au Nouveau-Brunswick, et sur 13 500 km en 1987 au Nouveau-Brunswick ont été traitées par les entrepreneurs.

INTRODUCTION

Flying of two total field surveys initiated in 1988 in the Yukon and British Columbia was continued in 1989 and one additional total field survey in the Lincoln Sea was initiated, for a total of 57 000 line kilometres. One total field/gradiometer/VLF-EM survey was flown comprising an additional 30 000 km. Processing continued on three detailed surveys flown in 1988, one purchased survey, and one survey flown in 1987 in the Saint John area, New Brunswick (Teskey et al., 1989). Data acquired from Imperial Oil Limited from a survey in northern British Columbia and Alberta, previously released at 1:1 000 000 scale, were compiled and released at 1:250 000.

REGIONAL SURVEYS

Flying of the Northern Yukon survey (Teskey et al., 1989), which was suspended in November 1988 due to unfavourable weather conditions, was continued in the spring of 1989. Difficulties were again experienced by the contractor due to a combination of weather and navigational problems, and the flying was suspended after completion of 25 000 line kilometres of the originally planned 57 000 kilometres. The remaining portion of the survey, which was designed to examine the structure under sedimentary cover in the Old Crow Basin, Dave Lord Uplift, and Eagle Plain, will be recontracted in 1990 if funding is available.

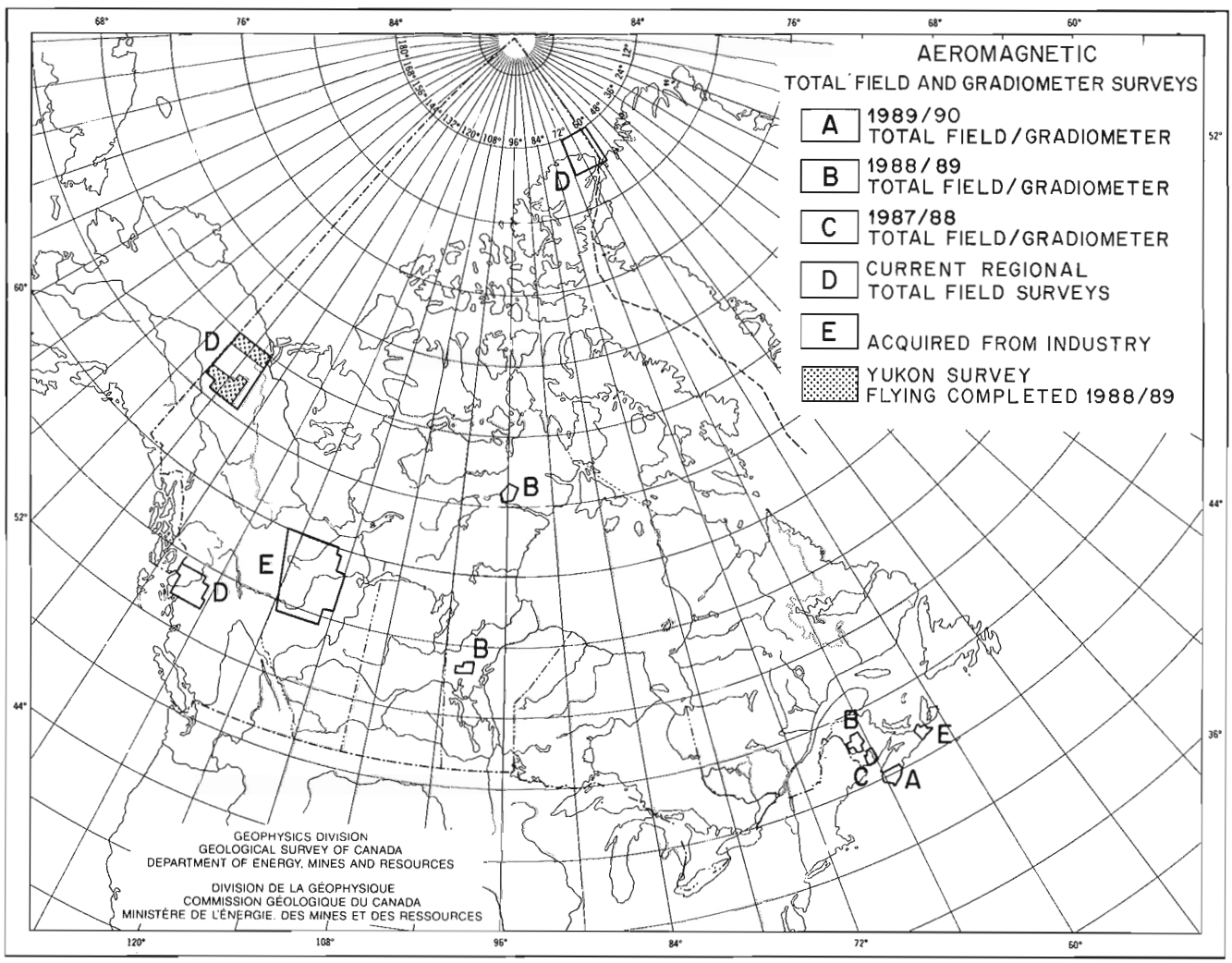

Figure 1. Locations of aeromagnetic total field and total field/gradiometer/VLF surveys for 1989-90.

Table 1. Aeromagnetic surveys

Survey	Type	Km	Line Spacing	Altitude (m)
New Brunswick (1987-88)	Aeromagnetic Total Field Gradiometer VLF	13 524	300 m	150 Radar
Northwest Territories (1988-89)	Aeromagnetic Total Field Gradiometer VLF	6 855	300 m	150 Radar
Manitoba (1988-89)	Aeromagnetic Total Field Gradiometer VLF	8 180	300 m	150 Radar
New Brunswick (1988-89)	Aeromagnetic Total Field Gradiometer VLF	10 322	300 m	150 Radar
Nova Scotia (Private)	Aeromagnetic Total Field Gradiometer VLF	4 200	300 m	150 Radar
Yukon (1988-90)	Regional Aeromagnetics	24 840	2 km (southern portion) 3 km (northern portion)	9 000 Bar 7 000 Bar
British Columbia (1988-90)	Regional Aeromagnetics	21 636	2 km	9 500 Bar
Nova Scotia (1989-90)	Aeromagnetic Total Field Gradiometer VLF	30 000	300 m	150 Radar
Lincoln Sea (1989)	Aeromagnetic Total Field	10 742	4 km	305 Radar
British Columbia/ Alberta (Private)	Aeromagnetic Total Field	BC 90 000 Alta 200 000	150 m 1000 m & 1500 m	Various alt. blocks constant bar 200 Radar

The Prince Rupert, British Columbia survey (Teskey et al., 1989), which was designed to help define lithologies and faults in the coastal range adjacent to the Queen Charlotte Basin, also experienced severe weather problems in 1988 and was discontinued after collection of approximately 20 percent of the data. The area was recontracted in 1989 and flying has been completed (22 000 line kilometres). The portion flown in 1988 was released as GSC open file. 2101 in September 1989.

The Lincoln Sea survey (north of Ellesmere Island) was flown in May 1989 by the National Aeronautical Establishment Convair 580 aircraft as a joint NAE/DREP/GSC project to investigate the structure of the polar continental margin (Hardwick et al., 1990, this volume). Processing is expected to be completed by late 1989.

Twenty-six 1:250 000 maps of total field data in northern British Columbia and Alberta compiled from maps originally supplied by Imperial Oil Limited were released in September 1989.

AEROMAGNETIC TOTAL FIELD GRADIOMETER/VLF-EM SURVEY

The aeromagnetic total field/gradiometer/VLF-EM survey in the Yarmouth area of Nova Scotia was designed to assist in the detailed structural mapping of this area as part of the Canada-Nova Scotia Mineral Development Agreement to stimulate mineral exploration. Flying of this survey was completed by September 1989 and compilation is scheduled to be completed by April 1990.

REFERENCES

Hardwick, C.D., Nelson, J.B., Bower, M.E., Marcotte, D.L., Forsyth, D., MacNab, R., and Teskey, D.
1990: Procedures and preliminary results of an aeromagnetic survey in the Lincoln Sea; *in* Current Research, Part D, Geological Survey of Canada, Paper 90-1D.

Teskey, D.J., Ready, E.E., Stone, P.E., Ellis, B., Tod, J., and Gibb, R.A.
1989: Aeromagnetic survey program of the Geological Survey of Canada 1988-89; *in* Current Research, Part F, Geological Survey of Canada, Paper 89-1F, p. 51-53.

EDDI: a FORTRAN computer program to produce corrected electron-microprobe analyses of minerals using an energy dispersive X-ray spectrometer

G.J. Pringle
Mineral Resources Division

Pringle, G.J., EDDI: a FORTRAN computer program to produce corrected electron-microprobe analyses of minerals using an energy dispersive X-ray spectrometer; in Current Research, Part A, Geological Survey of Canada, Paper 90-1A, p. 5-8, 1990.

Abstract

EDDI is an interactive FORTRAN program designed to produce quantitative X-ray energy dispersive (EDS) analyses of minerals using an electron beam instrument. The program has been developed in the microbeam laboratory at the Geological Survey of Canada as an economical and effective way to convert an existing qualitative EDS system into a fully quantitative system. The source listing, detailed documentation, and operation manual are being published as GSC open file 2127. The software is designed to run in an IBM PC environment. It contains an extensive capability to prepare summary reports of stored analyses using several choices of formula calculation and averaging of related groups.

Résumé

L'EDDI est un programme FORTRAN interactif conçu pour produire des analyses quantitatives aux rayons X à dispersion d'énergie (EDS) de minéraux au moyen d'un instrument à faisceau électronique. Le programme a été mis au point au laboratoire à microfaisceaux de la Commission géologique du Canada et constitue une façon bon marché et efficace de convertir un spectromètre d'analyse qualitative EDS actuel, en un spectromètre d'analyse complètement quantitative. La liste des sources, la documentation détaillée et le manuel d'instructions sont publiés sous forme de documents accessibles au public (dossier public n° 2127) de la CGC. Le logiciel est conçu pour être exécuté sur un PC compatible IBM. Il offre la possibilité de préparer des rapports sommaires d'analyses emmagasinées en utilisant plusieurs options de calcul à l'aide de formules et en établissant des moyennes de groupes apparentés.

INTRODUCTION

The first energy dispersive spectrometer (EDS) in the electron microprobe laboratory at the Geological Survey of Canada was purchased in 1972 and subsequently three more such spectrometers have been added to our microprobes and scanning electron microscopes. Computer programs that produced quantitative analyses from EDS spectra were not available in the first years, consequently such a program was developed at the Geological Survey of Canada. This program was designed specifically for analysis of rock-forming silicate minerals. An increased demand developed in succeeding years for quantitative EDS analyses on a broader range of mineral compositions involving elements throughout the periodic table. Software purchased for this purpose in 1978 was not entirely satisfactory, with the result that we proceeded to develop another program by expanding on the existing silicate program. The newer software package has been named EDDI and is suitable for general mineralogical applications.

The program is segmented so that it may be overlaid in systems with small amounts of usable core and moderate disk storage capacity. In systems such as the IBM XT and AT compatibles, the program can be run as a monolith. The modular structure of the program also makes it convenient to design and introduce a menu that is customized to a laboratory's applications and preferred approach to work flow management.

Currently there are two operational versions of the system in the laboratory. One working version of EDDI is running in a PDP 11/03-L computer with 64K bytes of core memory and dual half-megabyte floppy disk drives. This is mounted in a KEVEX 7000 spectrometer that is fully integrated with the computer thereby providing direct access to the spectra from the software. The second version is in a HP1000 computer with a 12 megabyte hard disk and 56K bytes of usable core. Spectra are transferred to this system from a KEVEX 5100 spectrometer by means of an asynchronous serial interface card in the HP1000.

We have a version of the program running in an IBM XT compatible with a 30 megabyte hard disk and an 8087 math coprocessor. It is operational except that it requires a multichannel analyzer board and drivers for spectral acquisition, transfer, and display. Spectra can be transferred to this version with a standard communications software package.

The software can be used to convert an existing qualitative EDS system into a fully quantitative system. Any laboratory that has a detector, pulse processor, and analogue to digital converter (ADC) mounted on their electron column can use the EDDI package as an economical and effective way to add the capability for quantitative analysis. A version of EDDI has been successfully installed in an IBM AT compatible in the Earth Sciences Department at Carleton University, Ottawa. This installation has a multichannel analyzer (MCA) board that provides real-time access to the spectrometer. The cost of the firmware and associated software utilities needed to install this type of system should be less than $7000 at current prices. This includes the cost of the computer.

The program source, the calculation algorithms, and the operator's manual are being published in GSC open file 2127, in order to assist laboratories who might wish to make this conversion. The documentation also includes some programming notes to assist in configuring the system and a discussion of the theory and practice of EDS mineral analysis.

The FORTRAN source listings in the open file report are from the IBM XT version and the documentation presumes that any users attempting to install EDDI on their system will provide their own hardware and drivers to transfer spectra into the program. Some familiarity with FORTRAN is also necessary to convert the system dependent statements in the code.

ANALYSIS OUTLINE

In electron microprobe work a quantitative analysis consists of preparing a count ratio of X-ray emission between standard and sample and calculating in counts/second (cps):

(sample cps/standard cps) $\times$ standard composition = analyzed composition

Any matrix or instrument condition that affects the emission rate must not change between readings on standard and sample. If this condition is met, then any such effects will ratio out in the calculation. This requirement is also the reason for the stress placed on instrument stability, consistent sample preparation, and efficiency in getting from standard to sample.

The effects that cannot be ratioed out are background, overlap, and matrix (ZAF) interferences. These must be calculated and this is the most important job undertaken by the software.

A first-quality analysis involves the direct comparison of standards and sample. Since it is often necessary to work with less than ideal equipment and conditions, it is important to have fast processing times and few intermediate steps. In short, the comparison should be fast and direct. The EDDI system incorporates many of these criteria.

Analysis turnaround

It is important to be able to see the fully corrected result from the last point analyzed before choosing the next point. This can result in great economies if the analyst is sufficiently experienced in both the analytical method and the application of the results. Careful preparation and selection of analysis points beforehand is still necessary; however, a speedy turnaround provides the luxury of choice as the work proceeds. Speeds should be at least in the 2 to 3 minute range to be useful.

Standardization

Standards should be similar materials to the unknowns. In EDS analysis this means that the program must accept standards with overlapping peaks. Often this provides a further advantage in that fewer standards are necessary for a given analytical setup which in turn provides faster recalibration times.

Recalibration

Commercially available software packages assume that the spectrometer is fitted with stable pulse processing of the most recent design. In these systems it takes hours or even days of work to recalibrate the standards after there has been a change in spectral characteristics, which is a reasonable approach if the electronic processing remains perfectly stable. In actual practice the recalibration process should be fast enough to include in every analytical sequence making it practical to produce analyses with older electronics.

Overlap correction

Again, the commercially available software packages presume that the pulse processing has resolution stability and characteristics that are often not available. The overlap correction needs to be relatively insensitive to these parameters.

Output format

The operator needs to be fully in control of the display format of the results including mineral formula calculations. Often displays are cluttered with information that is rarely needed.

Analyzed elements

The system needs to have the capability to analyze at least 25 elements simultaneously.

Matrix correction

All the currently available matrix correction procedures fail with some element combinations. The correction needs to be accessible to the operator, allowing the substitution of corrections from other sources such as a second ZAF program or a set of empirical measurements. It is also necessary to be able to insert new mass absorption coefficients.

Reports

There is a requirement for an extensive report writing utility based on analyses stored during the analytical session. It should be possible to arrange any subset of the results in a table, include averages, and have a free choice of mineral formula and end member calculations.

Menus

Electron beam X-ray analysis often becomes a highly repetitive process after the analyst has established a method for a particular application. Menu driven software becomes an encumbrance in this situation, forcing the operator to make multiple responses to essentially unnecessary queries. An appropriate design has a command structure that allows direct access to all program functions without having to pace through menus and schedules. This has the obvious disadvantage that the novice operator must spend some time learning the essential commands. The benefit in the hands of an experienced operator is a very flexible and responsive software package.

CORRECTIONS

Background

The background correction is that given in Fiori et. al. (1976) and modified by Heinrich et. al. (p. 365-369, 1981).

Overlap

The correction for overlap is an empirical approach that uses factors expressing the fraction of overlap between analyzed peaks within the specified windows. These windows are the regions used to integrate observed counts per second and are set up by the program once the analyst has specified the elements and X-ray lines for analysis. The technique is well proven in our laboratory and in fact was the basis of our original EDS software.

Matrix

The calculated matrix corrections are based on those published in Love and Scott (1978, 1981), Love, Cox, and Scott (1977, 1978), and Reed (1965).

The usual method of applying matrix corrections to online electron-microprobe analyses is by means of a general program such as the Love-Scott treatment. This calculation is often the most time-consuming portion of the analytical procedure. The time problem can be avoided by putting the matrix correction in the form of a graphical fit expressed in a table of coefficients. These coefficients are generated by the matrix program during the process of creating an analytical routine and they are stored with the routine. The coefficients will duplicate the correction that the original program would produce, with the advantage that the calculation iterates to closure with much greater efficiency. This is the approach used in EDDI and it is based on the correction scheme outlined in Lachance and Traill (1966), and Lachance (1970, 1979).

Emission and edge energies, mass absorption coefficients

The fitting relationships used for emission and edge energies as well as mass absorption coefficients are essentially those given in Springer and Nolan (1976). The coefficient table for edge energies has some modifications provided by R. Rousseau of the Mineral Resources Division at the GSC.

ACKNOWLEDGMENT

EDDI is founded on work and concepts developed by G.R. Lachance during his career at the Geological Survey of Canada. The system would not have been developed without his encouragement and long hours of freely given advice.

REFERENCES

Fiori, C.E., Myklebust, R.L., Heinrich, K.F.J., and Yakowitz, H.
1976: Prediction of continuum intensity in energy-dispersive X-ray microanalysis; Analytical Chemistry, v. 48, no. 1, p. 172-176.

Heinrich, K.F.J., Newbury, D.E., Myklebust, R.L., and Fiori, C.E.
1981: Energy-dispersive X-ray spectrometry; National Bureau of Standards, Special Paper 604.

Lachance, G.R.
1970: Fundamental coefficients for X-ray spectrochemical analysis; Canadian Journal of Spectroscopy, v. 15, no. 3, p. 3-11.

Lachance, G.R.
1979: Theoretical aspects of alpha coefficients used in X-ray fluorescence analysis; Scientific and Technical Notes *in* Current Research, Part B, Geological Survey of Canada, Paper 79-1B, p. 416.

Lachance, G.R. and Traill, R.J.
1966: A practical solution to the matrix problem in X-ray analysis; Canadian Journal of Spectroscopy, v. 11, no. 2, p. 43-48.

Love, G. and Scott, V.D.
1978: Evaluation of a new correction procedure for quantitative electron-probe microanalysis; Journal of Physics D: Applied Physics, v. 11, p. 1369-1376.
1981: Updating correction procedures in quantitative electron-probe microanalysis; Scanning, v. 4, no. 3, p. 111-130.

Love, G., Cox, M.G.C., and Scott, V.D.
1977: A simple Monte Carlo method for simulating electron-solid interactions and its application to electron-probe microanalysis; Journal of Physics D: Applied Physics, v. 10, p. 7-23.
1978: A versatile atomic number correction for electron-probe microanalysis; Journal of Physics D: Applied Physics, v. 11, p. 7-21.

Reed, S.J.B.
1965: Characteristic fluorescence corrections in electron-probe microanalysis; British Journal of Applied Physics, v. 16, p. 913-926.

Springer, G. and Nolan, B.
1976: Mathematical expansion for the evaluation of X-ray emission and critical absorption energies, and of mass absorption coefficients; Canadian Journal of Spectroscopy, v. 21, no. 5, p. 134-138.

Uranium in Canada, 1989

V. Ruzicka
Mineral Resources Division

Ruzicka, V., Uranium in Canada, 1989; in Current Research, Part A , Geological Survey of Canada, Paper 90-1A, p. 9-19, 1990.

Abstract

In spite of high annual production of uranium, Canada's global resources have remained at the same level during the past five years. New uranium occurrences associated with the sub-Athabasca unconformity were discovered on the Wolly and McArthur River blocks in the Athabasca Basin region, Saskatchewan. Grade and tonnage models for uranium deposits associated with unconformities indicate that the Australian deposits exhibit a large range in tonnages of low grade ores, whereas the Canadian deposits display a large range in ore grades.Mineralogical studies of selected uranium occurrences from the Athabasca and Elliot Lake basins allow refinement of conceptual genetic models for unconformity-associated and conglomerate deposits respectively. Granitoid rocks in the Miramichi Anticlinorium, New Brunswick, contain locally uranium associated with non-radioactive elements, such as Sn, W, Mo, Cu, Pb, Zn, Ag, Au, and Bi; radiometric methods can, therefore, be used for their prospection.

Résumé

Malgré une forte production annuelle d'uranium, les ressources totales du Canada sont restées au même niveau au cours des cinq dernières années. De nouvelles manifestations d'uranium associées à la discordance sub-Athabasca ont été découvertes sur les blocs de Wolly et de McArthur River dans la région du bassin d'Athabasca, en Saskatchewan. Des modèles de la teneur et du tonnage de gisements d'uranium associés à des discordances indiquent que les gisements australiens présentent une grande variété de tonnages de minerai à faible teneur alors que les gisements canadiens montrent une grande variété de teneurs du minerai. Des études minéralogiques de certaines manifestations d'uranium des bassins d'Athabasca et d'Elliot Lake permettent d'améliorer des modèles génétiques conçus en fonction de gisements associés à des discordances et de gisements conglomératiques. Des roches granitoïdes de l'anticlinorium de Miramichi, au Nouveau-Brunswick, renferment par endroits de l'uranium associé avec des éléments non radioactifs comme le Sn, le W, le Mo, le Cu, le Pb, le Zn, l'Ag, l'Au et le Bi; on peut donc utiliser des méthodes radiométriques pour la prospection de ces métaux.

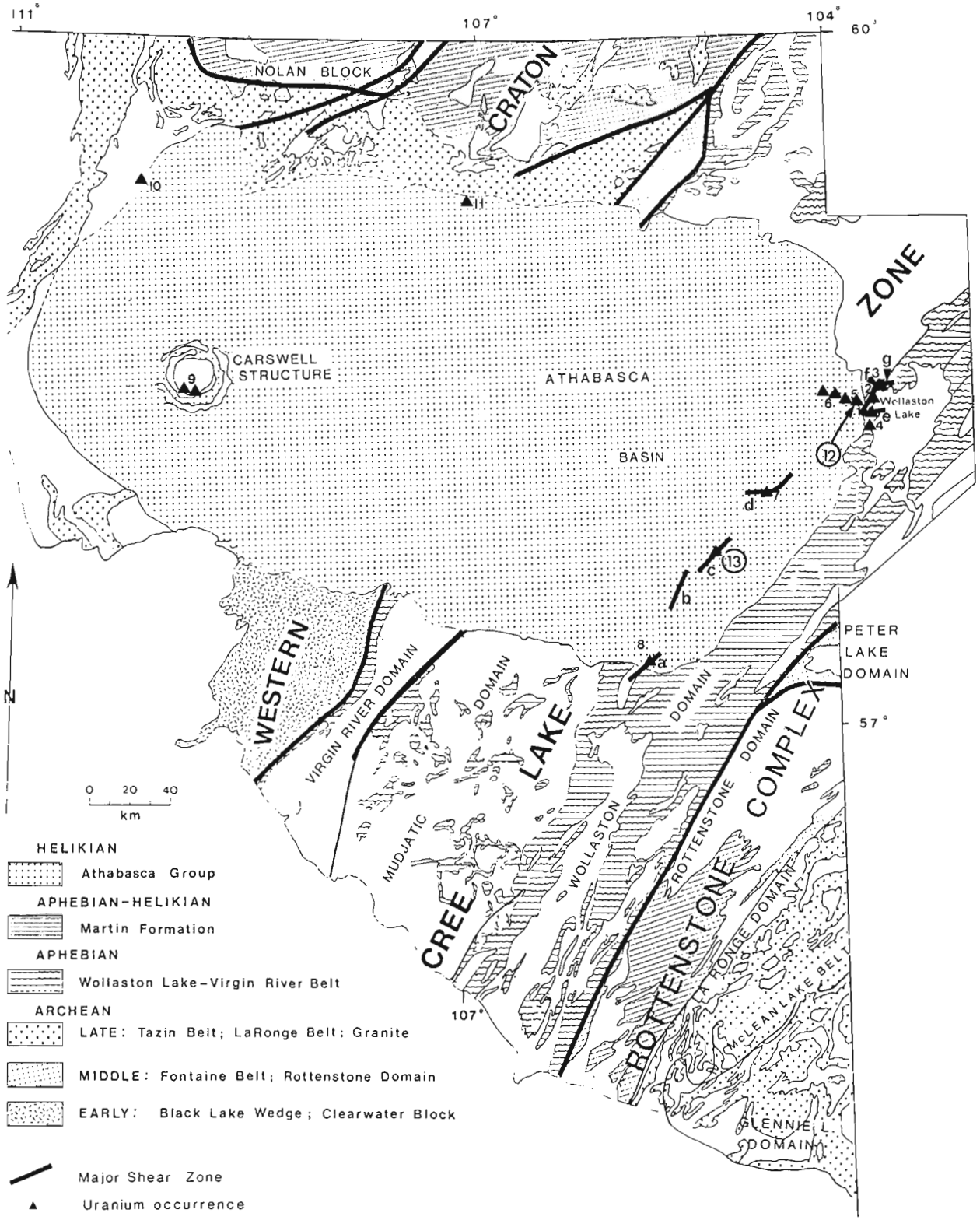

Figure 1. Selected uranium occurrences and structural trends controlling uranium mineralization in the Athabasca Basin region. Occurrences: 1 = Rabbit Lake; 2 = Collins Bay "A", "B" and "D"; 3 = Eagle Point; 4 = Raven and Horseshoe; 5 = McClean; 6 = Midwest and Dawn Lake; 7 = Cigar Lake; 8 = Key Lake; 9 = Cluff "D", Claude, OP, Dominique-Peter, Dominique-Janine, and South Dominique-Janine; 10 = Maurice Bay; 11 = Fond-du-Lac; 12 (circled) = Sue zone; 13 (circled) = P2N zone. Structures: a = Key Lake Fault; b = Hughes-Mann Lake Fault; c = P2 Fault; d = Cigar Lake Shear Zone; e = Rabbit Lake Fault; f = Collins Bay Fault Zone; g = Eagle Point Fault. Base map after Lewry and Sibbald (1979).

INTRODUCTION

From 1984 until the present, Canada has been the leading producer of uranium in the World Outside Centrally Planned Economies Areas (WOCA) with an annual output of 11 170 tonnes U in 1984 (i.e. 28.8 % of WOCA's production) and 12 400 tonnes U in 1988 (i.e. about 34.0 % of WOCA's production). During this period, Canada produced 58 610 tonnes U (OECD-NEA/IAEA, 1988; EMR, 1989). In 1988 and 1989 uranium was produced from 8 mines, namely: Denison, Quirke, Panel, and Stanleigh at Elliot Lake, Ontario; and Key Lake, Collins Bay "B", Claude, and Dominique-Peter in the Athabasca Basin region, Saskatchewan.

In spite of the high depletion of reserves in individual deposits, Canada's global mineable resources remained at about the same level since 1984. At the beginning of 1989 the mineable Reasonably Assured Resources in price categories up to $C300/kgU contained 310 000 tonnes U; the Estimated Additional Resources I amounted to 271 000 tonnes U; and the Estimated Additional Resources II comprised 380 000 tonnes of uranium metal (EMR, 1989).

As a result of exploration the depletion of resources was compensated by discoveries of new deposits, particularly in the Athabasca Basin region, where the exploration activity was most concentrated. The exploration activity in Canada reached the lowest point in 1985 (32 million Canadian dollars), but since then has gradually increased and reached 59 million dollars in 1988.

In the course of mineral resource appraisal, key deposits and areas in Canada were selected for detailed studies. Some results of the field, laboratory, and office studies by the author are presented in this paper.

SIGNIFICANT DISCOVERIES OF URANIUM OCCURRENCES

The 1989 exploration activity in Canada was focused predominantly on areas favourable for unconformity-associated deposits in the Athabasca Basin region, Saskatchewan and Alberta, in the Thelon Basin region, District of Keewatin, and in the Great Bear Lake region, District of Mackenzie. The exploration was based on conceptual genetic models postulating epigenetic mineralization controlled by Proterozoic unconformities, by conductive horizons in the basement rocks, by alteration zones, by faults, and by clastic sedimentary cover rocks.

Exploration drilling for possible extension of quartz-pebble conglomerate deposits was conducted in the Elliot Lake area, Ontario.

In New Brunswick, metallogenic studies under the Canada-New Brunswick Mineral Development Agreement (MDA) were concluded and a GSC paper on their results, prepared by A.L. McAllister and H.H. Hassan of the University of New Brunswick, is in the final stage of editing.

Most of the exploration activity was concentrated in the Athabasca Basin region, particularly in the area between Key Lake and Cigar Lake deposits, along the Collins Bay and Eagle Point faults, and on the Wolly block. In the western part of the basin the exploration was carried on in the Carswell Structure and its vicinity and in the Maybelle River area, Alberta.

Conceptual genetic modelling applied to exploration led to new discoveries on the Wolly block. Two deposits associated with the **Sue zone** have been delineated (Fig. 1). The discovery was made public in January 1989 (Total, 1989). The Sue zone, which occurs about 2.5 km east of the McClean deposit and immediately west of Cameco's Collins Bay "B" zone, represents a 4.2 km long structural trend. It contains at least two areas with significant uranium mineralization identified by drilling. One drillhole intersected 2.29 %U over a 12 m interval at a shallow depth. The deposits are spatially related to the Collins Bay Dome, with which also the Rabbit Lake, Collins Bay "A", Collins Bay "B", Collins Bay "D", and Eagle Point deposits are spatially associated. The deposits occur above the unconformity and contain polymetallic mineralization.

In the southeastern part of the Athabasca Basin, northeastern and eastern structural trends control uranium mineralization. These trends include dislocations, such as the Key Lake Fault, Rabbit Lake Fault, Collins Bay Thrust, Hughes-Mann Lake Fault, and the P2 Zone (Fig. 1). A significant uranium occurrence controlled by the P2 Zone was recently discovered by the Canadian Mining and Energy Corporation (Cameco; Star-Phoenix, 1989). The P2 Zone is a regional subvertical fault that extends horizontally for more than 20 km and dislocates the Aphebian basement and the Helikian Athabasca Group rocks. In its central part, in the vicinity of Boomerang Lake, i.e. on the McArthur River block, the zone is mineralized. Southwest of Boomerang Lake, uranium mineralization (called P2 South) occurs in altered arkose and sandstone within a short distance above the sub-Athabasca unconformity. The footwall beneath the unconformity consists of graphitic and pyritic pelitic gneiss and calc-silicate rocks. The principal constituent of the mineralization is pitchblende, about 300 Ma old (J. Marlatt, pers. comm. 1989). Northeast of Boomerang Lake, and about 5 km from the P2 South mineralization, the **P2 North** (P2N) occurrence was recently discovered. The high grade uranium mineralization occurs in silicified and dravitized sandstone at the sub-Athabasca unconformity (i.e. about 500 m below the surface; Star-Phoenix, 1989). The principal uranium mineral, pitchblende, was formed during the same mineralization episode (about 1.2 Ga ago; J. Marlatt, pers. comm. 1989) as other important deposits in the Athabasca Basin region (i.e. Key Lake, Cigar Lake, Rabbit Lake, Collins Bay "B", and Midwest). The discovery of the P2N occurrence was a result of successful application of a conceptual genetic model to geophysical and drilling data from previous stages of exploration. Several other uranium occurrences, such as BJ, (occurs outside the area of Fig. 1) have been identified on the McArthur River block in the past.

GRADE AND TONNAGE MODELS FOR URANIUM DEPOSITS ASSOCIATED WITH UNCONFORMITIES

In 1986 the United States Geological Survey (USGS) released some results of the USGS-INGEOMINAS Cooperative Mineral Resource Assessment of Colombia, which included 60 grade-tonnage conceptual models for selected types of mineral deposits (Cox and Singer, 1986). The models were based on estimated tonnages and grades from more than 3 900 well explored and well characterized deposits. The participants in the project had the most important immediate goal to "provide assistance to persons engaged in mineral resource assessment or exploration...and to upgrade the quality of their model compilation by encouraging input from those whose experience has not yet been captured in the existing models" (Cox and Singer, 1986). In order to facilitate preparation of standard figures for the grade-tonnage models, D.A. Singer and J.D. Bliss of the USGS developed an as yet unpublished program, called "G/T Modeler", for the data processing on a Macintosh computer. In order to test applicability of the method for quantitative assessment of deposits of one type, but hosted by different geological environments, the author prepared standard plots of grade and tonnage models for unconformity-associated deposits. The grade and tonnage data (Table 1) were used for deposits grouped in various configurations: for all known deposits of the world; for a group of deposits in Australia, all below the unconformity; for all Canadian deposits; for Canadian basement-hosted deposits, all below the unconformity; and for Canadian sandstone-hosted deposits, at and mainly above the unconformity (Fig. 2a to 2j).

Table 1. Tonnages and grades of ores and tonnages of uranium metal of the world's known unconformity-associated uranium deposits.

Deposit	Country	Ore kT	Grade %U	U T	Reference
Dyson's	Australia	157	0.29	452	Battey et al. (1987)
El Sherana	Australia	41	0.47	192	Battey et al. (1987)
El Sherana W	Australia	22	0.7	157	Battey et al. (1987)
Jabiluka 1	Australia	1373	0.21	2883	Battey et al. (1987)
Jabiluka 2	Australia	52422	0.33	172992	Battey et al. (1987)
Kintyre	Australia	5936	0.5	29680	G.C. Battey (pers. comm., 1989)
Koolpin Creek	Australia	3	0.11	3	Battey et al. (1987)
Koongarra	Australia	4946	0.228	11278	Battey et al. (1987)
Mt. Burton	Australia	6	0.18	11	Battey et al. (1987)
Mt. Fitch	Australia	290	0.44	1272	Battey et al. (1987)
Nabarlek	Australia	558	1.56	8700	Battey et al. (1987)
Palette	Australia	5	2.08	105	Battey et al. (1987)
Ranger 1	Australia	12057	0.273	32915	Battey et al. (1987)
Ranger 3	Australia	42425	0.17	72123	Battey et al. (1987)
Rockhole	Australia	14	0.95	129	Battey et al. (1987)
Rum Jungle S	Australia	665	0.37	2427	Battey et al. (1987)
Scinto 5	Australia	6	0.31	19	Battey et al. (1987)
Skull	Australia	1	0.42	3	Battey et al. (1987)
Sleisbeck	Australia	1	0.38	3	Battey et al. (1987)
White's	Australia	403	0.229	923	Battey et al. (1987)
Cigar Lake	Canada	902	12.2	110000	Fouques et al. (1986)
Claude	Canada	640	0.35	2240	Tona et al. (1985)
Cluff "D"	Canada	128	3.41	4370	Laine (1986)
Cluff "N"	Canada	505	0.34	1729	Laine (1986)
Cluff "OP"	Canada	53	0.28	150	Laine (1986)
Collins Bay "A"	Canada	135	4.83	6500	Ward (1988)
Collins Bay "B"	Canada	2585	0.61	15769	Ward (1988)
Collins Bay "D"	Canada	116	1.86	2154	Ward (1988)
Dawn Lake	Canada	794	1.7	13500	MacDougall (1988)
Dominique-Janine	Canada	250	0.32	800	Laine (1986)
Dominique-Peter	Canada	1761	0.66	11587	Laine (1986)
Eagle Point	Canada	3300	1.55	51152	Ward (1988)
Fond-du-Lac	Canada	183	0.21	385	Tremblay (1982)
Key Lake	Canada	3518	1.99	70000	Gardiner et al. (1988)
Kiggavik	Canada	3022	0.51	15384	Fuchs and Hilger (1987)
Maurice Bay	Canada	137	0.42	577	Tremblay (1982)
McClean	Canada	352	1.53	5385	Wallis et al. (1986)
Midwest	Canada	1200	1.6	19300	Ruzicka and LeCheminant (1987)
Rabbit Lake	Canada	5840	0.27	15769	Ward (1988)
Stewart Island	Canada	7	0.3	22	Homeniuk and Clark (1986)
West Bear	Canada	212	0.2	425	Tremblay (1982)
Total		146671	0.465	683465	

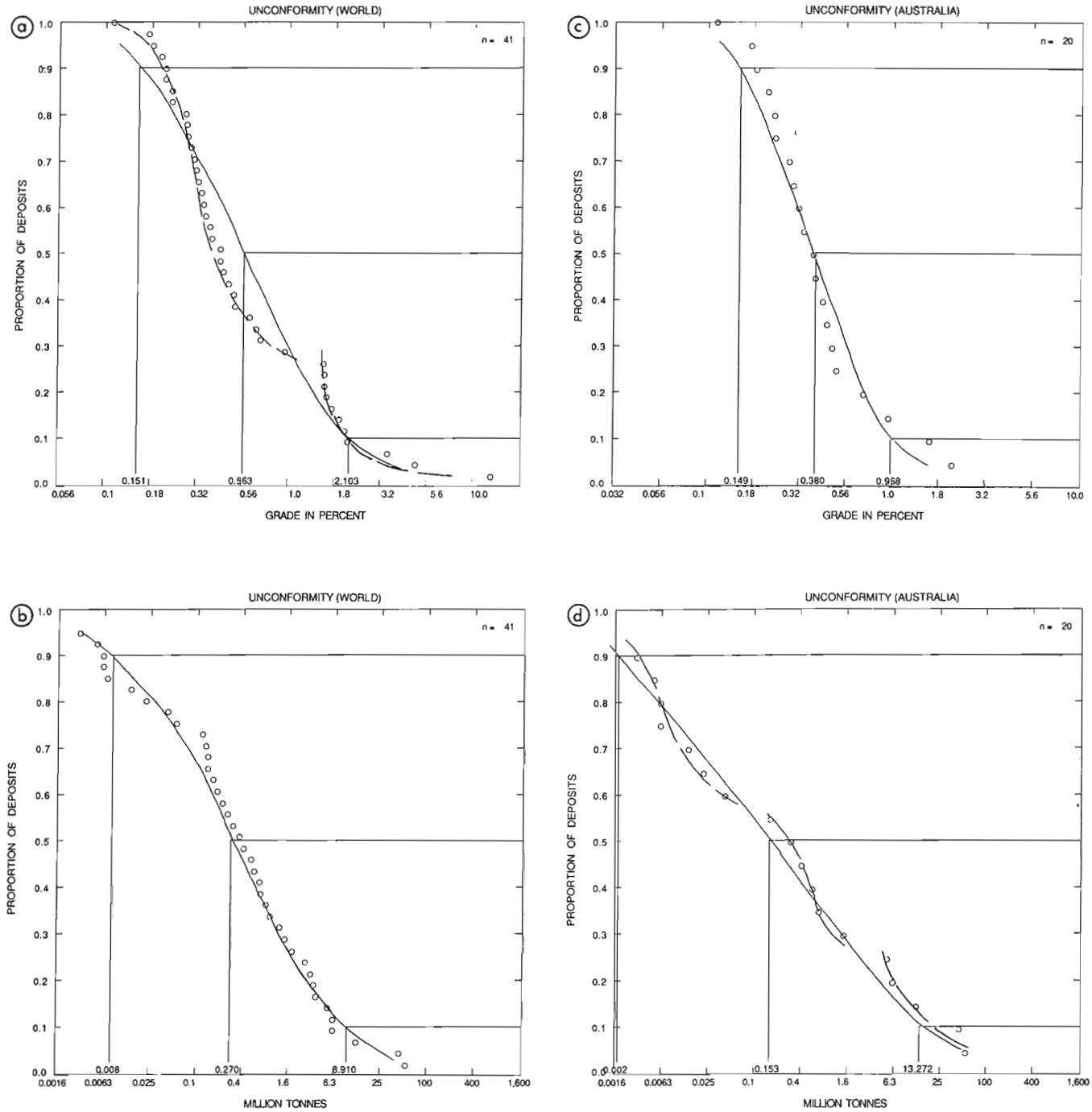

Figure 2. Grade and tonnage models for selected groups of unconformity-associated deposits: (a) grades and (b) tonnages of a composite group of world deposits; (c) grades and (d) tonnages of Australian deposits; (e) grades and (f) tonnages of Canadian deposits; (g) grades and (h) tonnages of Canadian basement-hosted deposits (i.e. below the unconformity); (i) grades and (j) tonnages of Canadian sandstone-hosted deposits (i.e. at or above the unconformity). The solid line summation curves represent interpretation of the data as following the program by D.A. Singer and J.D. Bliss (pers. comm. 1989); the dashed line summation curves denote possible interpretation of bimodal or trimodal populations.

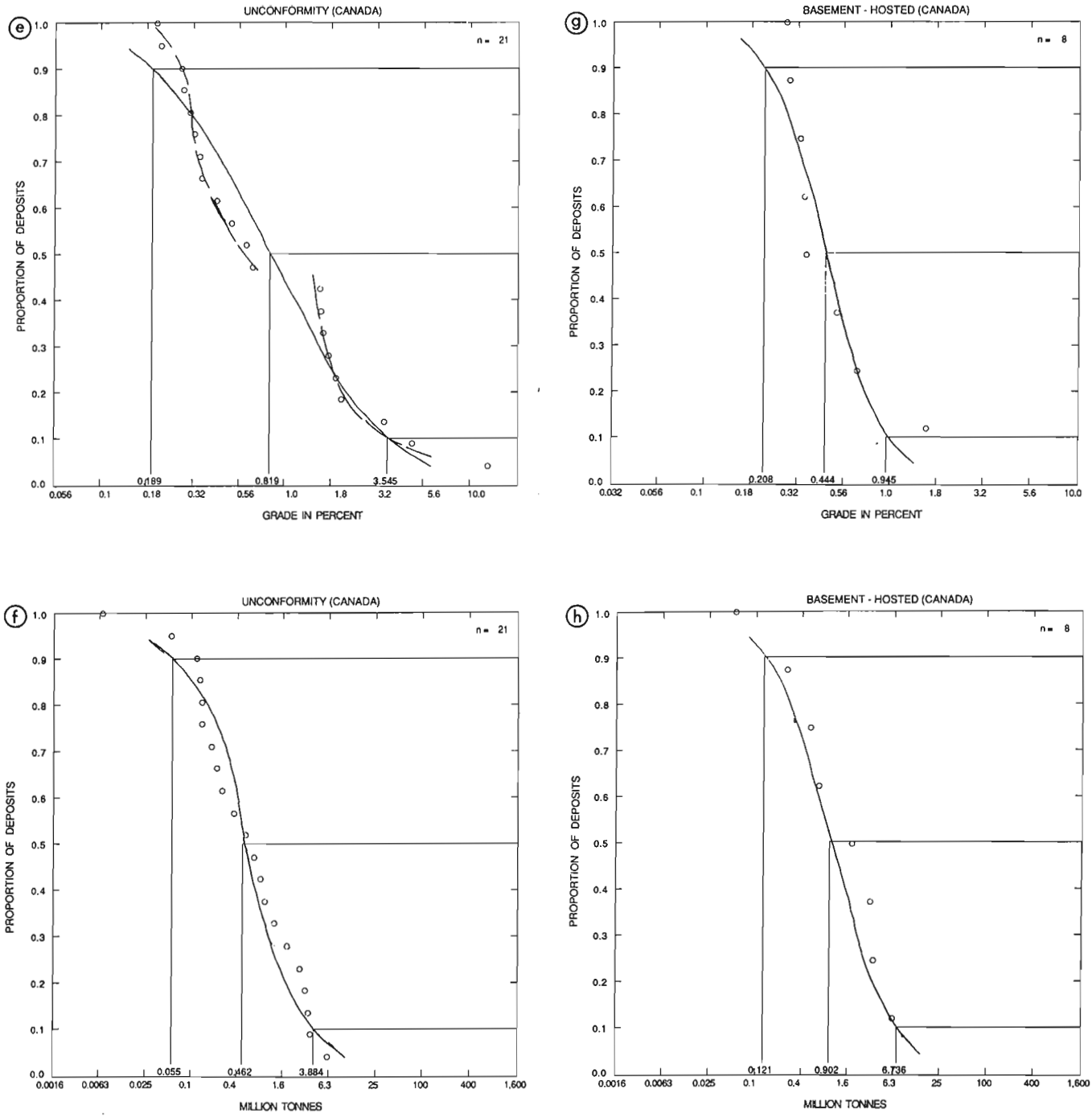

Figure 2. Continued

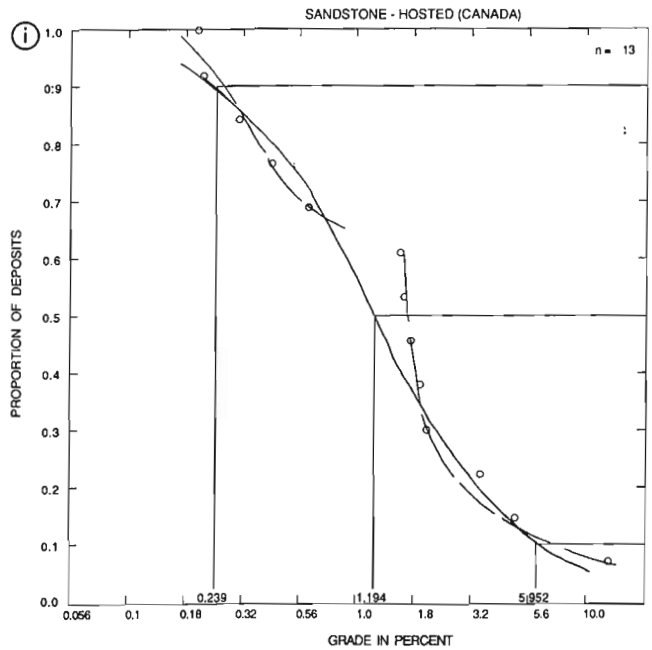

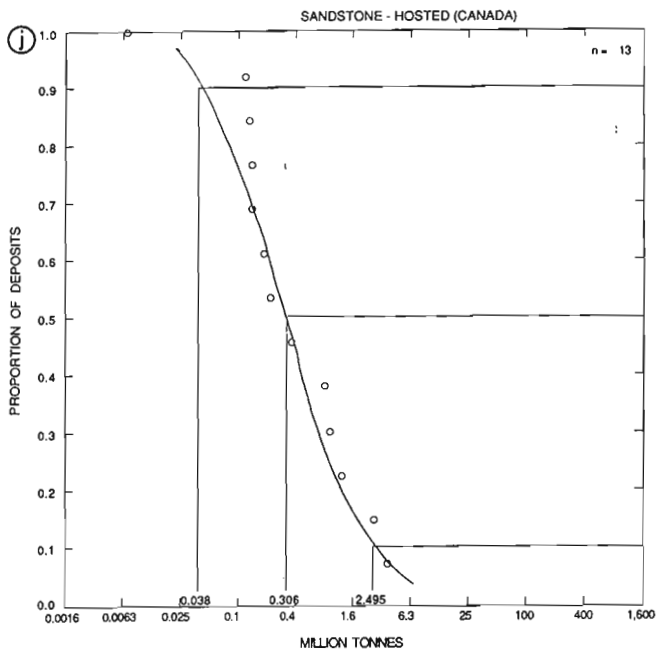

Figure 2. Continued

The plots, summation (frequency distribution) curves, and the 90th, 50th, and 10th percentiles for the grades and tonnages of all of the world's known unconformity-associated deposits (Fig. 2a and 2b) are roughly similar to those *in* Cox and Singer, (1986, p. 250).

However, individual groups of deposits display major differences in both grade and tonnage models: the Australian deposits exhibit a large range in tonnages (compare Fig. 2d and 2f); on the other hand Canadian deposits exhibit large range in grades (compare Fig. 2e and 2c). Further, the basement-hosted Canadian deposits generally cluster in the low grade segment of the grade summation curve (Fig. 2e), whereas the sandstone-hosted deposits, particularly those at the southeastern margin of the Athabasca Basin, occupy the high grade segment of the plot (Fig. 2e).

The differences in the grade distribution of the Canadian basement-hosted and sandstone-hosted (unconformity-type) deposits are apparent from the values of the 90th, 50th, and 10th percentiles of the statistical populations (Fig. 2g and 2i and Table 2). The data indicate that 90 percent of the known Canadian basement-hosted unconformity-associated deposits have grades of 0.21 % U or greater, 50 percent have grades of 0.44 % U or greater, and 10 percent have grades of 0.95 % U or greater; whereas 90 percent or more of the known Canadian sandstone-hosted unconformity-associated uranium deposits (particularly those occurring directly at the unconformity) have grades of 0.24 % U or greater, 50 percent have grades of 1.19 % U or greater, and 10 percent have grades of **5.95% U (!)** or greater.

Table 2. Percentiles (90th, 50th, and 10th) for grades and tonnages of ores of unconformity-associated uranium deposits sorted into various groups. The data refer to plots in Figures 2a to 2j.

Deposit Group	Grade%U			Tonnage Mt		
Percentile –>	90 th	50 th	10 th	90 th	50 th	10 th
World	0.151	0.563	2.103	0.008	0.270	8.910
Australia	0.149	0.380	0.968	0.002	0.153	13.272
Canada Global	0.189	0.819	3.545	0.055	0.462	3.884
Canada Basement	0.208	0.444	0.945	0.121	0.902	6.736
Canada Sandstone	0.239	1.194	5.952	0.038	0.306	2.495

Application of the grade and tonnage models to deposits of the same type but of different geological host environments is a useful tool for their quantitative classification. The analysis thus supports the statement that "...the grade and tonnage models are the fundamental means of translating geologists' resource assessments into a language that economists can use" (D.A. Singer, and J.D. Bliss pers. comm., 1989).

REFINEMENT OF CONCEPTUAL GENETIC MODELS

Samples from selected uranium occurrences from the Athabasca Basin, Saskatchewan (Collins Bay "B" and Dominique-Peter deposits) and Elliot Lake Basin, Ontario (Spine Road occurrence), were studied in order to further refine conceptual genetic models for unconformity-associated and conglomerate deposits respectively.

The **Collins Bay "B" zone** is a uranium-polymetallic deposit associated with the sub-Athabasca unconformity containing high grade, sandstone-hosted ores (for location **see** Fig. 1). Samples of the ores come from the northeastern wall of the open pit, about 10 m above the Collins Bay Fault. The samples contained coffinite as the principal uranium mineral and nickeline as the prevailing non-radioactive mineral. Other minerals are rammelsbergite, anatase, molybdenite, and zircon. The nickeline occurs in the deposit commonly in nodules, which are locally surrounded by coffinite (**see** autoradiograph, Fig. 3). The nickeline is intimately intergrown with rammelsbergite indicating simultaneous crystallization of the arsenides. Coffinite replaces nickeline (Fig. 4) and locally forms a thin granular mass of coffinite, nickeline, and rammelsbergite (Fig. 5). The coffinite contains elevated amounts of lead and titanium and traces of thorium, yttrium, phosphorus, and zirconium (Table 3, analyses 1 to 4). The titanium is apparently derived from rutile or anatase, which commonly occur in the ores. The position of coffinite in the paragenetic sequence and its chemical composition indicate that it formed after the main ore-forming phase from relatively low temperature (<200°C) residual solutions of negative Eh values. The nickeline-coffinite assemblages commonly occur in the periphery of the main orebodies, which consist mainly of pitchblende and nickel and cobalt arsenides, as is the case of the Collins Bay "B", the Key Lake, and other deposits.

The **Dominique-Peter deposit** is an unconformity-associated uranium deposit hosted by the Aphebian basement rocks. The uranium mineralization is hosted by rocks exhibiting carbonate, chlorite, and clay alteration, silicification, and locally strong mylonitization. It occurs in several forms: (a) as clusters of crystalline, thorium-free uraninite (U_3O_7?; Fig. 6); (b) as seams of massive pitchblende, some of which represent coalesced grains of the crystalline phase; (c) as coatings of and replacements by coffinite, which are locally associated with carbon (Fig. 7). Radiogenic lead occurs in stringers and euhedral grains of galena. Gangue contains Ca-, Mg-, Mn-, and Fe-carbonates (Fig. 6 and 7). The pitchblende contains elevated amounts of lead and calcium and traces of yttrium, titanium, and iron (Table 3, analyses 5 and 6). The coffinite is rich in calcium,

Figure 3. Autoradioluxograph of an ore specimen from the Collins Bay "B" deposit; positive image. See text for details.

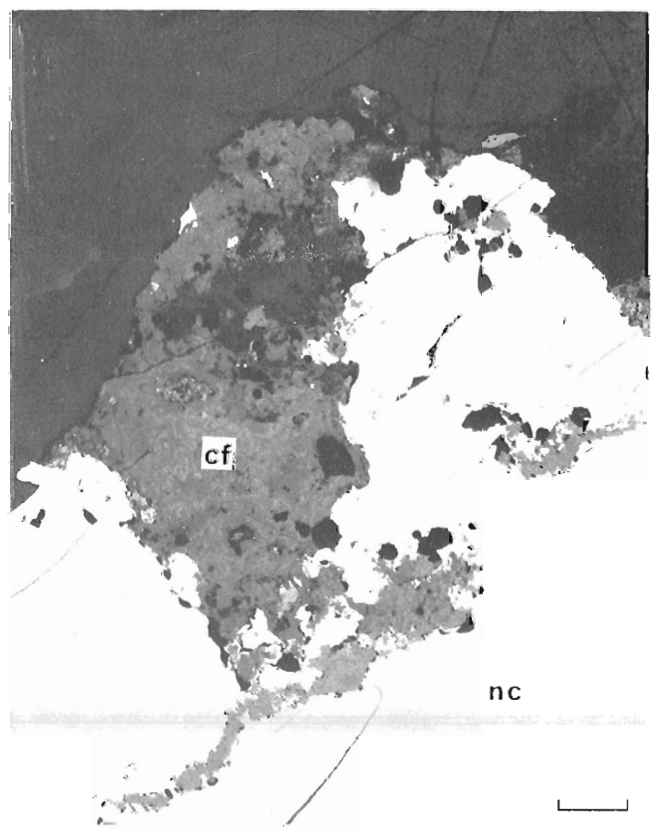

Figure 4. Coffinite (cf) surrounding and replacing nickeline (nc). Collins Bay "B" deposit. Photomicrograph, reflected light. Scale bar is equal to 100 μm.

Table 3. Microprobe analyses of ore-forming minerals from samples from the following localities: 1 to 4 of coffinite from Collins Bay "B" deposit; 5 and 6 of pitchblende from Dominique-Peter deposit; 7 and 8 of coffinite from Dominique-Peter deposit; 9 to 11 of U-Ti-(Si) phase ("brannerite") from Spine Road occurrence at Elliot Lake. Analyses of samples collected by the author were done by G.M. LeCheminant of the GSC Mineral Resources Division.

Constituent	Sample number										
	1	2	3	4	5	6	7	8	9	10	11
UO_2	73.598	80.36	75.472	74.072	84.077	83.574	72.092	70.284	26.635	28.081	34.567
Th_2O	0	0.028	0.043	0.009	0	0	0.065	0.034	1.442	1.171	1.677
PbO	1.816	2.984	1.356	0.86	8.735	9.328	0.132	0.075	0.922	0.712	0.288
Y_2O_3	0.067	0.052	0.104	0.147	0.274	0.189	0.704	1.003	0.858	0.547	2.711
$Zr°_2$	0.032	0.028	0.014	0.016	0	0	0	0	0	0.031	0.046
SiO_2	10.827	9.267	9.659	13.584	1.055	0.631	7.868	8.989	4.411	4.533	15.747
TiO_2	0.657	1.663	2.213	0.57	0.175	0.165	0	0	47.19	46.609	12.56
P_2O_5	0.362	0.293	0.284	0.323	0	0.142	0.504	0.534	0.025	0	0.211
SO_3	0.352	0.729	0.437	0.272	0.07	0.005	0	0	0.025	0.057	0.352
FeO	0.004	0.037	0.005	0	0.314	0.441	0.04	0.028	1.567	2.332	5.469
CaO	0.078	0.186	0.123	0.178	1.354	1.217	9.106	8.107	0.816	0.922	0.33
	87.795	91.083	89.711	90.033	96.055	95.693	90.511	89.055	83.891	84.996	73.959

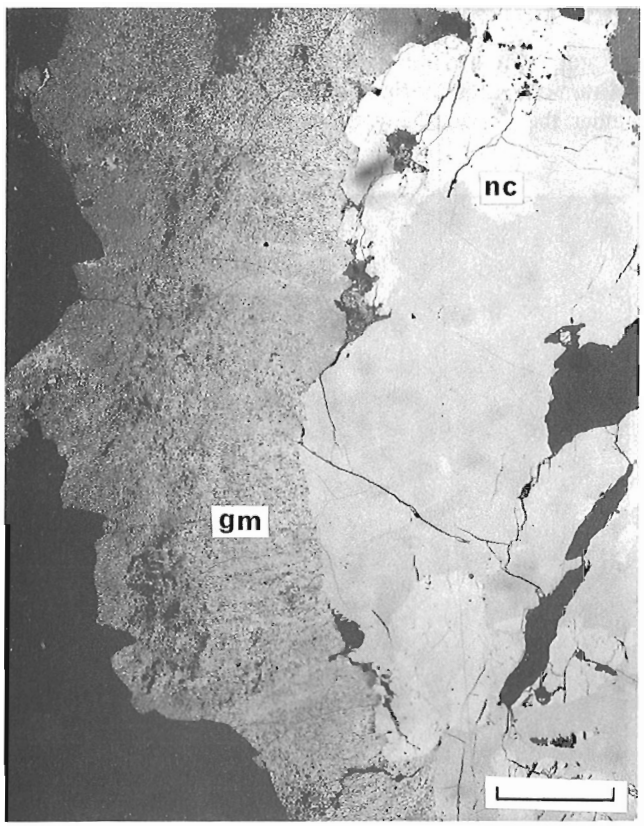

Figure 5. Granular mass (gm) consisting of coffinite, nickeline and rammelsbergite and rimming a nodule of nickeline (nc). Collins Bay "B" deposit. Photomicrograph, reflected light. Scale bar is equal to 100 μm.

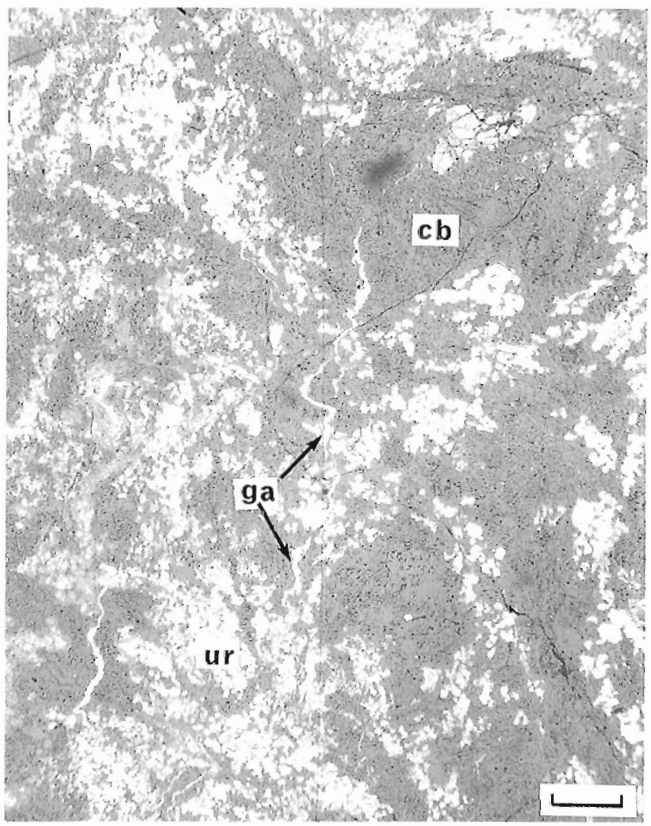

Figure 6. Thorium-free uraninite (U_3O_7?) (ur) forming clusters in carbonate (cb) matrix; white stringers are galena (ga). Dominique-Peter deposit. Photomicrograph, reflected light. Scale bar is equal to 100 μm.

yttrium, and phosphorus (Table 3, analyses 7 and 8). The calcium was derived from the matrix. Deposition of uranium minerals took place in at least three stages: (i) early deposition of crystalline uraninite; succeeded by (ii) massive pitchblende, which represents the main mineralization phase; and (iii) deposition of coffinite, accompanied by partial replacement of the crystalline uraninite and pitchblende. Mylonitization of the host rocks preceded uranium mineralization. Chloritization, kaolinization, illitization, silicification, and carbonatization accompanied deposition of uranium minerals. Carbonatization and silicification took place also after deposition of uranium.

The **Spine Road occurrence** is located in the town of Elliot Lake, Ontario, at the south shore of Elliot Lake. The occurrence is in several quartz-pebble conglomerate beds within the upper part of Matinenda Formation. Matrix of the conglomerate contains pyrite, chalcopyrite, monazite, zircon, a U-Ti-(Si) phase, anatase, mica, cerian allanite, and kerogen. The U-Ti-(Si) phase, called brannerite by Ramdohr (1957), is the principal uraniferous component of the conglomerate. Formation of brannerite from Pronto mine has been explained by Ramdohr (1957) as a result of hydrothermal processes, his "Pronto-Reaktion". Our observations on hand specimens collected from the Spine Road occurrence support Ramdohr's (1957) theory, but suggest that the authigenic uranium-titanium-silicon compound be simply designated as a U-Ti-(Si) phase. This phase is closely associated with anatase, which is apparently a breakdown product of ilmenite or magnetite-ilmenite. The uranium, associated with silicon, was scavenged from the ore-forming fluids by the titanium mineral. Backscattered electron photographs of anatase grains show the U-Ti-(Si) phases mostly at the rims of the anatase grains (Fig. 8), but also along fractures within the grains (Fig. 9). This process took place during the diagenetic stage of the conglomerate. In addition to uranium, titanium, and silicon, the U-Ti-(Si) phase contains thorium, lead, and yttrium (Table 3, analyses 9 to 11). This attests to derivation of the phase from original uraninite, which was dissolved in the diagenetic fluids and the constituents of which were deposited under reducing conditions on the surface and in fractures and cavities of the anatase in various (nonstoichiometric) proportions.

URANIUM METALLOGENY OF GRANITOIDS, MIRAMICHI ANTICLINORIUM, NEW BRUNSWICK

A study on uranium metallogeny of granitoids in the Miramichi Anticlinorium, New Brunswick, was carried on under the Canada-New Brunswick Mineral Development

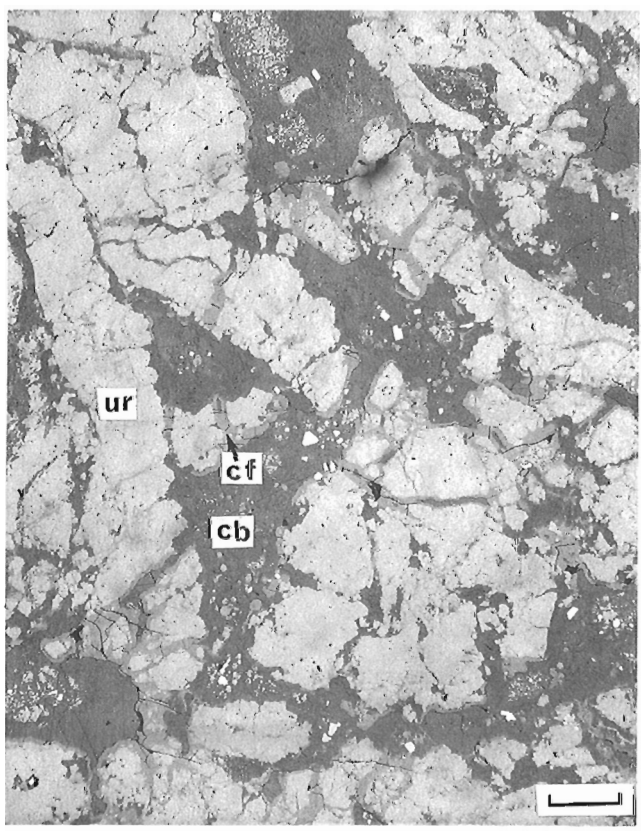

Figure 7. Coffinite (cf) coating thorium-free uraninite (ur) in carbonate (cb) matrix. Dominique-Peter deposit. Photomicrograph, reflected light. Scale bar is equal to 100 μm.

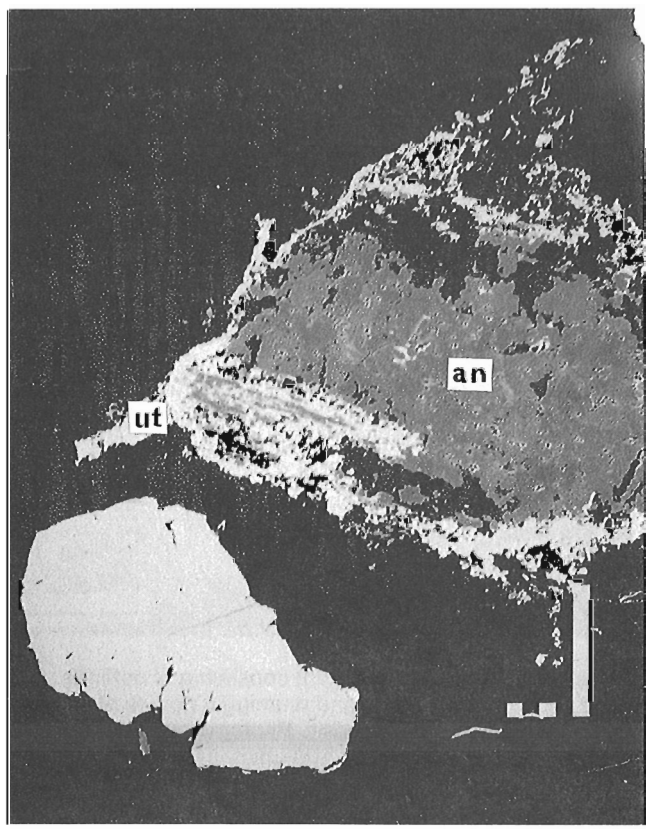

Figure 8. A U-Ti-(Si) phase ("brannerite") (ut) partly replacing rim of an anatase (an) grain. Spine Road occurrence, Elliot Lake. Backscattered electron photograph. Scale bar is equal to 100 μm.

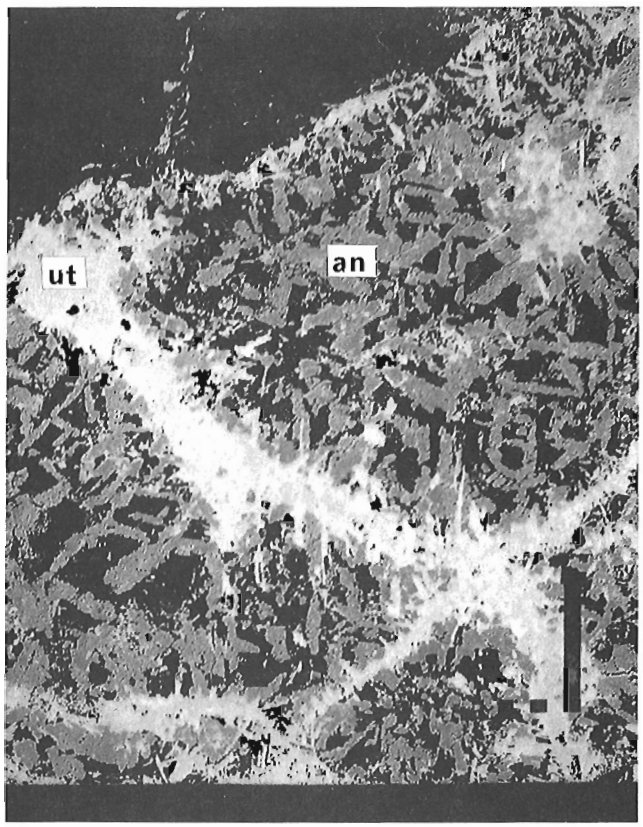

Figure 9. A U-Ti-(Si) phase ("brannerite") (ut) filling fractures in anatase (an). Spine Road occurrence, Elliot Lake. Backscattered electron photograph. Scale bar is equal to 100 μm.

Agreement by A.L. McAllister and H.H. Hassan at the University of New Brunswick. The study was based on geological, geochemical, and geophysical data acquired during their field work and on materials from geological mapping and exploration activities of other organizations. Results of the work (H.H. Hassan and A.L. McAllister, pers. comm., 1989) suggest that certain parts of the Burnthill, Dungarvon, Trout Brook, and Rocky Brook plutons contain elevated concentrations of uranium-polymetallic elemental assemblages, such as U, Sn, W, Mo, Cu, Pb, Zn, Ag, Au, and Bi. Radiometric methods can be, therefore, advantageously used in exploration for these commodities.

ACKNOWLEDGMENTS

The computer program G/T Modeler for Macintosh, which was developed by D.A. Singer and J.D. Bliss, was supplied by W.I. Finch of the United States Geological Survey, Denver, Colorado. Mineral identification and microprobe analyses of the specimens by G.M. LeCheminant of the Mineral Resources Division are sincerely appreciated. Critical reading of the paper by R.T. Bell is gratefully acknowledged.

REFERENCES

Battey, G.C., Miezitis, Y., and McKay, A.D.
1987: Australian uranium resources; Australia, Bureau of Mineral Resources and Geophysics, Resource Report 1, Canberra, 67 p.

Cox, D.P. and Singer, D.A. (editors)
1986: Mineral Deposit Models; United States Geological Survey, Bulletin 1693, Washington, 379 p.

EMR
1989: Canadian Uranium Industry, Fact Sheet; Energy, Mines and Resources, Ottawa, 1 p.

Fouques, J.P., Fowler, M., Knipping, H.D., and Schimann, K.
1986: The Cigar Lake uranium deposit: discovery and geological characteristics; *in* Uranium Deposits of Canada, edited by E.L. Evans, The Canadian Institute of Mining and Metallurgy, Special Volume 33, p. 218-229.

Fuchs, H.D. and Hilger, W.
1987: Kiggavik (Lone Gull): an unconformity related uranium deposit in the Thelon Basin, Northwest Territories, Canada; *in* Uranium Resources and Geology of North America, International Atomic Energy Agency, TECDOC-500, Vienna, p. 411-428.

Gardiner, C.D., Razvi, N., and Spencer, L.M. (editors)
1988: Canadian Mines Handbook 1988-89; Northern Miner Press Limited, 604 p.

Homeniuk, L.A. and Clark, R.J.McH.
1986: North Rim deposits, Athabasca Basin; *in* Uranium Deposits of Canada, edited by E.L. Evans, The Canadian Institute of Mining and Metallurgy, Special Volume 33, p. 230-240.

Laine, R.
1986: Uranium deposits of the Carswell Structure; *in* Uranium Deposits of Canada, edited by E.L. Evans, The Canadian Institute of Mining and Metallurgy, Special Volume 33, p. 155-169.

Lewry, J.F. and Sibbald, T.I.I.
1979: A review of pre-Athabasca basement geology in Northern Saskatchewan; *in* Uranium Exploration Techniques, Proceedings of a Symposium held in Regina, 1978, November 16-17, edited by G.R. Parslow, Saskatchewan Geological Society, Special Publication 4, p. 19-58.

MacDougall, D.G.
1988: Metallogenic Map Series: Wollaston Lake, NTS Area 64L; Saskatchewan Energy and Mines, Saskatchewan Geological Survey, Report 254, 40 p.

OECD-NEA/IAEA,
1988: Uranium Resources, Production and Demand; A Joint Report, Organization for Economic Co-operation and Development, Nuclear Energy Agency, Paris, 194 p.

Ramdohr, P.
1957: Die "Pronto-Reaktion"; Neues Jahrbuch fuer Mineralogie Monatshefte, p. 217-222.

Ruzicka, V. and LeCheminant, G.M.
1987: Uranium investigations in Canada, 1986; *in* Current Research, Part A, Geological Survey of Canada, Paper 87-1A, p. 249-262.

Star-Phoenix
1989: Major new uranium deposit discovered; Saturday, April 22, 1989 edition, Saskatoon, Saskatchewan.

Tona, F., Alonso, D., and Svab, M.
1985: Geology and mineralization in the Carswell Structure — a general approach; *in* The Carswell Structure Uranium Deposits, Saskatchewan, edited by R. Laine, D. Alonso, and M. Svab, Geological Association of Canada, Special Paper 29, p. 1-18.

Total
1989: Minatco Limited; press release of January 20, 1989, Calgary, Alberta, 1 p.

Tremblay, L.P.
1982: Geology of the uranium deposits related to the sub-Athabasca unconformity, Saskatchewan; Geological Survey of Canada, Paper 81-20, 56 p.

Wallis, R.H., Saracoglu, N., Brummer, J.J., and Golightly, J.P.
1986: The geology of the McClean uranium deposits, northern Saskatchewan; *in* Uranium Deposits of Canada, edited by E.L. Evans, The Canadian Institute of Mining and Metallurgy, Special Volume 33, p. 193-217.

Ward, D.M.
1988: Exploration and geology; *in* Rabbit Lake, Eldor 0Mines Ltd., Edmonton, p. 8-15.

A technique for cataloguing and retrieving large sets of marine magnetic and aeromagnetic data

J. Verhoef[1], R. Macnab[1], G. Oakey[1]
K. Usow[2], and P. Hull[2]
Atlantic Geoscience Centre, Dartmouth

Verhoef, J., Macnab, R., Oakey, G., Usow, K., and Hull, P., A technique for cataloguing and retrieving large sets of marine magnetic and aeromagnetic data; in Current Research, Part A, Geological Survey of Canada, Paper 90-1A, p. 21-25, 1990.

Abstract

In a major data compilation project for the Arctic and North Atlantic oceans, many large sets of digital magnetic observations are being assembled to create a coherent data base that can be applied to the construction of accurate magnetic anomaly maps and quantitative investigations. To ensure effective indexing and retrieval of selected data sets, a technique has been devised in which summary information that describes the data base is stored on line, and is queried interactively to locate and to extract information from the main data base, which is stored off line. In its present form, the method can handle additional data collected concurrently with magnetic observations (i.e. bathymetry, gravity); in theory, it can be extended to cope with many other kinds of data that are gathered from moving platforms.

Résumé

Dans un important projet de compilation de données portant sur les océans Arctique et Atlantique Nord, on regroupe de nombreux grands ensembles d'observations magnétiques numériques pour créer une base de données cohérente qu'on peut appliquer à l'établissement de cartes des anomalies magnétiques précises et à des études quantitatives. Afin d'assurer une indexation et une récupération efficaces d'ensembles de données choisis, on a mis au point une technique aux termes de laquelle des données sommaires qui décrivent la base de données sont stockées en direct puis interrogées interactivement afin de localiser et d'extraire des données de la base de données principale qui, elle, est stockée hors ligne. Présentée sous sa forme actuelle, la méthode peut traiter des données supplémentaires recueillies en même temps que des observations magnétiques (c'est-à-dire bathymétriques, gravimétriques); en principe, on peut l'étendre à de nombreux autres types de données qu'on recueille à partir de plates-formes mobiles.

[1] Blue Vajra Computing, 1107 South Park Street, Halifax Nova Scotia B3H 2W6

INTRODUCTION

A major compilation project has been initiated to assemble all available digital magnetic observations from international sources, for the purpose of producing a coherent data base for the Arctic and North Atlantic oceans and adjacent land areas. When completed, the data base will be used for the production of accurate magnetic anomaly maps, as well as for quantitative interpretations relating to plate reconstructions, the structure and formation of passive continental margins, and the history of seafloor spreading. For a description of the rationale, scope, and methodology of the project, see Macnab et al. (1990, this volume).

With the compilation covering such a large area of interest and with so many potential sources of observations, a significant aspect of the project concerns the efficient handling and management of data. The project has already accumulated numerous data sets that feature tremendous diversity: type of observation (marine magnetic or aeromagnetic); volume of data (from kilobytes to megabytes); form of storage (computer-readable media or printed maps); and format (grids, time series along ship tracks, fiducial observations along aircraft flight lines, or contours digitized from printed maps).

The project's rate of progress depends largely on our ability to select, manipulate, and merge these many distinct data sets on the way to creating a final homogeneous product: not only must the process be practical for handling large data sets in their entirety, but it must be equally effective at searching for and correcting single erroneous data points among millions.

Clearly, it is essential to have a set of tools and procedures that are fast, reliable, and easy to operate. A fundamental requirement is an efficient indexing system that allows the rapid selection and retrieval of data sets. Such an index and retrieval system has been designed, and is now being implemented.

POTENTIAL FIELDS SOFTWARE AT AGC

Figure 1 presents a general overview of the procedures and software tools for handling and processing potential field data at the Atlantic Geoscience Centre. These are based on a suite of about 150 programs running with a standard user interface in a networked VMS environment, and operating on common file formats to simplify the exchange of data between software modules.

Many of the functions shown in Figure 1 are multipurpose, i.e. they are applicable to other tasks besides the magnetic data compilation project: the management of other kinds of data, scientific analysis and interpretation, special displays, etc.

Largely within the context of the magnetic compilation project, the remainder of this paper will describe the two initial functions shown in Figure 1: **data capture** (the accumulation and preparation of information to load in the data base) and **data retrieval** (the selection and retrieval of information from the data base).

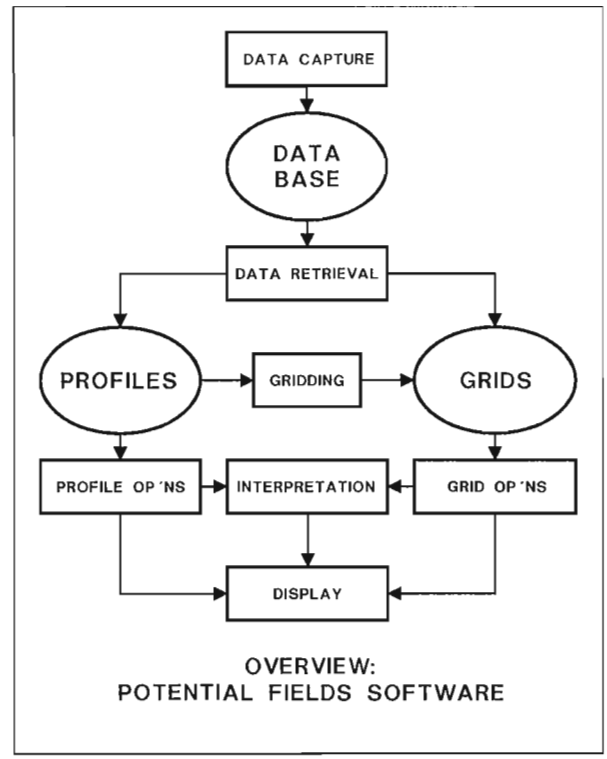

Figure 1. An overview of the software tools used to handle, process, and display potential fields data at the Atlantic Geoscience Centre. These consist of about 150 programs presently operating in a networked VMS environment (a conversion to UNIX is in the offing), and featuring a standard user interface and common file formats.

DATA CAPTURE AND PREPARATION

Magnetic observations for the compilation project are assembled from a variety of sources, as shown in the upper part of Figure 2. Most data are obtained on computer-readable media, but provision does exist for digitizing contour maps if the data are available in no other form.

Data centres such as the U.S. National Geophysical Data Center in Boulder, Colorado are valuable repositories of historical data holdings in digital form. Usually, the data receive only minimal quality control, but this is outweighed by the convenience of having large volumes of information already accumulated in one place and in a standard storage format.

Institutions such as universities and government laboratories collect and archive magnetic data in support of their own mapping and research objectives, and usually release these holdings when they have been analyzed and the results published. Data obtained from these organizations tend to have varying quality and to be stored in a great assortment of formats.

Commercial organizations such as oil and geophysical exploration companies collect and maintain large inventories of data; these tend to be proprietary for the most part, however, and so tend to receive only limited distribution.

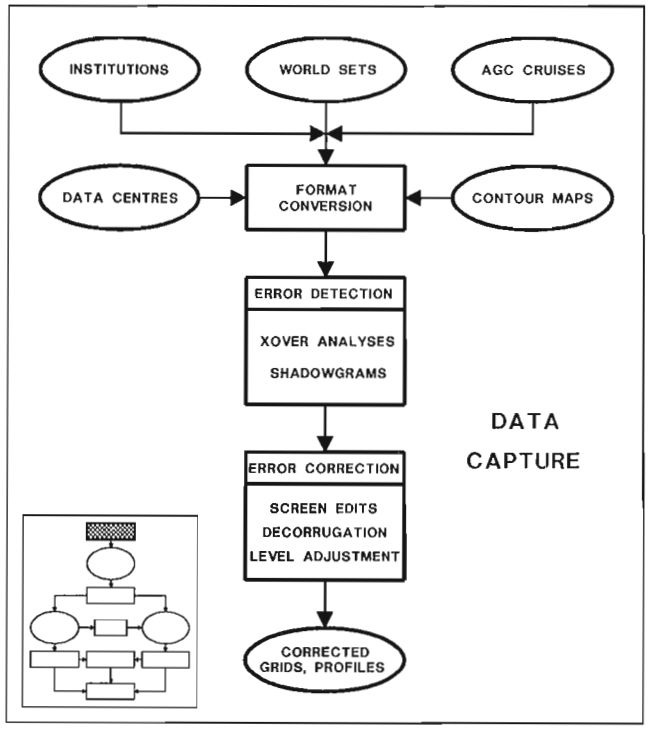

Figure 2. Steps involved in assembling data sets from different sources, and in preparing them prior to loading in the data base.

World sets consist of collections of observations with global or near global coverage, e.g. the bathymetric-topographic grid of ETOPO5 (ETOPO5, 1986), or SEASAT sea-surface altimetry measurements that can be converted mathematically to gravity values (Haxby, 1987). The MAGSAT data set is the only global collection of magnetic data, but as it contains only long wavelength features originating from sources in the Earth's core, its relevance to the present magnetic compilation is somewhat limited.

Cruises sponsored by the Geological Survey of Canada account for a large part of the total data base. These consist of systematic mapping expeditions carried out in co-operation with the Canadian Hydrographic Service, or of mission-oriented cruises organized to solve specific scientific problems (Verhoef and Macnab, 1987).

Upon receipt, all data sets are converted to a standard internal format to facilitate subsequent handling by common input-output routines. Series of marine magnetic or aeromagnetic observations (known as profile data) are stored in time ordered multifield records that can accommodate up to seven concurrently observed parameters, e.g. bathymetry, gravity, etc. Grids are reorganized if necessary into a standard row and column order. Digitized contours are converted to grids and are stored in a similar fashion.

During conversion, a formatted header record is created for each data set, which contains all available descriptors and qualifiers, e.g. type of data, sponsoring organization, time frame, area limits, etc. Supplementing this information is a large free-format comment area for recording items that don't fit into the categories above.

For the time being, all data are archived on 6250 bpi magnetic tape; however, we are investigating alternative technologies that feature compressed storage and fast access (such as optical discs).

To date, about 9 000 000 marine magnetic observations have been assembled, representing over 750 cruises. A third of these observations have been generated on about 90 cruises sponsored by the Geological Survey of Canada. Aeromagnetic surveys account for an additional 7 000 000 observations over land and sea; most observations over the Canadian land mass have been compiled and provided in gridded form by the Geophysics Division of the Geological Survey of Canada (Geological Survey of Canada, 1987), whereas most offshore data have been assembled as profiles along aircraft flight lines.

Following conversion, each data set is subjected to various error detection and correction procedures, as detailed by Macnab et al. (1987) and by Verhoef and Macnab (1987). An important procedure with marine profile data is the analysis of discrepancies at track crossover points, which can be related to diurnal variations, navigation errors, or failure of the International Geomagnetic Reference Field (IGRF) to model adequately the magnetic secular variation in certain regions (Verhoef and Macnab, 1987). Grid errors are most often detected by means of shaded relief plots that emphasize problems in the data; see the

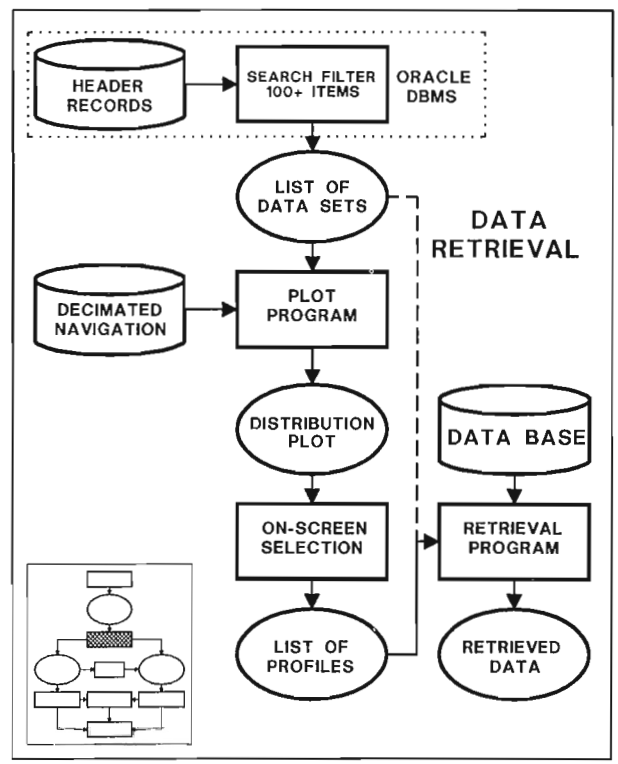

Figure 3. Index and retrieval procedures: header records and decimated navigation are stored on line and are queried interactively (depending on the user's needs, the production of a track plot from the decimated navigation is an optional step that can be bypassed); the output is a set of batch commands for extracting selected data sets from the main data base, which is stored off line.

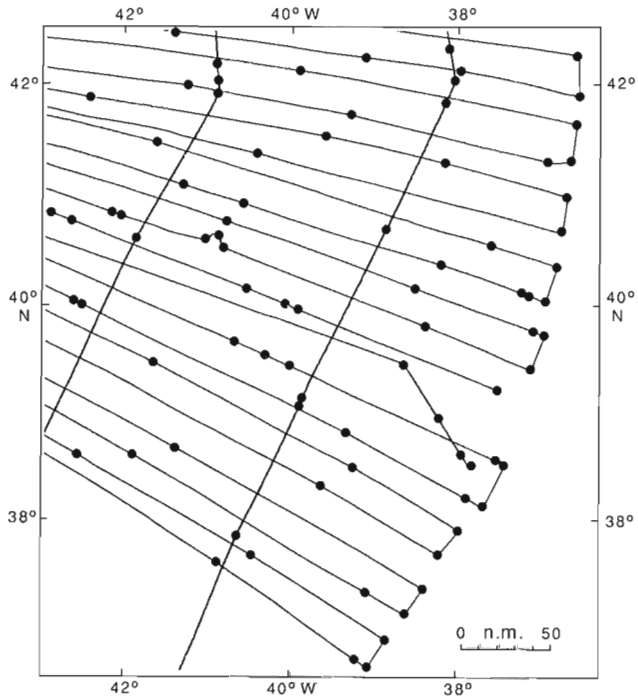

Figure 4. Significant compression factors can be achieved by decimating the navigation information that describes ships' tracks or aircraft flight lines. This figure is a partial plot of the lines flown in a regional aeromagnetic survey. The dots mark the locations of course or speed changes that exceeded preset limits, as detected by a decimation algorithm. Representing a fraction of the original data points, the dots can accurately reconstitute the complete survey pattern: in this particular case, 468 decimated points replicate the survey's 126 338 original fixes.

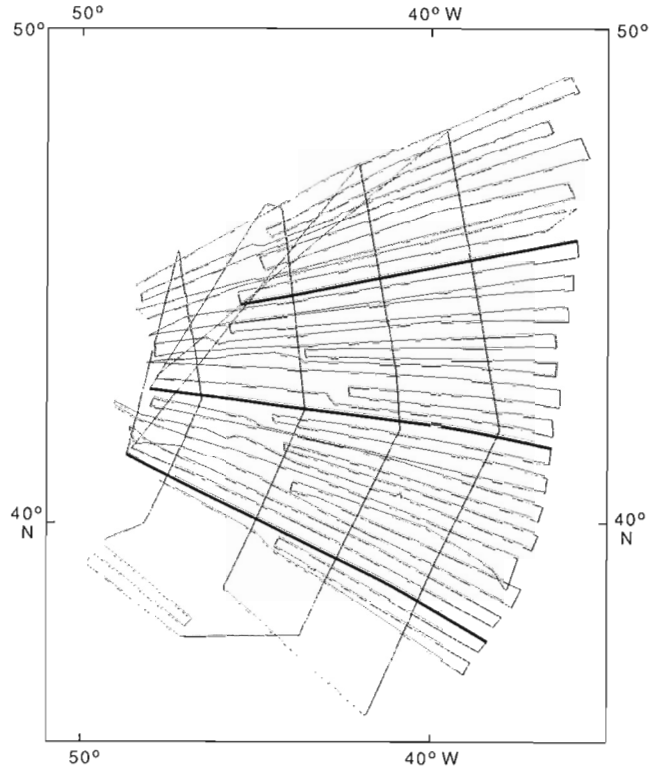

Figure 5. Example of interactive selection on a graphics terminal: the index and retrieval system has identified and displayed the flight lines from an aeromagnetic survey that meets selection criteria within a specified area. From these the operator has selected three track segments, which are highlighted and which will be subsequently retrieved from off-line storage in a batch operation.

example given by Macnab et al (1987). Corrective action can take several forms, including interactive editing on graphics workstations, level adjustments, and specialized procedures, e.g. decorrugation in selected areas.

At this stage, each data set should be clean and internally self-consistent. Some kinds of errors, e.g. failures of the IGRF to model adequately the time-varying components of the magnetic field, may only become evident when the data sets are being merged. Depending on the type of problem, the above corrections may be re-applied, or a different treatment may be necessary.

THE ON-LINE INDEX

The data base accumulated for the compilation project is far too voluminous for affordable on-line storage. At an early stage of the project, it was accordingly decided that all data sets would be stored off line, but that an on-line indexing or cataloguing system would be implemented for rapid searches in the data base and for semi-automated retrieval of data subsets selected according to various criteria, e.g. entire cruises or aeromagnetic surveys, observations within defined geographic limits, specific profiles, individual points, etc.

The on-line index consists of software and two disc files containing summary information that is sufficient to describe the data base for purposes of selecting and retrieving profile data (Fig. 3). The first file is organized as an ORACLE data base, and holds the headers for all data sets; this is accessed through modules of ORACLE software.

The second index file is written in a standard binary format, and holds decimated navigation information for all data sets, along with codes that identify type and availability of observations; this is accessed through custom-built programs. The decimated navigation consists of critical locations necessary to reconstitute the major features of a given ship's track or aircraft flight line: start of line, significant course and speed changes, end of line, and presence or absence of data points (Fig. 4). The decimation algorithm can typically achieve a compression ratio of a hundred to one, and was adapted from an algorithm that was originally implemented in house to accelerate the plotting of coastline data.

DATA RETRIEVAL

Extracting profile information from the data base is a three-step process (Fig. 3):

1. (Interactive) With appropriate search parameters, scan the header records that are stored in the ORACLE data base,

and identify those that meet selection requirements. Two procedure files are automatically created: the first for retrieving the corresponding positions in the decimated navigation file; the second for recovering the selected data sets from off-line storage.

2. (Interactive) Invoke the first procedure file on a graphics terminal to create a track or flight line plot that indicates the data distribution in the area corresponding to the selected data set(s). This step is optional and need not be followed if the user wishes to retrieve all data in the area: its main utility is for the user who wants to select only certain profiles out of the retrieval set, as shown in Figure 5.

3. (Batch) Invoke the second procedure file, which specifies which tape(s) to mount and which file(s) to read, in order to retrieve the desired data. The product of this step is a disc file that contains the required data.

INDEXING AND RETRIEVING GRIDDED AND OTHER FORMS OF DATA

The foregoing has described procedures implemented specifically for profile data, i.e. time series of observations along ship tracks, or fiducial observations along aircraft flight lines. Comparable functions are now being developed for data archived in grid form. The basic design of the index and retrieval scheme is flexible enough that it can be expanded and adapted to handle other forms of geographically referenced data, such as depths to seismically reflective layers, multibeam bathymetry, and digital sidescan data.

REFERENCES

ETOPO5
1986: Relief map of the Earth's surface; EOS, Transactions of the American Geophysical Union, v. 67, p. 121.

Geological Survey of Canada
1987: Magnetic Anomaly Map of Canada, Fifth Edition; Geological Survey of Canada, Map 1255A, scale 1:5 000 000.

Haxby, W.F.
1987: A portrayal of gridded geophysical data derived from SEASAT radar altimeter measurements of the shape of the ocean surface; National Geophysical Data Center, Boulder, Colorado, Report GG-3, 1 sheet.

Macnab, R., Verhoef, J., and Srivastava, S.P.
1990: A compilation of magnetic data from the Arctic and North Atlantic oceans; *in* Current Research, Part D, Geological Survey of Canada, Paper 90-1D.

Macnab, R., Verhoef, J., and Woodside, J.
1987: Techniques for the display and editing of marine potential field data; *in* Current Research, Part A, Geological Survey of Canada, Paper 87-1A, p. 865-875.

Verhoef, J. and Macnab, R.
1987: Magnetic data over the continental margin of eastern Canada: preparation of a data base and construction of a 1:5 million magnetic anomaly map; Geological Survey of Canada, Open File 1504, 95 p.

Predicting geographic variations in indoor radon using airborne gamma-ray spectrometry

P.J. Doyle[1], R.L. Grasty, and B.W. Charbonneau
Mineral Resources Division

Doyle, P.J., Grasty, R.L., and Charbonneau, B.W., Predicting geographic variations in indoor radon using airborne gamma-ray spectrometry; in Current Research, Part A, Geological Survey of Canada, Paper 90-1A, p. 27-32, 1990.

Abstract

Published airborne gamma-ray measurements of equivalent ground concentrations of uranium (eU_A) were used to select two communities in Quebec with contrasting radiometric environments for comparison of their indoor radon levels. The communities studied were Maniwaki (eU_A up to 2.4 ppm) and Ste-Agathe (<1 ppm eU_A). Data from a detailed airborne survey were used to further subdivide Maniwaki into "uraniferous" (> 2 ppm eU_A) and background (<2 ppm eU_A) areas. Indoor radon concentrations were measured over a five month period (January-May, 1988) in each community.

Trends for indoor radon essentially parallel those in the eU_A data. Thus lowest mean radon concentrations are associated with Ste-Agathe homes (first floors 10 Bq/m^3; basements 19 Bq/m^3), intermediate with those in the Maniwaki background area (first floors 31 Bq/m^3; basements 43 Bq/m^3) and highest with those in the "uraniferous" areas of Maniwaki (first floors 43 Bq/m^3; basements 91 Bq/m^3).

Results of this study suggest that both regional and detailed airborne gamma ray data are useful in predicting geographic variations in domestic radon exposure.

Résumé

On a utilisé des mesures publiées de concentrations d'équivalents au sol d'uranium (eU_A) établies par levés aériens des rayons gamma, pour choisir deux collectivités du Québec dont les environnements radiométriques contrastent, afin de comparer leur niveau de radon dans les intérieurs - Maniwaki (eU_A atteignant 2,4 ppm) et Sainte-Agathe (eU_A<1 ppm). Des données provenant d'un levé aérien détaillé ont été utilisées pour subdiviser Maniwaki en zones « uranifères » (≥2 ppm eU_A) et en zones de bruit de fond (<2 ppm eU_A). Les concentrations de radon dans les intérieurs ont été mesurées sur une période de cinq mois (de janvier à mai 1988) dans chaque collectivité.

Les tendances caractérisant le radon dans les intérieurs sont parallèles à celles des données d'eU_A. Ainsi, les concentrations moyennes de radon les plus faibles sont associées à des maisons de Sainte-Agathe (premiers étages, 10 Bq/m^3; sous-sols, 19 Bq/m^3), les concentrations intermédiaires à celles de la zone de bruit de fond de Maniwaki (premiers étages, 31 Bq/m^3; sous-sols, 43 Bq/m^3) et les plus élevées à celles des zones « uranifères » de Maniwaki (premiers étages, 43 Bq/m^3; sous-sols, 91 Bq/m^3).

Les résultats de cette étude semblent indiquer que les données des levés aériens des rayons gamma, de nature aussi bien régionale que détaillées, sont utiles dans la prévision des variations géographiques de l'exposition au radon domestique.

1 5-1939 Carling Ave, Ottawa, Ontario, K2A 1B9

INTRODUCTION

Surficial soil and rock are generally considered to be the major sources of indoor radon. The soil and rock properties that control indoor radon levels are the soil permeability and a source strength term, such as the radon release rate, which is dependent on the uranium concentration and emanation power of the rock or soil (Eaton and Scott, 1984).

The association between areas of elevated airborne gamma ray activity and enhanced average indoor radon levels has been reported by workers in the United States (Duval, 1989) and Sweden (Akerblom and Wilson, 1982). Recently, a large study by the New Jersey Department of Environmental Protection also found good correlation between indoor radon and airborne gamma-ray measurements (K.W. Muessig, pers. comm., 1987).

In Canada, earlier work by Taniguchi and Vasudev (1980), revealed that homes in the vicinity of a strong uranium anomaly were not necessarily characterized by elevated levels of radon decay products. However, the anomalous area was small, and because of the region's rural character, the study included very few homes. On the other hand, Wagner (1983) found that homes within uranium-enriched (>1 ppm eU_A) areas of northern Saskatchewan, defined on the basis of the Geological Survey of Canada's regional eU_A maps, were characterized by radon daughter activities over fourfold higher than those for homes from background (<1 ppm eU_A) areas.

This paper describes the results of a detailed study that examines the value of airborne equivalent uranium data (eU_A) in identifying potential radon problem areas. In addition, the importance of radon emanation rates of rocks and soils in controlling indoor radon levels was also assessed.

Two communuties in southwestern Quebec with differing geological and radioactive environments were selected for study on the basis of published gamma-ray data for the Mount Laurier map sheet. This regional survey had been flown with a 5 km line spacing, and was published at a scale of 1:250 000 (Geological Survey of Canada, 1979). The two communities selected, Maniwaki and Ste-Agathe (Fig. 1), are similar in size with populations of 5 000 - 10 000. Maniwaki was associated with an eU_A anomaly of 2.4 ppm, and Ste-Agathe with an area of low (<1 ppm) eU_A. Since preliminary field studies indicated that uranium-rich rocks occur only locally in the Maniwaki area, a detailed airborne gamma-ray survey (line spacing 100-200 m) was undertaken in late 1987 (Geological Survey of Canada, 1988). The resultant eU_A data were used to define "uraniferous" (≥ 2 ppm eU_A) areas and a background (<2 ppm eU_A) area within the town.

DESCRIPTION OF AREAS

Ste-Agathe

The town of Ste-Agathe is located on a large anorthosite complex (Baer et al., 1971) of low radioactivity. The area studied is underlain principally by brown-weathering, massive anorthosite and gabbro. This rock is typically medium- to coarse-grained, very dark grey pyroxene leucogabbro, containing 15 % clinopyroxene, 1-2 % magnetite, 1-2 % amphibole, and almost 80 % plagioclase feldspar. Bedrock is typically overlain by one or more metres of noncalcareous glacial till, which is in turn locally covered by deposits of medium grained alluvial sand. Texturally, the till is composed mostly of fine red-brown sand. Both the till and alluvial deposits are relatively permeable.

Maniwaki area

The town of Maniwaki is underlain by both uranium- and thorium-enriched pegmatite and granite, and radioelement-poor gneiss and marble (Wilson, 1924). A relatively large body of pegmatite-granite underlies the northeastern portion of the rocky promontory in the central part of the town. Elsewhere, this unit occurs mostly as small irregular masses within the gneiss and marble.

The radioactive rocks are typically composed of 40 % microcline, 20 % plagioclase, 15 % quartz, up to 20 % dark green clinopyroxene, and trace amounts of biotite and magnetite. Radioactive minerals readily identifiable on autoradiographs are zircon, sphene, and small yellow grains of thorite. Most of the uranium and thorium in these rocks is associated with the thorite (mineral identification courtesy of G.M. LeCheminant, Geological Survey of Canada).

Three major soil parent materials are recognized within the town; glacial till, laminated silty clay, and silty alluvium. The till is generally quite thin, but where significant thicknesses do occur, it was observed to be composed of relatively permeable, poorly sorted materials, including large numbers of predominantly gneissic rock fragments. The lacustrine clay and silty alluvium are typically a metre or more thick. Like the till, the alluvium is structureless and relatively permeable. The clay, on the other hand, is comparatively impermeable despite a locally blocky structure due to fracturing.

A contour map based on eU_A data from the Geological Survey of Canada's detailed airborne gamma-ray survey of the town of Maniwaki is presented in Figure 2. Shaded areas, characterized by eU_A values of 2 ppm or more, were defined as "uraniferous". The large shaded region in the

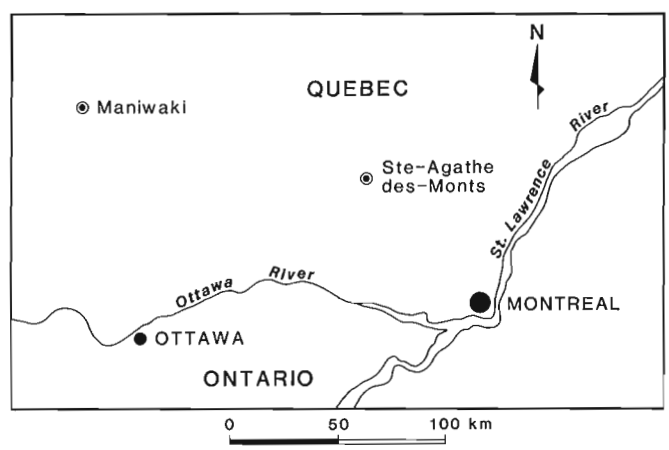

Figure 1. Location of Maniwaki and Ste-Agathe study areas.

centre of the map outlines approximately the rocky promontory mentioned previously. The 3.0 ppm contour is centred on the main body of radioelement-rich pegmatite-granite.

METHODS

Selection and description of homes

In Maniwaki, a total of 115 homes were selected for study — 35 in the "uraniferous" areas and 80 in the background area. In Ste-Agathe, 80 homes were selected. No particular criteria were used to limit home eligibility, although in general an attempt was made to select detached dwellings with basements. Information on house features that could influence indoor radon levels — such as the presence or absence of a basement, type of building materials, and age of structure — was noted.

Measurement of indoor radon

Alpha track dosemeters were used to estimate domestic radon exposure. The dosemeters were supplied and the track densities subsequently measured by the Environmental Radiation Hazards Division of Health and Welfare Canada. The method has been described in detail by McGregor et al. (1987). These detectors were installed in both first floor living areas and basements in January 1988 in Maniwaki, and in early February 1988 in Ste-Agathe. They were retrieved about five months later. Results of replicate measurements indicated that at low concentrations (<150 Bq/m^3, typical of about 90% of sites investigated in this study), the alpha track method was relatively imprecise (precision ±94%, at the 95% confidence level). At higher concentrations (150-800 Bq/m^3) however, precision is considerably improved (±23%, at 95% confidence level).

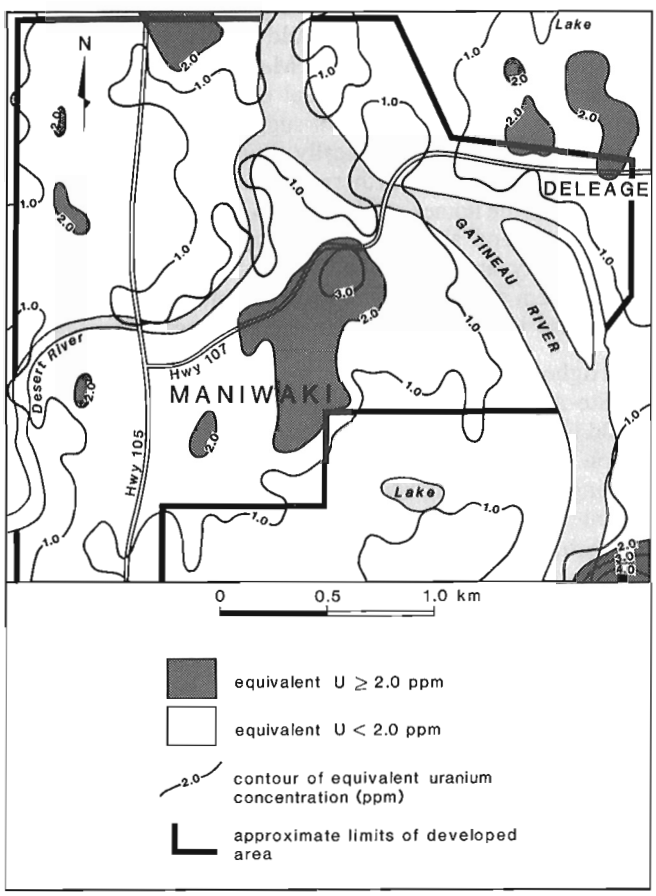

Figure 2. Contour map of eU_A data, Maniwaki area, as determined by the detailed airborne gamma-ray survey (Geological Survey of Canada, 1988).

Soil and rock investigations

Initially a Geometrics Model GRS-101 scintillometer and soil probe (capable of taking 2 cm diameter cores down to depths of 1 m) were used to evaluate the general nature of surficial geological materials around a home. This information was used to locate appropriate sites for more detailed study. Generally only one soil site was evaluated in detail at each property. Ideally the site was between about 3 and 15 m from the house and was representative of soil thought to be at the foundation level of the home. Where scintillometer readings indicated the presence of a radiometric anomaly near the home, the site was generally chosen to be at least partially representative of the radioelement-rich area.

After an appropriate soil site was chosen, a McPhar Spectra 44D portable gamma-ray spectrometer was used to measure the "in situ" equivalent uranium (eU_G) content of the surface materials. Also, at every house in Maniwaki and at every third house in Ste-Agathe, a 100-300 g soil sample was obtained, typically from depths of 60-75 cm. This material was used for subsequent radon emanation rate measurements. Finally, if bedrock outcropped near the home, additional gamma-ray spectrometer readings and samples for radon emanation rate measurement were taken at these rock exposures.

Measurement of radon emanation rates

Radon emanation rates (RnE) for soil and rock samples were measured using an alpha track procedure similar to that described by McCorkell et al. (1981). 100 g of air dried soil or 50 g of ground (less than 100 mesh) rock material were sealed in plastic bags (which were permeable to radon, but impermeable to thoron) and placed in 250 mL glass jars. Cellulose nitrate detectors were then affixed to the underside of jar covers and the jars were sealed for up to two months. After etching detectors in 2.5 M NaOH, track densities were determined visually using a microscope. The relationship between track density and RnE was determined by applying the same procedure to Certified Reference Materials with known radon emanation rates (McCorkell, 1986). Analytical precision, estimated from duplicate analyses, was approximately ±15% at the 95% confidence level.

RESULTS

As shown in Table 1, mean eU_G and RnE values for Ste-Agathe rock and soil are typically considerably below those for Maniwaki. Furthermore, highest overall means are generally associated with "uraniferous" areas, and inter-

Table 1. Comparison of surficial equivalent uranium (eU_G) and radon emanation rate (RnE) measurements for rock and soil near Maniwaki and Ste-Agathe homes.

Material	Parameter	Statistic*	Maniwaki		Ste-Agathe
			Uraniferous Areas	Background Area	
Rock	eU_G (ppm)	GM	2.40	2.51	0.14
		GD	2.7	3.5	3.8
		Max	17.0	19.5	0.4
		N	23	13	4
	RnE (Bq/g/s)	GM	8.71×10^{-9}	4.47×10^{-9}	1.51×10^{-9}
		GD	3.2	2.7	1.3
		Max	8.91×10^{-8}	3.09×10^{-8}	2.24×10^{-9}
		N	20	11	4
Soil	eU_G (ppm)	GM	1.17	0.74	0.62
		GD	2.1	1.6	1.6
		Max	8.4	3.2	1.3
		N	32	78	78
	RnE (Bq/g/s)	GM	2.09×10^{-8}	1.32×10^{-8}	3.39×10^{-9}
		GD	2.7	1.6	1.5
		Max	2.69×10^{-7}	7.49×10^{-8}	7.76×10^{-9}
		N	31	79	27

* GM = geometric mean, GD = geometric deviation, Max = maximum value observed, N = number of observations.

Table 2. Summary of indoor radon data for Maniwaki and Ste-Agathe.

Area of home	Statistic*	Indoor Radon		
		Maniwaki		Ste-Agathe
		Uraniferous Areas	Background Area	
First Floors	GM (Bq/m^3)	43	31	10
	GD (Bq/m^3)	4.3	3.6	4.1
	Max (Bq/m^3)	813	550	87
	N (total)	35	70	70
	N > 800 Bq/m^3	2(6%)	0	0
	N > 150 Bq/m^3	7(20%)	6(9%)	0
Basements	GM (Bq/m^3)	91	43	19
	GD (Bq/m^3)	2.3	3.1	3.5
	Max (Bq/m^3)	380	708	116
	N (total)	20	70	69
	N > 800 Bq/m^3	0	0	0
	N > 150 Bq/m^3	7(35%)	6(9%)	0

* GM = geometric mean, GD = geometric deviation, Max = maximum value observed, N = number of measurements (N (total) is usually less than the total number of homes visited because, not all homes had accessible basements and first floor areas, and some of the radon detectors deployed were not successfully retrieved; the value in brackets = % of corresponding N (total)).

mediate values with the background area of Maniwaki. Since these trends are consistent with those for both the regional and detailed eU_A maps, it is concluded that eU_A patterns do reflect differences in source strength of surficial geological materials. Similar findings have been reported recently by Duval (1989).

Table 1 shows that in Maniwaki, the mean eU_G for the rock material in the "uraniferous" areas is slightly lower than that for the background area. This is attributable to the fact that much of the southwestern half of the large "uraniferous" region in the centre of Figure 2 (where the majority of the "uraniferous" homes are located) is underlain by nonradioactive gneiss and marble, which only locally includes masses of uranium-rich pegmatite-granite. The high mean eU_G value for Ste-Agathe soil (0.62 ppm) relative to that for rock (0.14 ppm) can be explained, at least in part, by glacially transported granitic and gneissic boulders which were observed to be intermixed in the predominantly basic Ste-Agathe till.

Radon levels for first floors and basements in Maniwaki and Ste-Agathe are compared in Table 2. Trends in these data are consistent with those in Table 1, in that the lowest means are associated with the Ste-Agathe homes, intermediate with those in the Maniwaki background area, and highest with those in the "uraniferous" areas of Maniwaki. Comparing the numbers of homes with >150 Bq/m^3 indoor radon, none were found in Ste-Agathe, whereas 9% of homes in the background area and 20-35% (depending upon whether first floor or basement data are considered) of those in the "uraniferous" areas of Maniwaki had values above 150 Bq/m^3. Concentrations in excess of 800 Bq/m^3, the Federal Government guideline, were detected in only two homes, both located within the "uraniferous" part of Maniwaki.

DISCUSSION

A variety of factors, such as soil permeability and differences in house construction could be responsible for the enhanced indoor radon levels in Maniwaki relative to those for Ste-Agathe. However, visual examination of surficial deposits in the two communities suggests that the permeability of Maniwaki soils is typically similar to or less than that of Ste-Agathe soils. Furthermore, the construction styles and ages of the homes selected in Maniwaki and Ste-Agathe were in general similar. Consequently, differences in the radioactivity and emanation rates of local rock and soil would seem to be the factors responsible for the observed difference in indoor radon levels in the two towns.

Higher mean indoor radon levels in Maniwaki compared to Ste-Agathe indicate that 1:250 000 scale eU_A maps could be of value in predicting regional variations in indoor radon levels. Care however, must be exercised when interpreting the local significance of regional eU_A data. Thus despite the fact that Maniwaki is associated with a radiometric high, because of the limited distribution of uranium-rich rock and overburden, only a small fraction of the homes in the town are actually built on this material. As a result, the absolute magnitudes of the mean indoor radon concentrations for Maniwaki were considerably lower than originally expected, and values of over 800 Bq/m^3 (the Federal Government guideline) were found in the living areas of only 2 of the 115 Maniwaki homes tested.

Equivalent uranium data from the detailed aerial survey, on the other hand, appear to be much more useful in describing local source strength. Thus, as shown in Figure 2, only a small percentage of the town of Maniwaki is indicated to be "uraniferous" ($eU_A \geq 2$ ppm), and within this anomalous area RnE rates for both rock and soil, and soil eU_G values are all typically elevated (Table 1). Care however

must be exercised in interpreting even this detailed map. For example, as noted previously, detailed field studies revealed that much of the southwestern half of the large "uraniferous" area in Figure 2 is in fact underlain by nonradioactive gneiss and marble, which only locally includes masses of uranium-rich pegmatite-granite. Thus a relatively large percentage of the homes investigated in the "uraniferous" areas were actually built on uranium-poor bedrock and not anomalous granite-pegmatite. As a result the observed contrast in source strength between "uraniferous" and background areas is somewhat less than was originally expected.

The elevated indoor radon levels found in the "uraniferous" areas in Maniwaki are believed to be mainly attributable to elevated radon release rates for rock and soil in these areas. As shown elsewhere (unpublished report submitted to the Exploration Geophysics Subdivision, Geological Survey of Canada by P.J. Doyle, 1989), variations in soil permeability appear to have little effect on indoor radon distribution patterns in Maniwaki. The influence of variations in construction style, however, cannot be ruled out. Because of the proximity of bedrock to the surface throughout most of the "uraniferous" areas, a high proportion (40 %) of the homes sampled had crawl spaces — which were open to the ground below and were generally well sealed during the winter months — instead of basements. Since only about 5 % of the homes in the background area had crawl spaces, the higher indoor radon levels in the "uraniferous" areas (Table 2) could also be a partial consequence of structural differences in the homes selected.

The association between areas of elevated airborne gamma-ray activity and enhanced average indoor radon levels noted in this study, has also been found recently in a large study of approximately 5 700 homes in New Jersey by the New Jersey Department of Environmental Protection (K.W. Muessig, pers. comm., 1987). In this study it was found that in areas with eU_A values >2.1 ppm over 30 % of the homes had radon levels greater than 150 Bq/m^3 indoor radon, and in the 3.5-6.0 ppm eU_A range, an average of 40 % to 60 % of the homes had levels greater than 150 Bq/m^3. These results are consistent with those reported in this study, since as noted in Table 2, in the "uraniferous" parts of Maniwaki (≥ 2.0 ppm eU_A) 20 % of the first floor areas and 35 % of the basements sampled were characterized by radon levels above 150 Bq/m^3.

Although in the areas studied, variations in soil permeability appear to have had very little effect on observed indoor radon distribution patterns, this situation cannot be assumed elsewhere. Grasty (1989), for example, has attributed high indoor radon levels in Winnipeg in part to fracturing of glacial lake clays, and consequent enhancement of local soil permeability. Similarly Duval (1989), citing studies in the U.S. Pacific Northwest, has concluded that although aerial gamma-ray data can be useful in identifying potential radon problem areas, information on soil permeability must also be considered.

CONCLUSION

Results of this study suggest that both regional and local variations in indoor radon can be predicted using airborne gamma-ray survey data. On a regional scale, use could be made of the Geological Survey of Canada's 1:250 000 scale equivalent uranium maps. Maps of this type are currently available for large portions of Canada. On a local scale, for example in comparing areas within communities, detailed airborne gamma-ray surveys could be undertaken. Other factors being equal, areas characterized by higher eU_A values would be expected to have, on average, higher indoor radon levels. However, available information on local bedrock and surficial geology — and in particular soil permeability — should also be consulted when interpreting the significance of airborne gamma-ray data.

ACKNOWLEDGMENTS

Financial support for this project was provided by the Science and Professional Services Directorate of Supply and Services Canada (Contract #23233-7-1372/01-SS), along with the Exploration Geophysics Subdivision of the Geological Survey of Canada. The Environmental Radiation Hazards Division of Health and Welfare Canada supplied the alpha track detectors for measuring indoor radon. The Mineral Sciences Laboratories of the Canada Centre for Mineral and Energy Technology (CANMET) provided the laboratory space and equipment necessary for the radon emanation measurements. Special thanks are extended to R.H. McCorkell of CANMET who generously made his extensive experience in the alpha track method available to the authors, and to Robert Phillips who provided valuable assistance in the field component of the work. Finally, the authors wish to thank the many individuals in both Maniwaki and Ste-Agathe who kindly volunteered to cooperate in this investigation.

REFERENCES

Akerblom, G. and Wilson, C.
1982: Radon — geological aspects of an environmental problem; Geological Survey of Sweden, Rapporter och meddelanden, nr. 30, 47 p.

Baer, A.J., Poole, W.H., and Sanford, B.V.
1971: Rivière Gatineau. Geological Survey of Canada Map 1334A.

Duval, J.S.
1989: Indoor radon prediction using gamma ray spectrometric data; Eos, v. 70, no.15, p. 496 (abstract).

Eaton, R.S. and Scott, A.G.
1984: Understanding radon transport into houses; Radiation Protection Dosimetry, v. 7, nos. 1-4, p. 251-253.

Geological Survey of Canada
1979: Airborne gamma ray contour maps, Mount Laurier, Quebec; Geological Survey of Canada, Geophysics Series 36031G.
1988: Airborne geophysical survey, 1987, Maniwaki area, Quebec; Geological Survey of Canada, Open File 1729.

Grasty, R.L.
1989: The relationship of geology and gamma-ray spectrometry to radon in homes; Eos, v. 70, no. 15, p. 496 (abstract).

McCorkell, R.H.
1986: Radon emanation rate studies: interlaboratory standard reference materials and the effects of powdering and pelletizing; Canadian Institute of Mining and Metallurgy Bulletin, v. 79, no. 894, p. 66-69.

McCorkell, R.H., Archaumbault, G., and Brameld, M.P.
1981: Laboratory apparatus for measuring radon emanation from solids; Canadian Institute of Mining and Metallurgy Bulletin, v. 74, no. 833, p. 90-96.

McGregor, R.G., Walker, W.B., and Eaton, R.S.
1987: Experiences in the development of a CR-39 alpha track dosemeter for radon; *presented at* "Indoor Radon II", Specialty Conference, Air Pollution Control Association, Cherry Hill, New Jersey, April 6-10, 1987.

Taniguchi, H. and Vasudev, P.
1980: Radon and radon daughters due to natural uranium occurrences in a rural Ontario community; *in* The Natural Radiation Environment III, Proceedings of the 3rd International Conference on the Natural Radiation Environment, edited by T.F. Gesell and W.M. Louder, Technical Information Center, U.S. Department of Energy, Springfield, Virginia, p. 1623-1633.

Wagner, E.P.
1983: Radon monitoring in northern communities; Chronic Disease in Canada, v. 4, no. 1, p. 6-7.

Wilson, M.E.
1924: Arnprior-Quyon and Maniwaki areas, Ontario and Quebec; Geological Survey of Canada, Memoir 136, 152 p.

Observations on gold deposits in North China Platform

K.H. Poulsen[1], B.E. Taylor[1], F. Robert[1], and J.K. Mortensen[2]

Poulsen, K.H., Taylor, B.E., Robert, F., and Mortensen, J.K., Observations on gold deposits in North China Platform; in Current Research, Part A, Geological Survey of Canada, Paper 90-1A, p. 33-44, 1990.

Abstract

North China Platform contains many significant gold deposits that are concentrated within basement uplifts, such as Liaoxi and Jiaodong, in which Archean gneisses and Phanerozoic granitoid rocks occur in equal proportion. Many of the gold deposits are hosted by Archean rocks, but their restriction to late brittle faults, the local zoning of ore minerals about plutons, and their associated hydrothermal alteration suggest that they have a greater genetic affinity with Mesozoic magmatism than with Archean processes.

Résumé

La plateforme de la Chine septentrionale renferme plusieurs gîtes d'or importants, concentrés dans les soulèvements du socle, comme ceux de Liaoxi et Jiaodong, occupés par des proportions égales de gneiss archéens et des roches granitoïdes phanérozoïques. Plusieurs des gîtes d'or sont encaissés dans des roches archéennes, mais leur occurrence dans des failles cassantes tardives, de même qu'une zonalité métallique autour des plutons et que l'altération hydrothermale associée, suggèrent une relation génétique avec le magmatisme mésozoïque plutôt qu'avec des processus archéens.

[1] Mineral Resources Division
[2] Continental Geoscience Division

INTRODUCTION

North China Platform (NCP) is composed of an Archean/Early Proterozoic metamorphic basement that is typically covered by middle Proterozoic through Tertiary sedimentary and volcanic rocks. NCP also contains substantial volumes of granitoid rocks, most of which are of Mesozoic age and are presumably the products of eastward-driven subduction beneath the Asian continental margin (Fig. 1). Gold deposits that account for an estimated 20 percent of China's annual production are concentrated where windows of the metamorphic basement rocks are exposed in NCP. Most Chinese geologists regard this relationship between uplifts of Precambrian metamorphic rocks and gold to favour genesis of the deposits from Precambrian source beds, either by remobilization of existing Precambrian deposits or by extraction of gold from geochemically enriched source rocks of the amphibolite facies during younger hydrothermal events (Qin Nai et al., 1988). There is nonetheless an increasing awareness of the importance of Mesozoic magmatic activity as a focusing mechanism for many deposits (see for example, Guo Wenkui, 1989).

The authors spent five weeks in 1989 examining gold deposits in the Liaoxi Uplift near the border between Liaoning Province and Inner Mongolia Autonomous Region and in the Jiaodong Uplift in the eastern part of Shangdong Province (Fig. 1). The fieldwork was carried out under the guidance of Chinese colleagues Lin Baoqin, Shen Ershu, and Zhang Lidong of the Shenyang Institute of Geology and Mineral Resources and Shang Ling of the Liaoning Bureau of Geology and Mineral Resources. The study represents the second phase of a co-operative gold project under the terms of the Canada-China Memorandum of Understanding 1985-1990 (Poulsen et al., 1989). This report summarizes the authors' observations and represents a preliminary geological assessment of the gold deposits from a Canadian perspective.

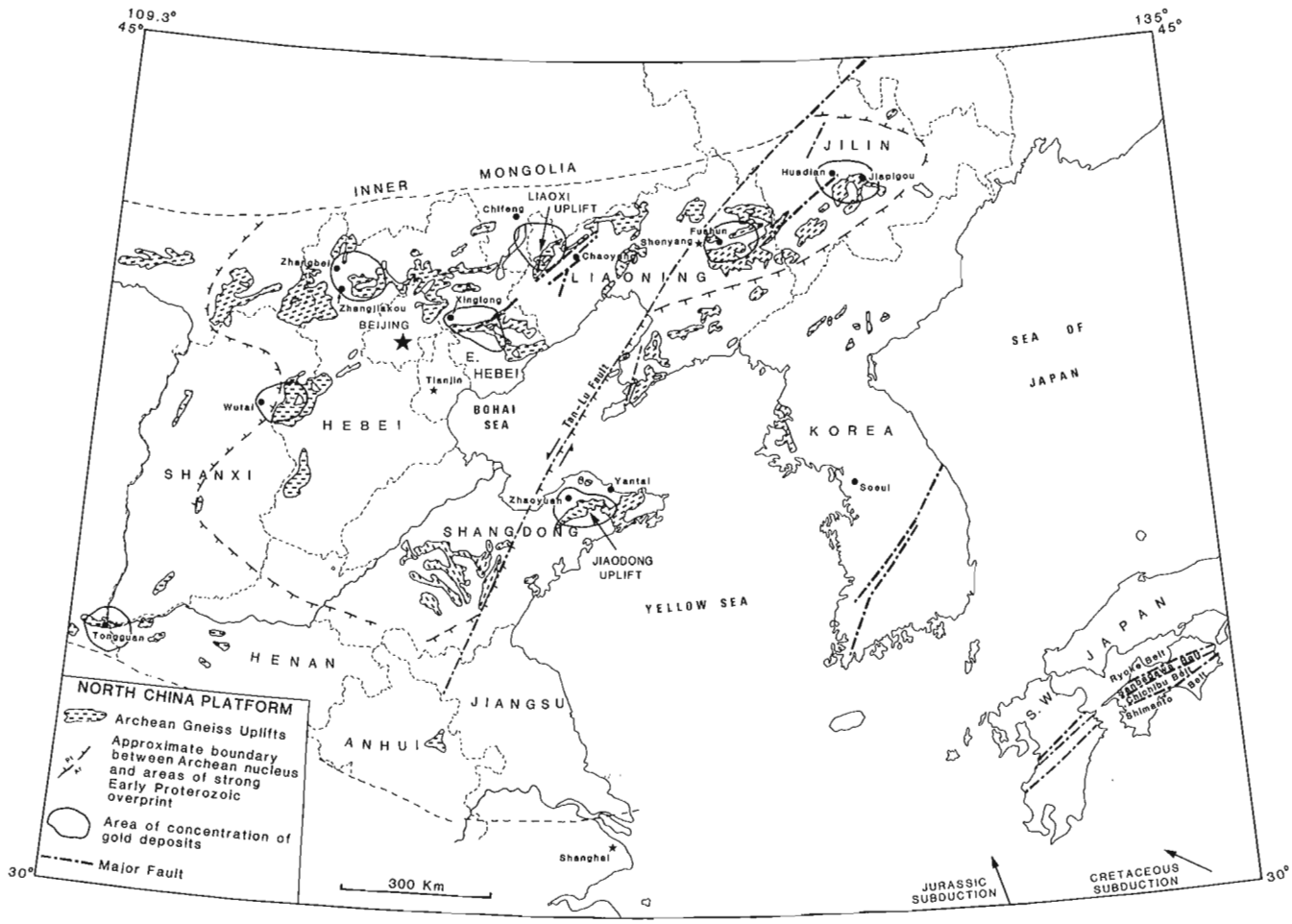

Figure 1. Geological map of North China Platform showing the distribution of Precambrian uplifts and areas of concentation of gold deposits. Adapted from Sheet 11 of the Geological Map of Asia (Anonymous, 1975) compiled by the Chinese Academy of Geological Sciences.

THE UPLIFTS

Liaoxi Uplift

The Liaoxi Uplift (Fig. 2) covers an area of approximately 1500 km^2 along the border of Liaoning Province and Inner Mongolia Autonomous Region and is one of a series of uplifts that compose the Nei Mongol Axis.

The inner part of the uplift is dominated lithologically by Archean gneisses and Mesozoic granitoid rocks. The Archean rocks are predominantly plagioclase-biotite-hornblende gneisses with subordinate amounts of amphibolite, feldspar megacrystic orthogneiss, granitic pegmatite, metapyroxenite, and laterally extensive sheets of quartz-magnetite rocks which appear to be metamorphosed oxide facies iron formations. Apart from the iron formations, which are mined on a small scale for iron ore, there is little preserved evidence to reveal the original protoliths of the gneisses. In most cases amphibolites appear to be metamorphosed mafic dykes. Hornblendite and metapyroxenite typically occur in lenticular masses, one to two kilometres in diameter, that may also represent metamorphosed intrusions. Granitic rocks of Phanerozoic age are approximately as abundant as Archean rocks in the Liaoxi Uplift. On existing geological maps they are subdivided into a number of suites, of which three are predominant (Fig. 2). The largest masses (γ4 on Chinese maps) are typically 25 to 50 km in diameter and are composed of relatively homogeneous, coarse grained, weakly foliated quartz monzonite. These bodies are commonly assigned a Hercynian age, although geochronological constraints are lacking. Smaller masses, 10 to 25 km in diameter and composed of granite and quartz monzonite, occur as scattered bodies that define the central axis of the uplift. The smallest plutons, 1 to 10 km across, are composed principally of medium grained granodiorite, diorite, and quartz monzonite and are locally porphyritic. The last two categories of intrusions are locally designated as ηo and γ5 on Chinese geological maps and are typically assigned a Mesozoic (Yanshanian) age. Jurassic and Lower Cretaceous cover rocks occur in the interior of the uplift, but are most abundant on its flanks. In both situations these cover rocks are predominantly terrestrial sandstones and subaerial volcanic flows, breccia, and tuff. There are two notable features in the disposition of the cover rocks. First of all, on the flanks of the uplift they overlie a two kilometre thick sequence of Sinian (Late Proterozoic) quartzite and dolomite that is absent from the interior of the uplift, whereas similar Mesozoic cover rocks rest directly on Precambrian basement in the interior of the uplift. Secondly, the Mesozoic sedimentary and volcanic rocks in both cases, like the Sinian, everywhere dip moderately to steeply despite the absence of penetrative deformation and recognizable metamorphism. These observations suggest that the uplift was established prior to, or during, Mesozoic magmatism and that uplift and tilting were achieved by fault-block rotation.

A number of elements contribute to the overall structure of the uplift. One of these, the northeasterly striking Beipaio-Chengde Fault, is a zone of fault gouge and breccia up to 10 m wide that, like its northern counterpart, the Chifeng Fault, is a reverse fault that establishes the limits of exposure of the Archean gneisses as well as the structural grain of the uplift as a whole (Fig. 1). The long axes of many of the Mesozoic granitoid bodies also are parallel to this trend, as is the mean strike of gneissosity in the Archean rocks. Numerous northeasterly- and northwesterly striking faults are transverse to this structural trend, the most prominent member of the northeasterly set having a sinistral offset of 25 km (Fig. 2). All of these structural elements are compatible with north-northwesterly compression across the uplift.

Jiaodong Uplift

The Jiaodong Uplift occupies the central part of the Shangdong Peninsula (Fig. 1). The western part of the uplift (Fig. 3) is marked by the Tan-Lu Fault, a major sinistral strike-slip structure that transects NCP. In this area the uplift is 50 km wide.

Precambrian schists and gneisses compose approximately 50 percent of the exposure in the uplift and these consist primarily of Archean rocks of the Jiaodong Group. Primary features in these metamorphic rocks are better preserved than those in the rocks of the Liaoxi Uplift and indicate that the Jiaodong Group is composed mainly of biotite schist of metasedimentary origin, with minor amphibolite representing metamorphosed dykes. Some of the metamorphic rocks in Jiaodong Uplift are reported to be biotite gneiss and metamorphosed granite of Early Proterozoic age, but they are not present near the main gold district and were not examined.

The Mesozoic granitoid rocks of this uplift occur mainly in a single batholithic complex comprising the voluminous biotite quartz monzonite of the Linglong Phase and the younger potassium-feldspar-porphyritic biotite-hornblende granodiorite of the Guojialing Phase. The Linglong Phase is commonly described as "migmatite", but this designation appears to be based on the presence of abundant xenoliths of schist and gneiss near its contacts with the Precambrian rocks. Small stocks of mid-Mesozoic (Yanshanian) granodiorite and granite occur throughout the uplift and compose the youngest granitoid phase. Mesozoic volcanic and sedimentary rocks occur on the flanks of the uplift but these were not examined.

The structure of the uplift is defined primarily by the notrheast axis of the Linglong and Guojialing granitoid rocks, by the east-northeast distribution of, and strike of foliation within, the Precambrian schists and gneisses, and by a set of north-northeast brittle faults that are parallel to the Tan-Lu Fault. Older faults such as the Zaoping and Jiaojia faults follow a sinuous course but strike, on average, east-northeast, whereas a younger set strikes northwest (Fig. 3).

GEOLOGICAL SETTING OF GOLD

Gold deposits are distributed throughout the central core of both uplifts (Fig. 2, and 3). The authors had the opportunity to examine and study eight gold deposits that included six small to medium sized mines in the Jinchanggouliang-Erdaogou, Xiaotazigou-Dongwujia, and Saijingou areas of Liaoxi Uplift and two large gold deposits in the Linglong and Jiaojia areas of Zhaoyuan gold district in the Jiaodong Uplift.

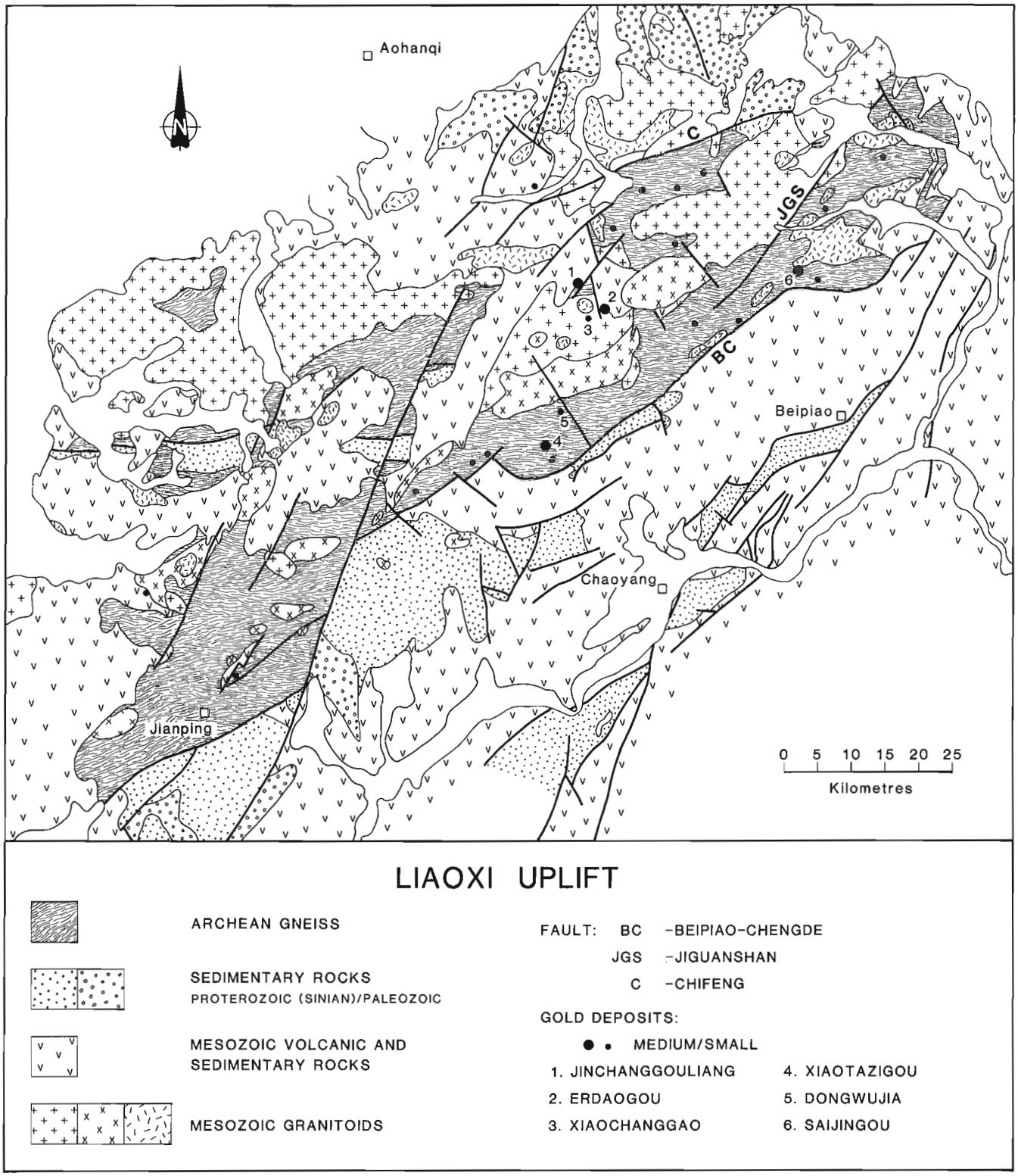

Figure 2. Geology and gold deposits of Liaoxi Uplift. Adapted from an unpublished 1:500 000 compilation map. Deposit locations by Lin Baoqin.

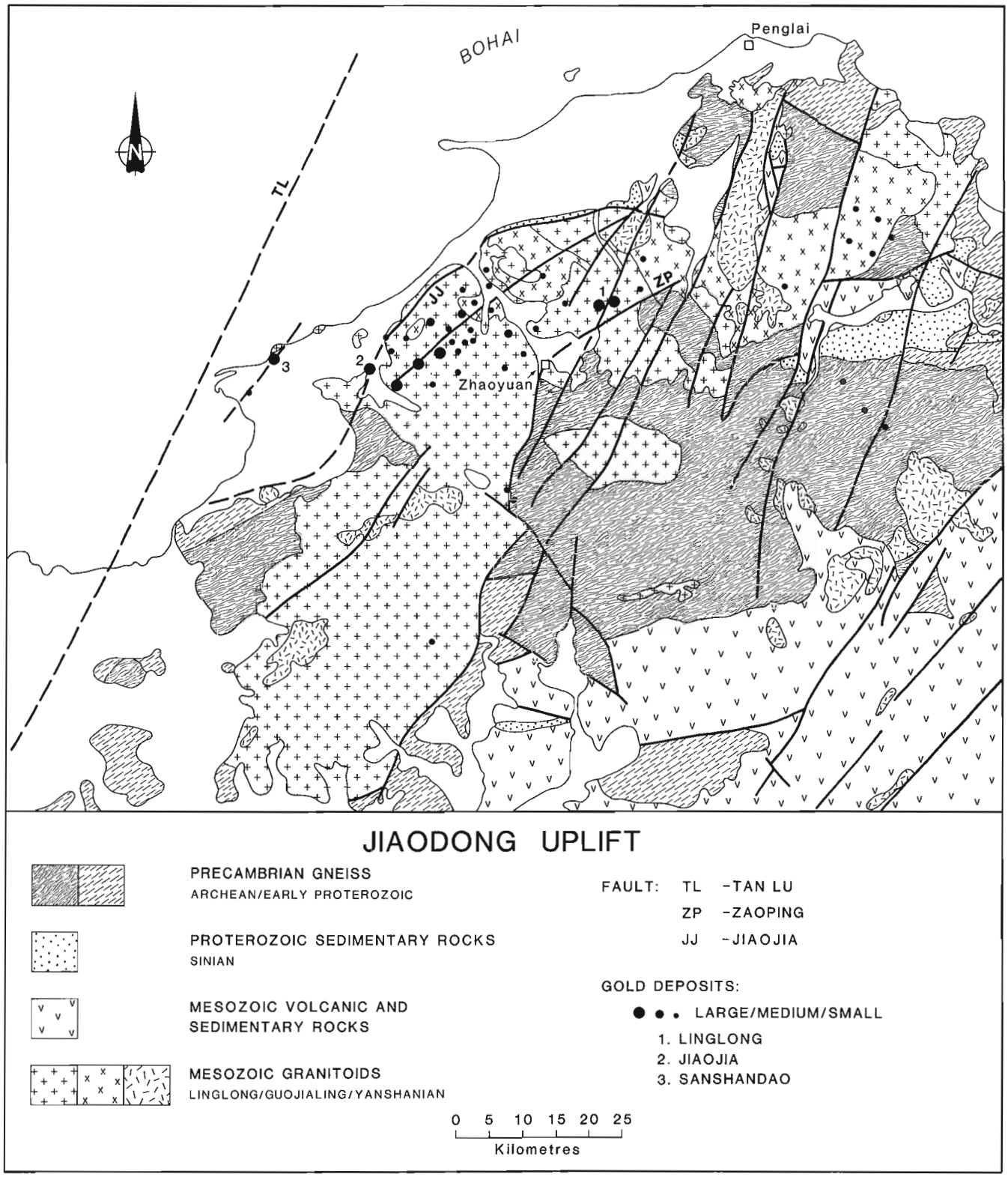

Figure 3. Geology and gold deposits of Jiaodong Uplift. After an unpublished compilation map by No. 6 Geological Team of Shandong Province.

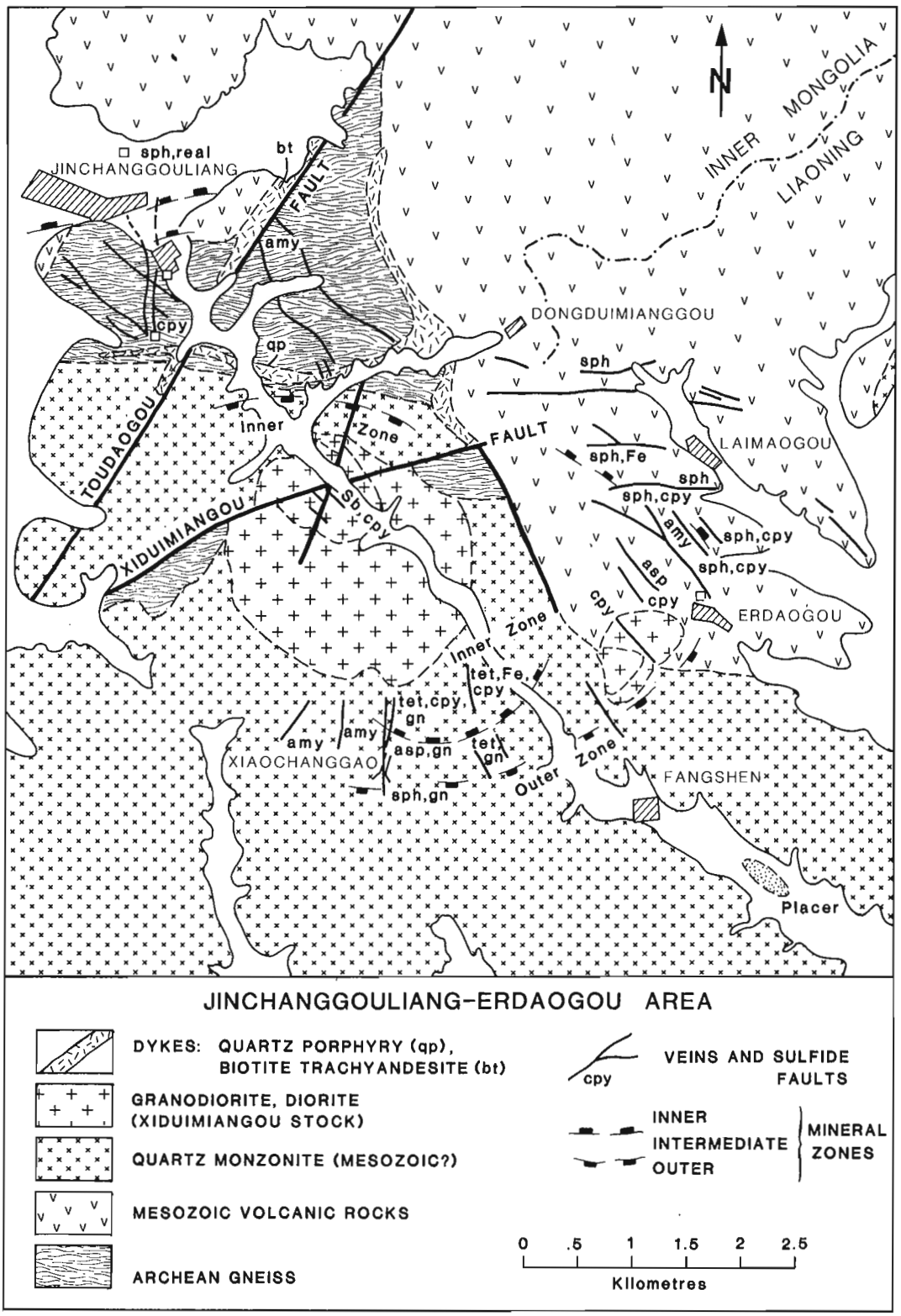

Figure 4. Map of the geology and gold veins in the Jinchanggouliang-Erdaogou area showing the boundaries of mineral zones. Mineral abbreviations are amy (amethyst), Fl (fluorite), tet (tetrahedrite), cpy (chalcopyrite), asp (arsenopyrite), sph (sphalerite), gn (galena), sb (stibnite), and real (realgar).

Jinchanggouliang-Erdaogou area

The gold deposits of this district (Fig. 4) are centred around the Xiduimiangou Stock, a zoned pluton with a margin of equigranular granodiorite and a core of porphyritic quartz monzonite which has a reported K-Ar feldspar age of 126 Ma. The stock intrudes Archean gneiss and a large mass of medium- to coarse-grained quartz monzonite. In the eastern part of the area, a sequence of Jurassic rhyolitic to andesitic flows, tuff, and breccia, with intercalated immature sandstone, dips moderately to steeply east-northeast, away from the gneissic and granitoid rocks. The contact between the volcanic rocks and the gneissic and granitoid rocks is everywhere occupied by faults and small intrusions, but local conglomerate within the volcanic sequence contains abundant boulders of gneiss. A small stock of granodiorite to diorite at the Erdaogou Mine cuts both the volcanic rocks and the large quartz monzonite mass. Dykes, which have a wide range in composition from diorite and porphyritic rhyolite to dacite and biotite trachyte, are ubiquitous throughout the area, and most commonly strike north to northwest. A "T-shaped" dyke east of Jinchanggouliang (Fig. 4) is notable because it varies along strike from homogeneous quartz-phyric rhyolite, to flow-banded rhyolite, to a breccia of porphyritic rhyolite fragments in an aphanitic matrix, and thus likely is, in part, a pebble dyke. Although they show complex crosscutting relationships with one another, the dykes collectively represent the youngest magmatic activity in the area in that they were observed to cut all other rock units including the Xiduimiangou Stock. The dykes are cut by the numerous faults in the area, but in many cases occupy the same structural sites as faults, including those faults that host veins.

The **Jinchanggouliang** deposit occurs in Archean gneiss within the hanging wall of the northerly dipping Toudaogou

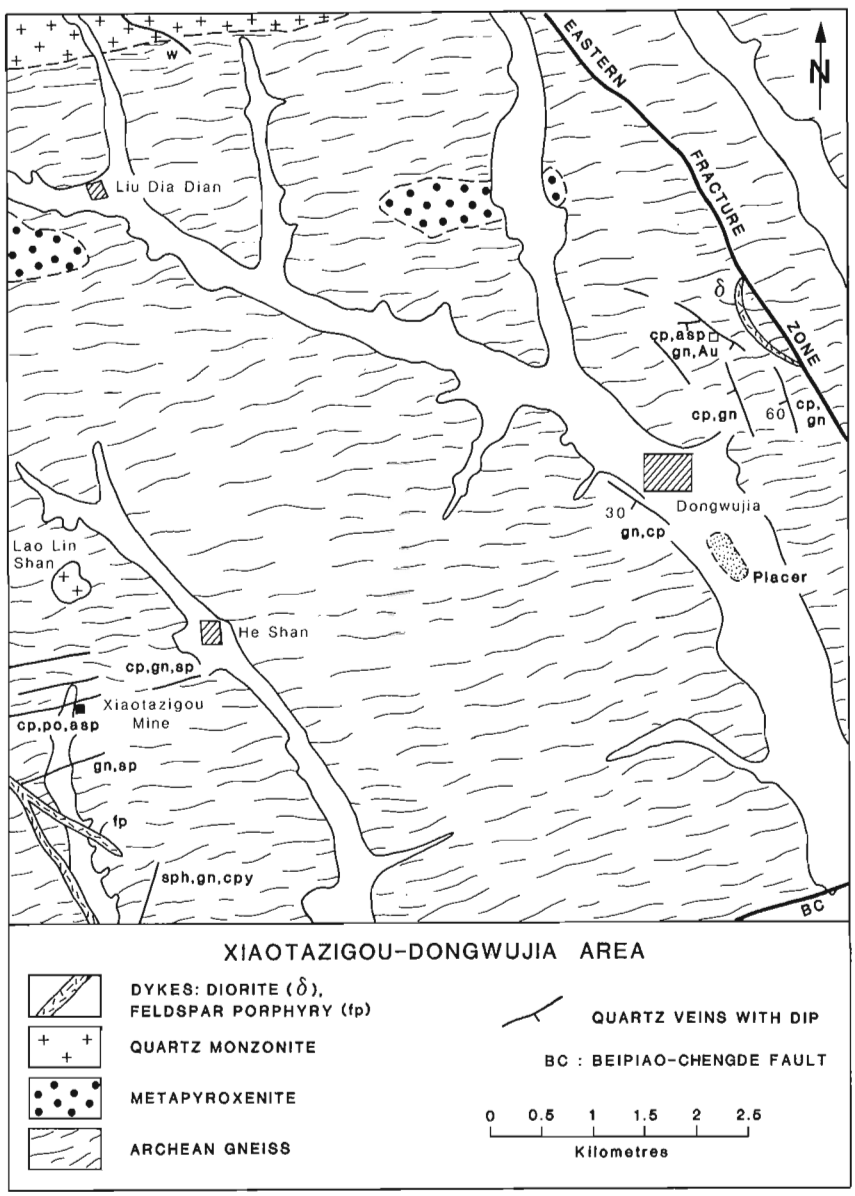

Figure 5. Map of the geology and gold veins in the Xiaotazigou-Dongwujia area. Mineral abbreviations as in Figure 4 with the inclusion of po (pyrrhotite) and W (wolframite).

Fault (Fig. 4). The orebodies occur in faults that cut across the gneissic grain of the Archean rocks and that locally offset Mesozoic dykes. Numerous individual orebodies have been mined over a vertical interval of 300 m. The **Erdaogou** deposit is hosted by faults cutting flow-banded rhyolite, diorite dykes, and a granodiorite stock (Fig. 4). The orebodies are being mined over a vertical interval of 200 m. The **Xiaochanggao** deposit is hosted by a large mass of equigranular quartz monzonite (Fig. 4) but, in detail, the orebodies occur in faults that are approximately parallel to, but that also cut, dykes composed of diorite and porphyritic andesite. The largest orebody within this deposit is 800 m long and 300 m deep.

Xiaotazigou-Dongwujia area

The Xiaotazigou and Dongwujia deposits are located seven kilometres apart in an area dominated by Archean gneisses of the Xiaotazigou Formation (Fig. 5). Narrow stratiform magnetite iron formation units are prominent in this area and are generally parallel to the dominant east-northeast gneissosity. Mesozoic intrusions include a small stock, the Lao Lin Shan pluton, of quartz monzonite composition, numerous dykes composed of diorite and porphyritic dacite, and a large mass of quartz monzonite that flanks the area on the north.

Quartz veins that cut this quartz monzonite body, as well as Archean gneiss (Fig. 5), contain wolframite and molybdenite and are sites of small-scale tungsten mines. The gold deposits occur to the north of the Beipiao-Chengde Fault and to the west of the Eastern Fracture Zone (Fig.5) in minor faults that are parallel to both of these major structures. The **Xiaotazigou** deposit consists of an array of quartz vein that are parallel to faults composed of gouge. The chalcopyrite-arsenopyrite-pyrrhotite-gold ore is typically located in the gouge zones rather than the adjacent ribboned quartz veins. The **Dongwujia** deposit contains ribboned quartz veins as much as three metres wide. Gold occurs in the veins within shoots containing high concentrations of chalcopyrite and galena, and in sulphide-rich gouge and breccia adjacent to veins. The largest orebody is 300 m long and 200 m deep.

Saijingou area

At Saijingou (Fig. 2), an extensive quartz vein system is hosted by an apophysis of a granodiorite-diorite stock that has intruded Archean gneiss. The apophysis is composed mainly of diorite that contains abundant gneissic xenoliths and that is cut by an amygdaloidal breccia dyke, 250 m wide, and by numerous dykes of aplite. The **Saijingou** deposit is centred on a northwesterly striking, northeasterly dipping fault zone. Arrays of northwesterly and easterly dipping quartz veins containing gold and minor sulphides extend up to one kilometre away from the fault into its footwall rocks. However, most production has come from veins that are in the immediate hanging wall of the fault and parallel to it.

Linglong Area

This area (Fig. 6) is underlain entirely by the Linglong Phase biotite quartz monzonite which is cut by a swarm of

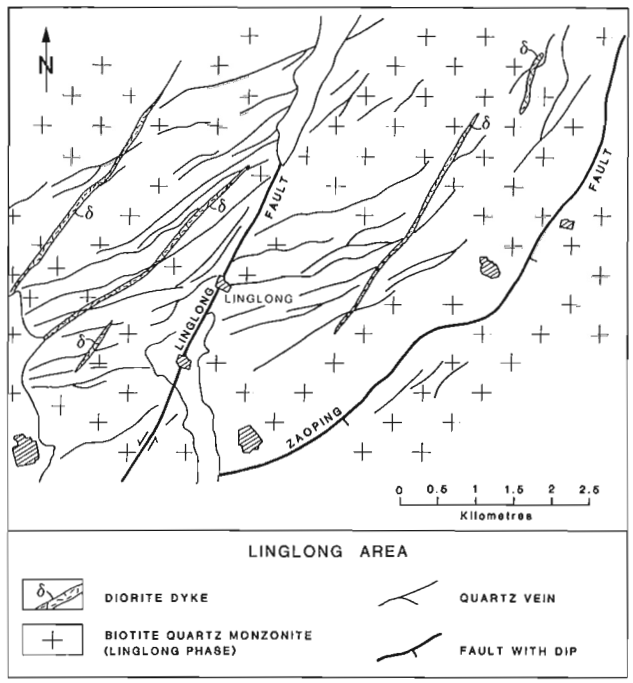

Figure 6. Map of the geology and gold veins in the Linglong area. From map by Li Shi Xian (pers. comm., 1989).

northeast-striking diorite and lamprophyre dykes. More than 100 quartz veins, ranging from 10 cm to 5 m wide, dip steeply north-northwest and occur in the footwall of the southeast-dipping Zaoping Fault (Fig. 6). The veins and dykes are offset 30 m sinistrally by the Linglong Fault.

At the **Linglong** deposit, there are two centres of production, Linglong and Lingshan. Gold is mined over a vertical interval of 400 m and is known to extend to 1000 m below surface. Ore from upper elevations is of quartz vein type, whereas non-vein disseminated ore (''alteration-type'' or ''Jiaojia-type'') occurs at greater depth. The Zaoping Fault is mineralized with Jiaojia-type ore at depth, and individual vein structures, depending on vertical position, may contain barren quartz grading downward to quartz vein ore and ultimately to Jiaojia-type ore.

Jiaojia area

The Jiaojia area (Fig. 7) is underlain in part by granitoid rocks of the Linglong Phase, and these are cut by a stock composed of Guojialing Phase granodiorite with feldspar phenocrysts up to 10 cm long. Archean gneisses occupy the hanging wall of the northwesterly dipping Jiaojia Fault, a sinuous zone of fault gouge, up to three metres wide, that merges with several smaller splay faults.

The **Jiaojia** deposit, the largest of six of this type in the area, occurs within the footwall of the Jiaojia Fault. It is composed of Jiaojia-type ore, disseminated pyrite, gold, and minor base metals in a sericitized cataclastic matrix of Linglong Phase quartz monzonite. The deposits are composed of several en echelon lenses adjacent and parallel to the Jiaojia Fault. The largest lens is 1300 m long and is, on average, four metres wide, although locally it is as wide as

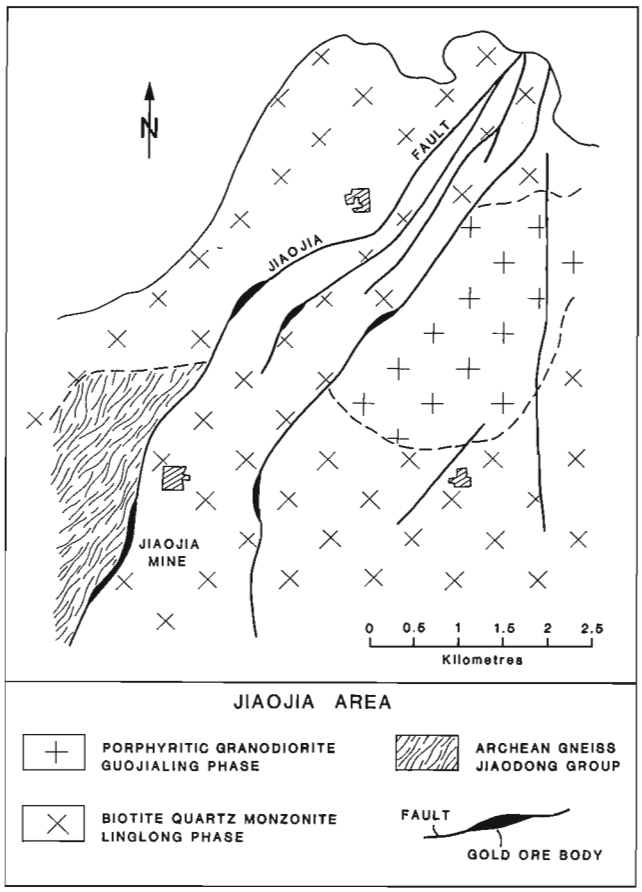

Figure 7. Map of the geology and gold deposits in the Jiaojia area. From map by Li Shi Xian (pers. comm., 1989).

30 m. Farther from the fault, lenses contain increasing amounts of vein quartz.

CHARACTERISTICS OF THE OREBODIES

All of the deposits that we examined have points of similarity and difference with regard to their structure, mineralogy, and hydrothermal alteration.

Structure

In all cases, faults are the primary loci for orebodies, of which three structural styles were encountered: i) fault gouge, vuggy veins, hydrothermal breccia; ii) ribbon quartz veins; and iii) cataclastic replacement zones.

At Erdaogou, Jinchanggouliang, Xiaochanggao, Xiaotazigou and Dongwujia much of the ore occurs in veins controlled by sinuous, anastomosed, gouge-rich faults. Although there are many variations, even within a single vein, there are several recurring elements within these structures. Sulphide-rich gouge and fault breccia are the common forms of ore that directly occupy the faults. The veins are not everywhere brecciated, but recemented vein breccia and the presence of vein fragments in gouge indicate fault movement continued in places after vein formation. Striated fault surfaces are abundant and, together with observed offsets on dykes, indicate that most of these faults experienced oblique slip and that some have had more than one direction of slip. In some cases, sulphide veinlets were observed to transect the gouge and breccia, so mineral deposition likely overlapped even with the latest episodes of active faulting. Hydrothermal breccia and quartz-sulphide veinlets are particularly common where gouge zones bifurcate. The veinlets are mainly of extensional type (i.e. are often symmetrical, with mineral growth orthogonal to vein walls), and typically are obligue linking structures between fault strands. Both veinlets and hydrothermal breccias commonly are filled with well formed vuggy crystals of quartz, amethyst, and sulphide minerals; vugs remain in places.

Metre-wide quartz veins were observed at Xiaotazigou, Dongwujia, Saijingou, and Linglong. The veins commonly have a ribbon texture and are composed of massive vitreous quartz with minor sulphide minerals. Where sulphides are abundant, they occupy fractures that cut the quartz. Gouge and cataclasite are well developed along vein margins and appear to have formed after the veins.

The cataclastic ores at Jiaojia and Linglong are fine grained, nonfoliated, dark grey rocks containing disseminated fine grained sulphide minerals and gold. A continuous progression was observed outward, from fine grained ore to less mineralized, sericitized coarse quartz monzonite, to fresh quartz monzonite that is neither altered nor deformed. Given the shape and distribution of the orebodies, it is likely that they represent incipient cataclastic zones that did not develop into faults, but that were favourable loci for fluid movement.

Ore mineralogy

All of the deposits contain the same suite of ore minerals, including electrum, pyrite, and chalcopyrite. Galena and sphalerite are also common but have a more restricted distribution. The content of silver exceeds that of gold at all deposits (7:1 to 1:1), and, although most of the silver is accounted for by electrum, tetrahedrite occurs at some deposits, notably at Xiaochanggao. Rarer ocurrences of ore minerals include arsenopyrite at Xiaotazigou, Xiaochanggao, and Erdaogou, realgar and orpiment at Jinchanggouliang, stibnite in a vein south of Jinchanggouliang, and pyrrhotite at Xiaotazigou.

The type and abundance of the ore minerals were noted to differ from vein to vein in a given district so that the authors and their Chinese colleagues collected data in an attempt to establish whether there were patterns of mineral zoning. This was done most thoroughly in the Jinchanggouliang-Erdaogou area where many veins were examined in underground workings and in surface exposures. Three apparently concentric zones are indicated from this compilation (Fig. 4). An inner Sb-Cu zone is characterized by the presence of tetrahedrite and stibnite and abundant chalcopyrite, an intermediate pyrite zone characterized by sparse base metal content but with common pyrite and local chalcopyrite and arsenopyrite, and an outer Zn zone where sphalerite is particularly abundant and is locally accompanied by realgar and orpiment. Galena is present in all of the zones and fluorite was noted at a few localities in

the inner zone. Gold has been extracted from veins within all of the zones, but it is perhaps significant that most of the productive orebodies at the larger deposits are contained in the intermediate zone. Although not fully established, the zones appear to be centred about the Xiduimiangou granodiorite stock (Fig. 4).

A similar distinction between copper-bearing and zinc-bearing zones can be made in a qualitative way for the Xiaotazigou-Dongwujia area. Here, the main gold orebodies contain abundant chalcopyrite, but veins south of Xiaotazigou mine (Fig. 5) also contain substantial sphalerite.

Attempts to establish whether vertical zoning was also present at these deposits were unsuccessful, mainly due to the limited depth of most workings. Personal communication from mine geologists suggests that some vertical variations do exist. For example, upward increases in gold grade and abundance of base metals were reported for individual veins at Saijingou, Linglong, and Jiaojia.

Hydrothermal alteration

In all of the mines examined, host rocks to veins and breccia zones exhibit evidence of hydrothermal alteration in varying amounts. Hydrothermal alteration was mapped in detail in only a few locations, but could be generally useful in documenting the paleogeothermal systems in which ore was deposited. The alteration mineralogy and its distribution reflect both the chemical composition and permeability of the host rock. The general types of alteration include: i) sericitic alteration (sericitization, silicification, pyritization) in felsic rocks; ii) propylitic alteration (chloritization, carbonatization, pyritization), dominantly in mafic rocks; and iii) argillic alteration, which is primarily present in vein-bearing faults in both rock types. Presumably argillization of wall-rock fragments in (or adjacent to) vein-bearing faults occurred as the geothermal systems in each area cooled; clay gouge may have eventually sealed fluid pathways. Broadly similar mineral assemblages developed in several deposits, although physico-chemical conditions of alteration and mineralization may have differed in detail. Except for an apparent tendency for epidote to occur in rocks where veins contained chalcopyrite at Jinchanggouliang, no obvious variation in alteration mineralogy with sulphide mineralogy was observed. Ore grade, however, seemed to vary directly with the sulphide (especially pyrite) contents of veins and altered wall rocks.

The most striking example of silicification was examined in rhyolite wall rocks at Erdaogou. Here, medium grey zones as wide as two metres were developed around veins, preserving the overall texture of the rhyolitic rocks (welded ash flows, in part). Within the zone of silicification, and for several metres beyond its abrupt limit, 0.5-1.0 mm pyrite cubes constitute about 3 – 5 % of the altered rocks. Silicification of granitic rocks at Jiaojia is also accompanied by pyrite and chalcopyrite in ore. In other mines, silicification was less pronounced, and consisted primarily of closely-spaced veins and/or veinlets of quartz rather than pervasive replacement of groundmass.

Sericitization and pyritization, principal components along with quartz of sericitic alteration, are typically restricted to wall-rock fragments in vein-bearing faults, to vein selvedges, one to several centimetres-thick, or to coatings on vein walls or along fractures through veins. Although developed farther from the vein-bearing faults in the felsic rocks, diorite dykes in Erdaogou and Jinchanggouliang mines were replaced by sericite (+ pyrite) as far as 10 cm away from veins. Where zoning developed (e.g. Erdaogou), pyrite and sericite occur farther from veins than zones of marked silicification. This potassic alteration is also characterized by quartz plus potassium feldspar farther from vein centres in the Jiaojia deposit.

Chloritization of wall rocks, and the occurrence of chlorite as a vein mineral, is predominant at Jinchanggouliang where wall rocks (largely amphibolites, and biotite-hornblende schists) contain abundant mafic minerals. Pyrite and calcite, and, locally, epidote (+chalcopyrite) accompany the chlorite. In rocks of intermediate composition, chlorite is found with sericite.

Calcite accompanied the alteration of mafic and intermediate rocks, and locally constitutes the sole vein mineral in subsidiary veinlets adjacent to the principal vein-bearing faults. Pervasive carbonatization of mafic dykes that occupy vein-bearing faults was noted at both Erdaogou and Jinchanggouliang, and local ferroan dolomite was noted as an alteration mineral at Dongwujia and Saijingou. However, unlike altered rocks adjacent to many mesothermal quartz veins in the Canadian Shield, carbonatization does not appear to predominate over hydration of the rocks.

DISCUSSION

Chinese geologists employ a host rock classification for gold deposits. The deposits described above are therefore thought to be representative of a migmatite type (Jiaojia, Linglong), a granite type (Xiaochanggao, Saijingou), an Archean type (Jinchanggouliang, Xiaotazigou, Dongwujia), and a volcanic type (Erdaogou). However, if we consider all of the characteristics of the deposits, including their relative time of formation, overall distribution, structural style, mineralogical composition, and hydrothermal alteration, we must conclude that all of these deposits belong to a single class transitional in their geological attributes between the conventional epithermal and mesothermal types (Panteleyev, 1986). Furthermore, it seems inescapable that all of the deposits that we examined are of probable magmatic hydrothermal origin. Magmatic heat, volatiles (e.g. H_2O, S, and C), and perhaps metals were added to meteoric geothermal fluids localized by active faults that were eventually sealed by veins. Many of the alteration-, ore-, and vein-forming constituents were probably also redistributed from the sedimentary, volcanic, and plutonic host rocks, and this is a subject of continuing research.

Perhaps the closest North American analogues to the setting of these Chinese deposits examined are presented by those Tertiary deposits in Colorado and New Mexico which are hosted by Precambrian rocks, or for which Precambrian rocks compose the principal basement rocks. These include, among others, deposits in the so-called Colorado Mineral Belt, which extends from Central City in the Colorado Front Range, to the San Juan volcanic field in southwestern Colorado.

In these instances, as for the Chinese deposits, Mesozoic (to Tertiary) gold vein deposits formed about high-level intrusions in uplifts of Precambrian basement. Largely because of their young age, many of the Tertiary deposits are less deeply eroded than those examined in China, and are clearly of epithermal affinity (e.g. Hayba et al., 1986). Consequently, a broad relationship between volcanic rocks and subvolcanic plutons is well illustrated. The earlier volcanic structures (e.g. calderas) have provided conduits for mineralization-related intrusions and circulation of meteoric geothermal fluids (e.g. Lipman et al., 1976). Polymetallic gold vein systems explored in the Lake City caldera, Colorado (see for example, Slack, 1980), reflect a base metal and precious metal zoning generally similar to that discovered in the Jinchanggouliang-Erdaogou area.

The geological setting and style of mineralization, as well as the scale and pattern of mineral zoning encountered in the Jinchanggouliang-Erdaogou area, also compare favourably with several Canadian examples, particularly the Rossland District in British Columbia (Thorpe, 1967; Fyles, 1984). The Blackdome deposit in Southern British Columbia also shares many attributes with the Erdaogou deposit. Both are hosted by gouge-rich faults that cut similar andesite-rhyolite successions. The deposits share a similar mineralogy and 5:1 ratio of silver to gold.

Although many of the Chinese deposits are hosted by Archean rocks, they differ considerably from Archean deposits of the Canadian Shield, particularly by their lack of extensive carbonate alteration, by the relative brittleness of their host structures, and by their relative enrichment of silver relative to gold. Nonetheless, the ribbon quartz veins at the Linglong, Dongwujia, and Saijingou deposits are mesoscopically similar to the veins of greenstone belt deposits with respect to their dimensions, mineralogy, and internal structure.

The "Jiaojia-type" is the most unique of all of the styles of mineralization that the authors examined in China. It is similar in some respects to a type of cataclastic ore that is found at some Abitibi gold deposits (Eldrich in the Rouyn area, McDermott in the Harker-Holloway area). The potential of material of this type (i.e. diseminated gold in mineralized wall rocks) to be ore might easily be overlooked in districts where gold has been traditionally extracted from quartz veins. Furthermore the grade-width-tonnage characteristics of the Jiaojia type deposits are such that they would be viable in the North American economic context.

FUTURE WORK

Geothermal systems leave a marked imprint on host rocks both from the mineralogical and isotopic standpoint. Because of the dominance of surface-derived waters in magmatically-heated geothermal systems, oxygen and hydrogen isotope geochemistry is particularly well suited to the documentation of the extent and temperature of paleogeothermal systems. Samples were collected for the purpose of mapping the shift in $^{18}O/^{16}O$ in wall rocks affected by the heated waters. This should allow detection of higher temperature, higher fluid-flux regions which have been shown in other systems to be associated with areas of higher ore grade (e.g. references in Taylor, 1987). In continental meteoric geothermal systems, wall rocks in such areas are usually characterized by extreme depletion in ^{18}O. Isotopic study of carbon and sulphur in collected samples will allow physicochemical aspects of the mineralizing hydrothermal system(s) to be deduced as well as the extent of mixing between magmatic and nonmagmatic sources of these elements.

The existing geochronological data for NCP are limited and it is therefore difficult to fully evaluate the relationship of gold deposits to the magmatic and structural history of these regions. Suites of samples were collected from the Liaoxi and Jiaodong uplifts during the course of our fieldwork for both geochronological and isotopic tracer studies. This work will be directed toward: i) understanding the magmatic history and age of major structures in each area; ii) establishing the age of gold mineralization; and iii) providing constraints on the genesis of magmas and source(s) of ore fluids. U-Pb, K-Ar, and Ar-Ar dating, and Pb, Sr, and Nd isotopic tracer studies of these samples are in progress.

ACKNOWLEDGMENTS

The authors wish to acknowledge the collaboration of our Chinese colleagues and the warm welcome extended by the Chinese Academy of Geological Sciences and the leaders of the numerous mines that were visited. Our knowledge of the Shandong area was mainly derived from field excursions and information provided by Mr. Li Shi Xian of the No. 6 Geological Team of Shandong and Mr. Qiu Youshou of the Shenyang Institute of Geology and Mineral Resources. R.I. Thorpe provided a careful review of the manuscript.

REFERENCES

Anonymous
1975: Geological Map of Asia; Academy of Geological Sciences of China, Beijing, People's Republic of China.

Fyles, J.T.
1984: Geological setting of the Rossland mining camp; British Columbia Ministry of Energy, Mines and Petroleum Resources, Bulletin 74, 61 p.

Guo Wenkui
1989: Significant geological features of vein gold metallogeny in China; Global Tectonics and Metallogeny, v. 3, p. 91-100.

Hayba, D.O., Bethke, P.M., Heald, P., and Foley, N.K.
1986: Geologic, mineralogic, and geochemical characteristics of volcanic-hosted epithermal precious-metal deposits; Reviews in Economic Geology, v. 2, p. 129-167.

Lipman, P.W., Fisher, F.S., Mehnert, H.H., Naeser, C.W., Luedke, R.G., and Steven, T.A.
1976: Multiple ages of mid-Tertiary mineralization and alteration in the western San Juan Mountains, Colorado; Economic Geology, v. 71, p. 571-588.

Panteleyev, A.
1986: A Canadian Cordilleran model for epithermal gold-silver deposits; Geoscience Canada, v. 13, p. 101-111.

Poulsen, K.H., Brommecker, R., Green, S.B., Baker, K.A., Lin Baoqin, Shang Ling, Shen Ershu, Zhang Lidong, Diamond, L., and Marshall, D.
1989: Contrasts in setting and style of gold deposits in duo Archean terranes: Rice Lake District, Canada, and Western Liaoning District, China; *in* Current Research, Part C, Geological Survey of Canada, Paper 89-1C, p. 121-25.

Qin Nai, Wang Konghai, Pang Qingbang, Qiu Youshou, Mu Ruishen, Yu Changtao, Wei Yongfu, Li Wenkang, and Lu Yingie
1988: Regional metallogenic conditions of main gold deposit types in China; Shenyang Institute of Geology and Mineral Resources Publishing House, 127 p.

Slack, J.S.
1980: Multistage vein ores of the Lake City district, western San Juan mountains, Colorado; Economic Geology, v. 75, p. 963-991.

Taylor, B.E.
1987: Stable isotope geochemistry of ore-forming fluids; Chapter 8: Short Course in Stable Isotope Geochemistry of Low Temperature Fluids, Mineralogical Association of Canada, v. 13, p. 337-445.

Thorpe, R.I.
1967: Mineralogy and zoning of the Rossland area; Ph.D. thesis, University of Wisconsin, Madison, Wisconsin.

The character and some effects of the major magnetic storm of 13-14 March, 1989

J. Hruska, R.L. Coles, H.-L. Lam, and G. Jansen van Beek
Geophysics Division

Hruska, J., Coles, R.L., Lam, H.-L., and Jansen van Beek, G., The character and some effects of the major magnetic storm of 13-14 March, 1989; in Current Research, Part A, Geological Survey of Canada, Paper 90-1A, p. 45-56, 1990.

Abstract

Extensive coverage of the major magnetic storm of 13-14 March was obtained by the thirteen magnetic observatories in Canada. This storm exhibited a diverse morphology. Excursions over 2 000 nT were observed in the subauroral zone and intense Pc5 pulsations with amplitudes of 300 nT were recorded at subauroral and auroral observatories. The impact of this storm in Canada was greater than that of any previous storm. A major electric power blackout occurred in Quebec, and many other power utilities in Canada experienced problems. Large decreases in pipe-to-soil potentials were recorded on pipeline systems, and effects on ionospheric radio communication and on transatlantic communication systems were observed. An analysis of magnetic data around the time of the major power outage shows an equivalent ionospheric current system that changed rapidly in intensity. The timing of the storm was most opportune in strengthening the Canadian forecasting and warning services within the Geological Survey.

Résumé

Les 13 observatoires magnétiques du Canada ont permis d'obtenir une bonne couverture de l'important orage magnétique des 13 et 14 mars. L'orage a fait preuve d'une grande variété de morphologies. Des pointes de plus de 2000 nT ont été observées dans la zone subaurorale et des impulsions Pc5 intenses avec des amplitudes de 300 nT ont été enregistrées dans des observatoires subauroraux et auroraux. La répercussion de cet orage au Canada a été plus grande que celle de tout autre orage antérieur. Au Québec, il y a eu une importante panne d'électricité, et de nombreux services publics d'électricité du Canada ont également éprouvé des ennuis. D'importantes baisses de potentiel des canalisations au sol ont été enregistrées sur les réseaux de pipeline, et des effets ont été observés sur des systèmes de radiocommunication ionosphérique et sur des systèmes de télécommunications transatlantiques. Une analyse des données magnétiques vers l'époque de la grande panne de courant révèle un système de courant ionosphérique équivalent dont l'intensité a changé rapidement. L'orage s'est produit à un moment opportun puisqu'il a permis l'amélioration des services canadiens de prévision et d'alerte au sein de la Commission géologique.

INTRODUCTION

The storm of 13-14 March, 1989 was one of the largest magnetic storms on record. This particular storm was not only a major natural phenomenon, but it has also provided data for many future scientific studies on solar-terrestrial relationships, and has demonstrated the vulnerability of human enterprises to such events. The Working Group on Geomagnetic Applications at the first Solar-Terrestrial Predictions Workshop in Boulder, Colorado in 1979 recommended that communication and co-operation between industry and researchers should be improved so that effects from magnetic disturbances could be prevented, or at least diminished (Campbell et al., 1979). The effects of this major storm have proven to be positive in this sense. The affected industries have realized the value of geophysical research, with the result that co-operation between groups such as ours and relevant companies has been increased. In fact, high resolution data have been provided to us by industry for comparative studies on this topic.

In this paper, we describe briefly the character of the magnetic storm as observed in Canada, followed by short discussions of some of the reported effects on several technological systems.

THE CANADIAN MAGNETIC OBSERVATORY NETWORK

The Canadian Magnetic Observatory Network (Coles et al., 1987) consists of 13 digital observatories (Fig. 1), providing coverage of the three major magnetic regions in Canada, namely, the subauroral (SUB), auroral (AUR), and polar cap (POL) regions. At each observatory, the automatic magnetic observatory system (AMOS III) (Trigg and Nandi, 1984) records magnetic field vector and scalar data at one-minute intervals on cartridge tape. At three stations (Ottawa OTT, Meanook MEA, and Victoria VIC), the magnetic field is also sampled at ten second intervals. All observatories (except Alert ALE and Mould Bay MBC) are automatically interrogated by computer from headquarters in Ottawa every night in order to obtain summary data (hourly means and hourly ranges) and diagnostic information. Although digital data files are routinely produced, special data files for the period including this storm have been prepared.

In this paper, one-minute data, and ten-second data where available, have been used for magnetogram plots and rates of change analyses. Hourly ranges, HRX, of the X(north) component, and their daily mean DRX (Hruska and Coles, 1987; Lam, 1987) have also been used.

CHARACTERISTICS OF THIS STORM

Magnetic activity was high from the beginning of March and reached its peak when the impact of emissions from the active region 5395 on the Sun induced the major storm on March 13-14. This region 5395 produced many X-ray and optically intense flares, rich in particles and in radio emissions, and was clearly the solar source of this geomagnetic storm.

The storm started at 0128 UT on 13 March, 1989 with the sudden commencement seen by all the Canadian subauroral stations MEA, GLN (Glenlea), OTT, STJ (St. John's), and VIC (Fig. 2). After about five hours of moderate fluctuations of the geomagnetic field, the storm intensified at around 0730 UT when a rapid negative excursion was seen at all the subauroral stations (except VIC) and at our most easterly station in the auroral zone, Poste-de-la-Baleine (PBQ). This excursion appeared to progress northward as the northern stations registered its occurrence after

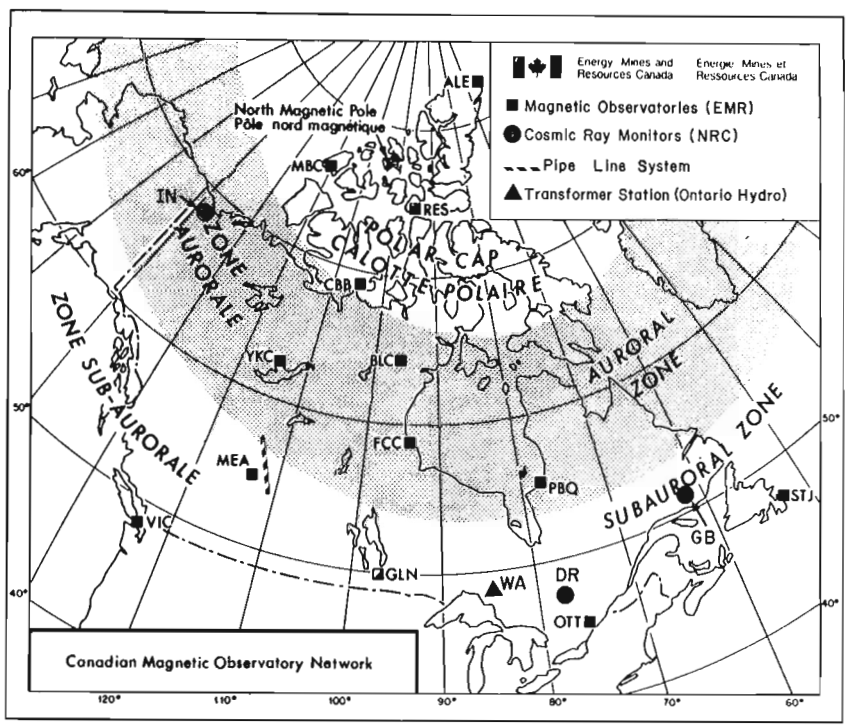

Figure 1. Map of the Canadian Magnetic Observatory Network operated by GSC, Canadian cosmic ray stations operated by NRC, the Ontario Hydro transformer station at Wawa, and the approximate location of the Home Oil Company pipeline system.

0800 UT. This particular excursion attained maximum amplitudes of well over 2 000 nT in MEA and GLN in the subauroral zone but the amplitude fell off to about 1 500 nT at Fort Churchill (FCC) to the north and PBQ to the northeast and about 1 000 nT at OTT to the southeast. Another major negative excursion occurred about three hours later around 1030 UT at the southern stations and later, at about 1100 UT, at the northern stations. This particular excursion reached a maximum amplitude of over 2 000 nT in the subauroral station of MEA, with the amplitude reduced somewhat to about 1 500 nT at the other subauroral stations of GLN and OTT and the auroral stations of FCC and PBQ. However, at Yellowknife (YKC), the western auroral station, the excursion still attained an amplitude of almost 2 000 nT. Thereafter, the field underwent some major fluctuations of lesser amplitudes, although at MEA, between 14-16 UT, there was a sharp negative excursion of 1 500 nT and at OTT, between 22-23 UT, there was another, positive excursion of 1 500 nT. Both excursions were less noticeable at the other stations. Throughout this 13 March, 1989 UT day, the subauroral stations of MEA, GLN, and OTT saw the most intense storm activities.

On 14 March, 1989, the storm appeared to be generally subsiding (Fig. 3), though some intense events did occur. A major negative excursion occurred at OTT and GLN between 01-02 UT with an amplitude of the order of 2 000 nT. Intense substorm activity was registered in the subauroral stations of MEA, GLN, and OTT in the local midnight sector between 06-09 UT while less intense substorm activity was also registered at the auroral stations of FCC and PBQ. As the stations rotated into the morning sector, Pc5 pulsations were recorded in the subauroral stations of MEA and GLN and the auroral stations of FCC and PBQ between 12-17 UT. The Pc5 pulsations were sinusoidal with large amplitudes of about 300 nT and persisted for about five hours. The average frequency was about 2.5 mHz which is within the low frequency portion of the Pc5 spectrum. According to the classification by Lam (in press), these pulsations could be referred to as Pc5A pulsations. Lam and Rostoker (1978) showed that Pc5 activity in the morning sector is colocated with the westward auroral electrojet. Thus, the Pc5 activity observed at the subauroral stations of MEA and GLN was indicative of a southward expansion of the auroral oval into the normal subauroral zone. Furthermore, Lam and Rostoker (1978) showed that Pc5 activity is enhanced in conjunction with a recovery of the electrojet from an interval of significant activity. On that basis, the intense pulsations between 13-15 UT were suggestive of a reconfiguration of the auroral oval that had expanded farther southward during previous stormy times, that is, the relaxation of the magnetosphere from a previously stressed state. Thus, toward the end of this UT day, the storm activity was subsiding in the subauroral zone although some minor positive excursions were still seen at the auroral and polar cap stations.

In the early 1970s a useful technique was developed for studying geomagnetic disturbances by calculating equivalent ionospheric line currents (Loomer and Jansen van Beek, 1971, 1972). The Biot-Savart law was adapted to give the equivalent line current for a magnetic disturbance at a magnetic observatory. These equivalent line currents (e.g. Fig. 4) were not meant to be a definitive analysis of magnetospheric and ionospheric current systems but merely to give an overall view of the storm current activity. Figure 4a gives the positions of the Canadian magnetic observatories used in this analysis. In Figures 4b, 4c, and 4d, the intensity of the line current is represented by the length of the vector, the positive direction of which indicated by the feathered asterisk. An estimate of the distance between the line current and the observatory is given by the straight line joining the midpoint of the current vector and the observatory position as shown by the box symbol. The scale is the same as the map scale. A flat earth is assumed with the current height set at about 110 km.

The outstanding effect of this magnetic storm in Canada was the Hydro-Quebec power outage associated with the large magnetic excursion centered in time at approximately 0800 UT. Consequently, a series of equivalent line current plots were made starting at 0726 UT and ending at 0900 UT. The diagrams in Figures 4b, 4c, and 4d are the most representative plots of this series.

The plots show that a well developed current system existed before the onset of the excursion at 0730 UT (Fig. 4b). The evidence suggests a westward flowing equivalent current which lay between PBQ and OTT, then swung north to flow between YKC and BLC (Baker Lake), and joined the eastwardly directed flow in the polar cap. The GLN, MEA, and VIC vectors indicate another current system to the southwest. As this negative magnetic excursion developed, the equivalent current pattern intensified and expanded in area. From the plots, the most westerly expansion of the system was at 0748 UT (Fig. 4c). At that time, GLN was directly under the current system which then turned northward to the southwest of MEA and to the west of YKC. This pattern then decreased in area except for occasional westward surges and large current intensifications between PBQ/OTT and between FCC/GLN. By 0900 UT, the coherent equivalent current pattern as seen by the Canadian magnetic observatories had collapsed into an apparent random configuration (Fig. 4d).

In summary, the major negative excursion centred in time at 0800 UT was the result of an enhancement of an established ionospheric current system (an unshown plot shows that this pattern existed as early as 0618 UT). This current system did not collapse until 0900 UT at which time short period activity appeared at latitudes of PBQ and farther south.

During this storm, decreases of over 10 percent in the cosmic ray neutron flux were recorded at the monitoring stations operated by the Herzberg Institute of Astrophysics, National Research Council (see Fig. 1 for locations). Normally, such decreases tend to coincide with the sudden commencement, or onset, of a storm (Haurwitz et al., 1965). This storm is interesting because the major decrease in neutron flux did not start at any of the monitoring stations until the magnetic storm reached its main phase. In Figure 5 are shown high resolution data from the Canadian neutron

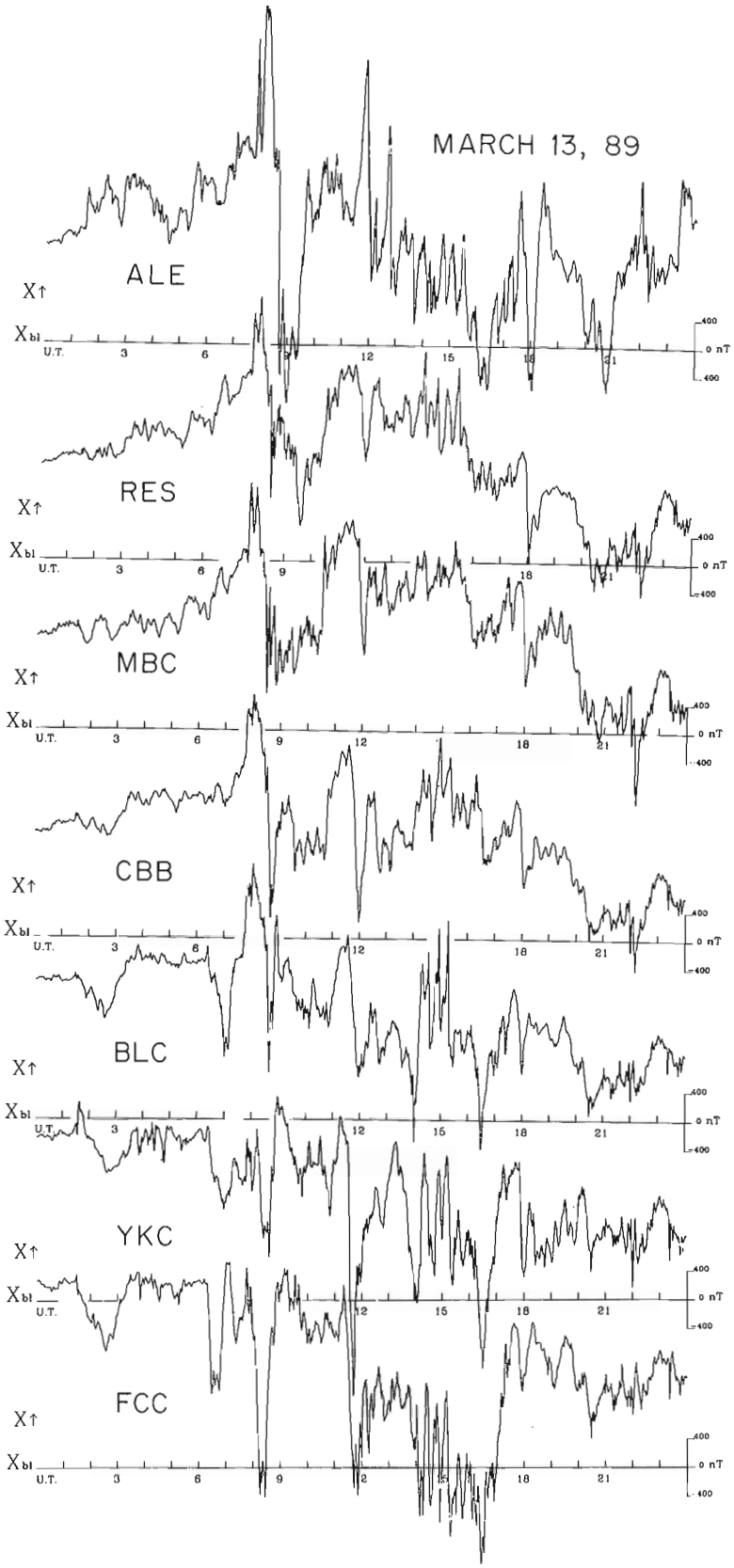

Figure 2. X component (northward) magnetograms from all of the Canadian magnetic observatories arranged in order of geomagnetic latitude for 13 March, 1989. Actual locations are shown in Figure 1.

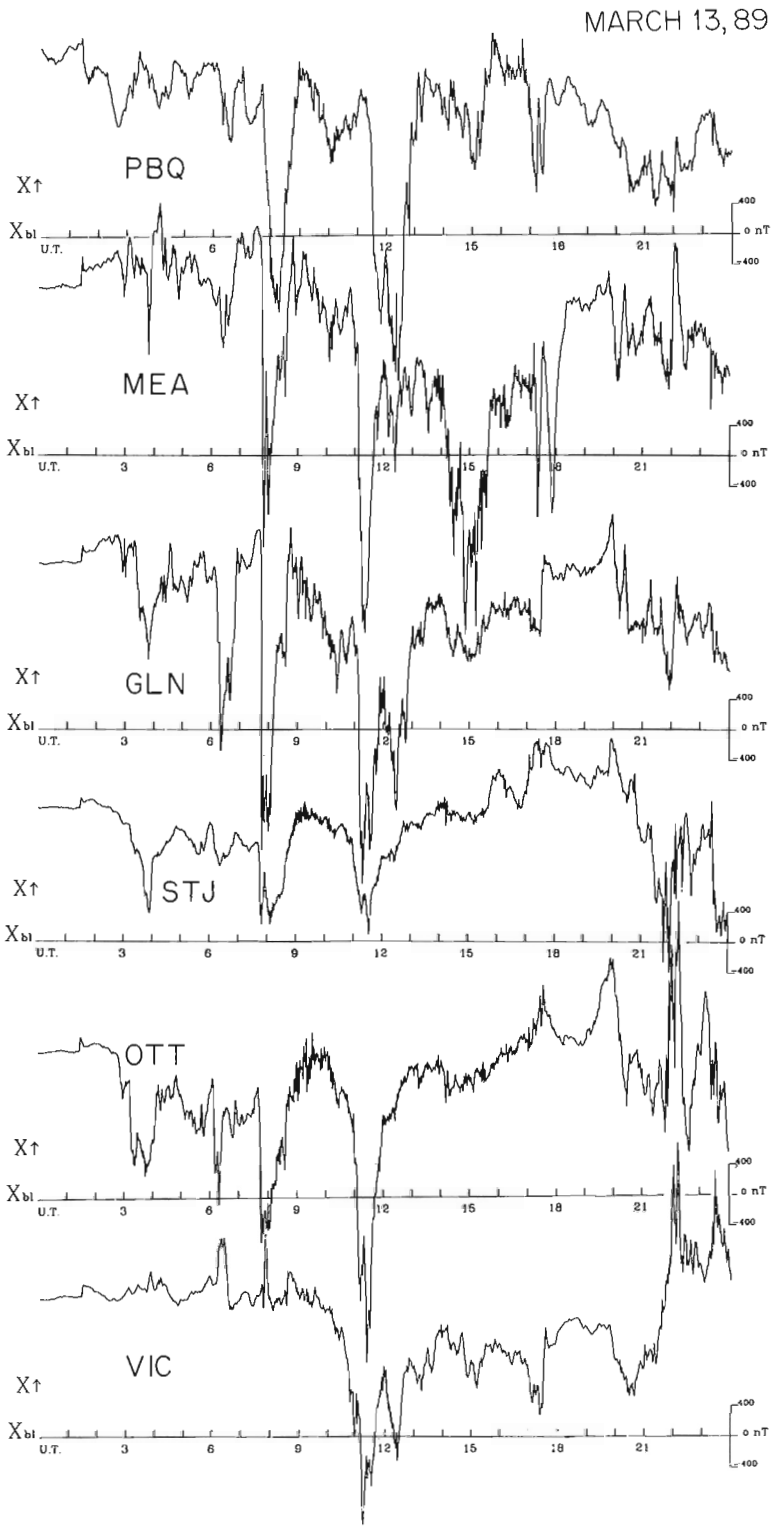

Figure 2. Continued

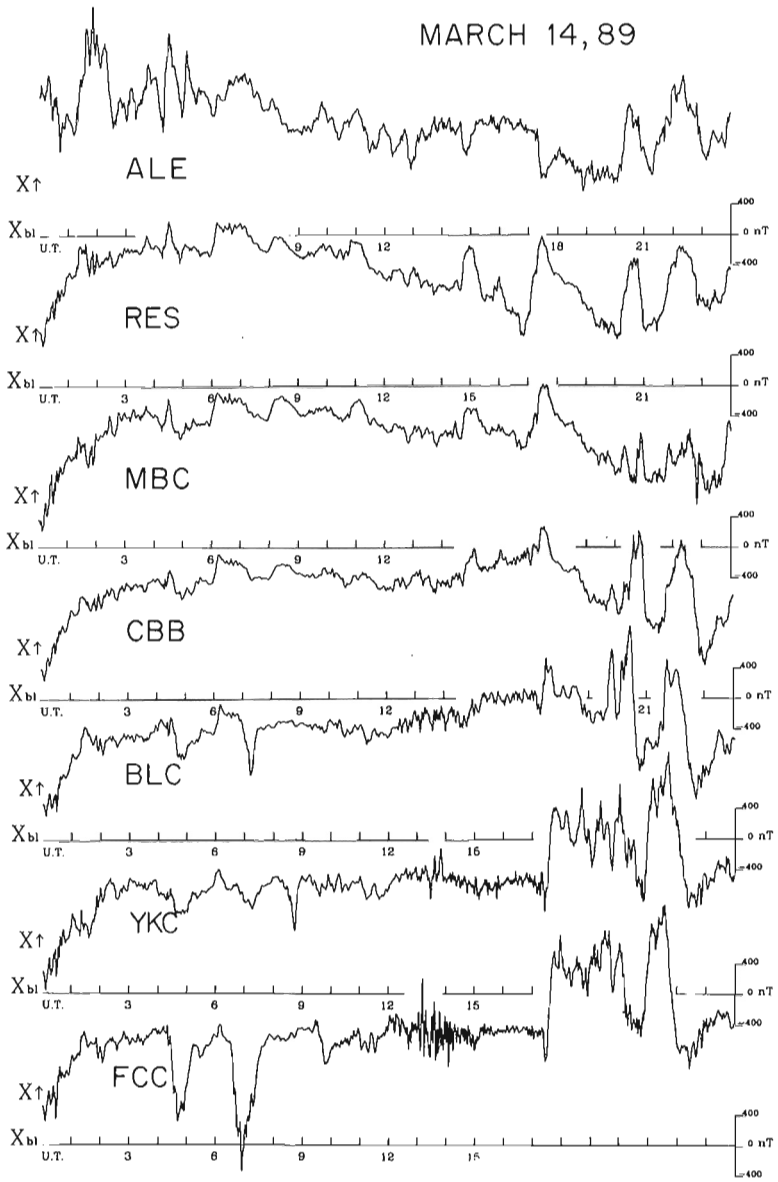

Figure 3. Same as Figure 2 except for 14 March, 1989.

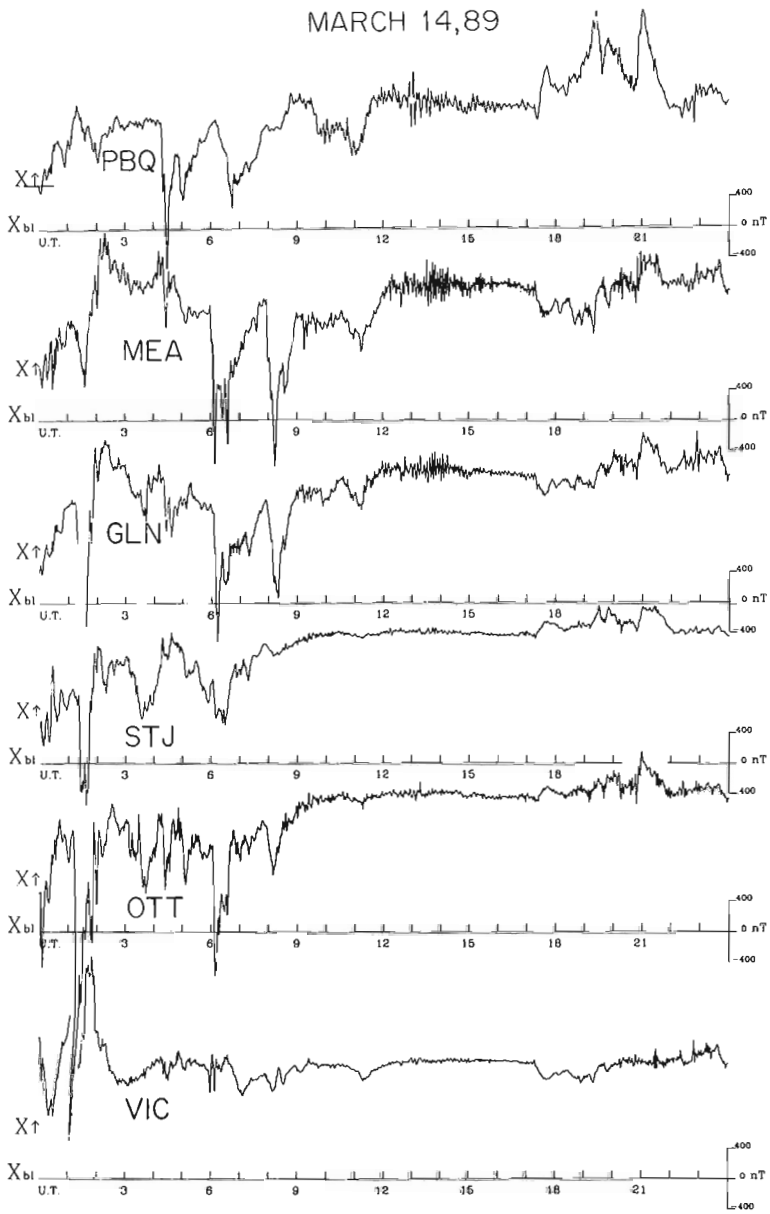

Figure 3. Continued

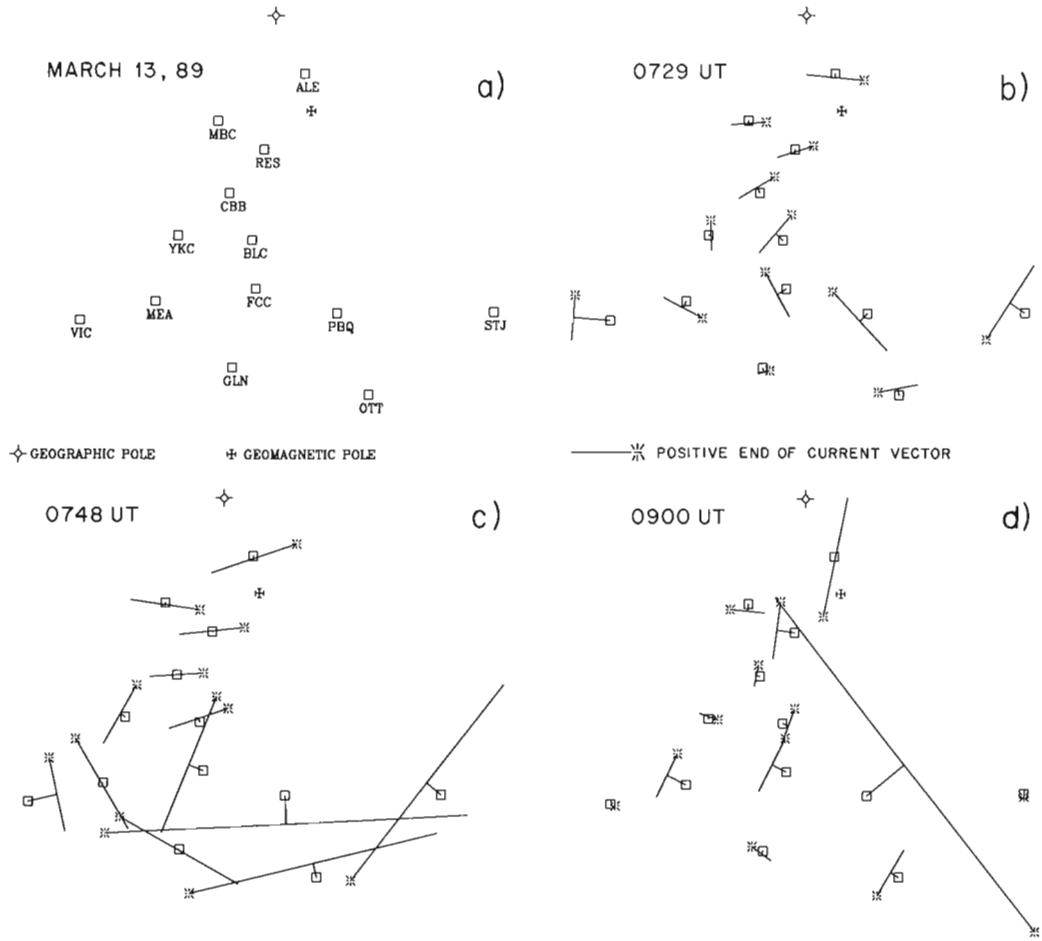

Figure 4. Equivalent line currents for the Canadian magnetic observatories. (a) Squares indicate positions of magnetic observatories used in this analysis. (b, c, and d) Equivalent line currents — at 0729 UT, 0748 UT, and 0900 UT, on 13 March, 1989. Asterisk shows positive end of current vector, and the line from the observatory is the distance between the line current and the observatory.

monitors at Deep River (DR), Goose Bay (GB), and Inuvik (IN) (M.D. Wilson, pers. comm., 1989) together with the X component of the geomagnetic field, as recorded at the Ottawa Magnetic Observatory. No significant effect at the time of the sudden commencement is seen. A slow decrease started around 0600 UT at Inuvik, the most northern station, and around 0800 UT at Deep River and at Goose Bay. A sharp decrease of about 3 to 4 percent occurred at all stations between 1000 to 1100 UT, with another of 7 to 8 percent between 1700 to 1900 UT. These decreases correlated with occurrences of large excursions in the geomagnetic field, especially at the northern observatories (see Fig. 2).

EFFECTS OF GEOMAGNETIC ACTIVITY ON TECHNOLOGY

The impacts of geomagnetic activity on technology are quite diverse in nature, but in most cases are economically significant. Some effects are immediately apparent, while others only become evident after a considerable elapsed time. Here we describe only a few events during this storm, each from a different industry, that have been correlated with data from the Canadian magnetic network.

Geomagnetically induced currents (GIC) and potentials, and their effects on long conductors, such as electrical power transmission systems, pipelines, and telecommunications systems, were recognized at the beginning of this century, and since then have been discussed by many authors (e.g. Anderson et al. (1974), Watanabe and Shier (1982), Campbell (1986), and Lanzerotti and Gregori (1986)).

GIC on electric power systems

This magnetic storm had the most serious effects on electric power systems ever observed in Canada. On 13 March at 0745 UT, the storm induced currents in the Hydro Quebec transmission lines running southward from the James Bay

region in northern Quebec. As a result, transformers were saturated, generating harmonics, with the subsequent tripping of protective relays on static compensators. This caused a generation loss of 9 450 MW. With a load of about 21 300 MW at that moment, the system was unable to withstand this sudden loss and collapsed within seconds, causing further loss of generation at other generating stations. The result was a total blackout for about six million people for about nine hours. Other utilities in Canada felt the effects of this storm in the form of power fluctuations, voltage depressions, and induced currents (Coles et al., 1989). The highest GIC levels observed by Ontario Hydro on 13 March were about 80 amperes, and Newfoundland and Labrador Hydro reported a GIC of about 150 amperes.

The correlations between time occurrences of major problems on electrical systems with the peaks of geomagnetic variations are excellent. Fig. 6 shows (a) an example of the GIC as recorded at ten-second intervals by Ontario Hydro at their transformer station at Wawa (K. Thompson, pers. comm., 1989), (b) the rate of change of the X (north) component of the magnetic field recorded at Ottawa Magnetic Observatory based on data sampled at ten second intervals, which are shown in (c). The point to note here is that the sustained rate of change of the magnetic field is the important factor, not the intensity. Of course, other factors such as the local earth conductivity and the electrical network configuration also play significant roles.

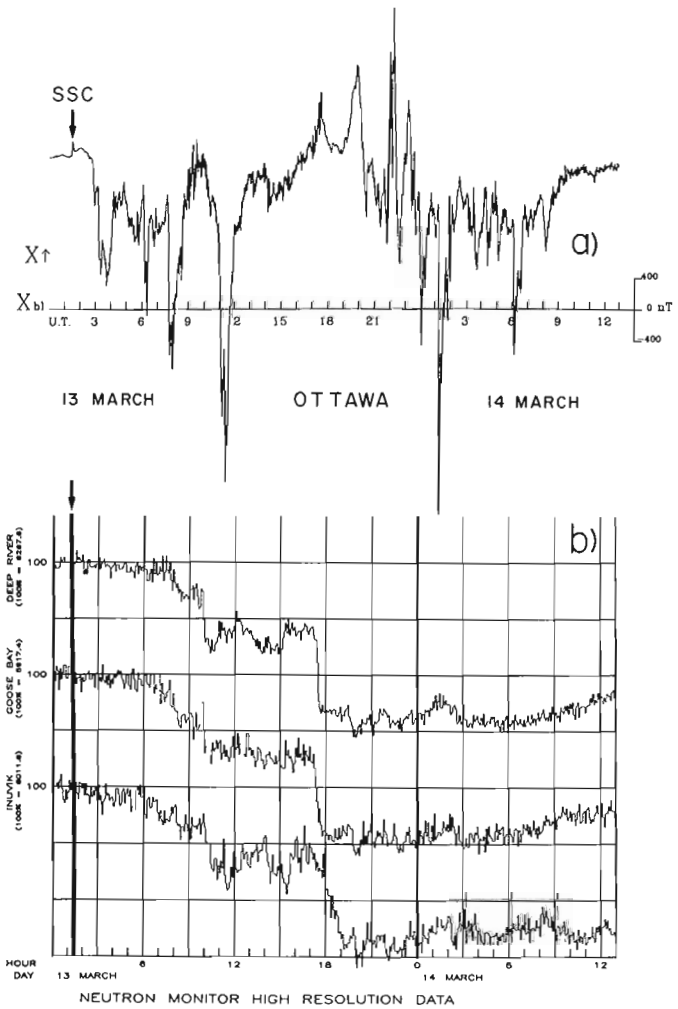

Figure 5. Neutron monitor data (5 min counts) at Deep River, Goose Bay, and Inuvik (b), and X (north) component (1 min resolution) of magnetic field from Ottawa(a), 13-14 March, 1989.

Potentials on pipelines

Normal cathodic protection systems on pipelines apply pipe-to-soil potentials of -850 mV (or more negative) to prevent electrolytic corrosion at flaws in the pipeline coating. These potentials are monitored to confirm that cathodic protection is in fact in operation. During magnetic storms, induced effects cause the potentials to vary rapidly and widely from the -850 mV level, rendering the monitoring system ineffective and the pipeline exposed to possible electrolytic corrosion. In fact, significant corrosion can occur when the pipe-to-soil potential becomes more positive than about -650 mV (Commonwealth Seager Group, 1987).

An example of induced potentials on a pipeline system was recorded during this March storm by the Home Oil Company on a pipeline located approximately 200 km northeast of Meanook Magnetic Observatory (Fig. 1) in western Canada. Figure 7 shows the record of pipe-to-soil potential (Home Oil Company, pers. comm., 1989) together with the magnetic record from Meanook Observatory. The straight line on Figure 7a is the -850 mV level; the first occurrence of disturbed values of the pipe-to-soil potential was coincident with the first major surge in the storm. Disturbed values, often more positive than -650 mV, persisted throughout the storm.

Potentials on a transatlantic telecommunications cable

The effects of magnetic storms on transatlantic telecommunications cables were reported in 1958 and again in 1972 when significant disruptions were observed Lanzerotti and Gregori (1986). At the time of this March 1989 storm, a new transatlantic telecommunications fiber-optic cable was in use. It did not experience a disruption, but large induced potentials were observed on the power supply cables. The largest voltage excursions were observed approximately at 1110 UT and 2145 UT on 13 March and at 0130 UT on 14 March (L.V. Medford, pers. comm., 1989). Figure 8 shows the X (north) component of magnetic field from St. John's Magnetic Observatory; the peaks of voltage excursions (marked by arrows, L.J. Lanzerotti, pers. comm., 1989) clearly correlate with the largest variations of magnetic field.

Ionospheric radio-wave propagation

To illustrate the effect of this storm on ionospheric propagation conditions we compare the radio propagation quality indices (RPQ) with the geomagnetic DRX indices, which characterized the geomagnetic conditions in three major magnetic zones in Canada. Radio propagation quality indices are routinely calculated for six circuits: from Nordeich

in West Germany to: England, Italy, Iran, Japan, Australia, and U.S.A. (New York). They represent the quality of propagation for a 24-hour interval for different HF frequencies (a description of the RPQ is given by Coffey (1985, 1989) and by Miller (1989)). The quality index from 0.1 to 1 represents very poor, 1.1 to 3.0 poor, 3.1 to 5.0 fair, and 5.1 to 7.0 normal propagation. In Figure 9 are shown DRX indices and RPQ indices during the interval from 1016 March 1989. On all circuits the RPQ reached "poor" level, with very poor (0.4) quality on the New York path. This latter circuit runs through the subauroral zone, which was the most disturbed region during this storm. The relation between DRX and RPQ has been investigated in detail by Miller (1989).

EFFECT ON CANADIAN MAGNETIC FORECASTING SERVICE

The impact of this magnetic storm was also considerable at the Associate Regional Warning Centre (ARWC) in the Geomagnetism Section, Geophysics Division, in the GSC. The ARWC Ottawa is one of a number of centres around the world, linked by Telex, FAX, and other means, for the purposes of exchanging timely data concerning the activity on the Sun and geomagnetic and ionospheric activity on Earth, and of producing forecasts. ARWC Ottawa routinely produces forecasts of geomagnetic activity. For about a year prior to the storm, discussions had been held with Ontario Hydro and, through them, with other electric power utilities

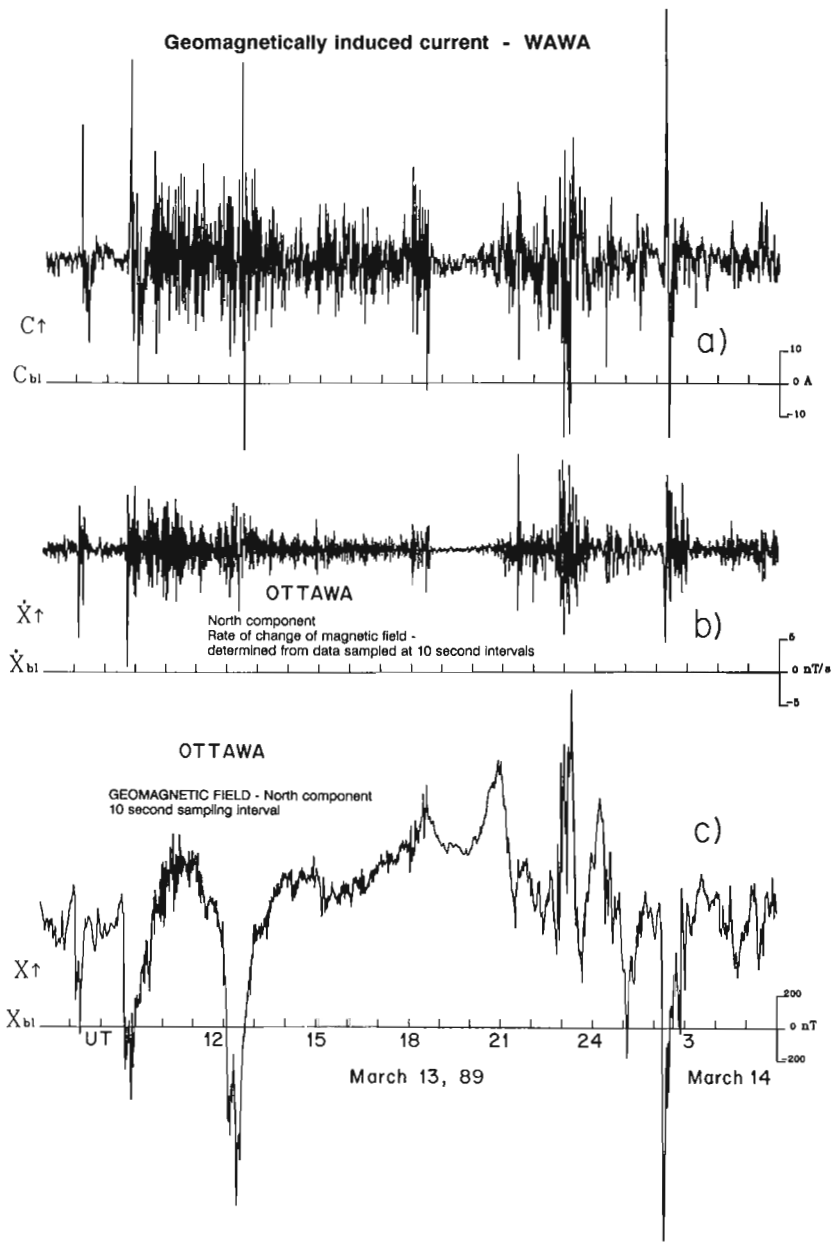

Figure 6. (a) GIC at Wawa transformer station, (b) rate of change of X (north) component of magnetic field at Ottawa, and (c) X component of magnetic field, at Ottawa Magnetic Observatory, 13-14 March, 1989.

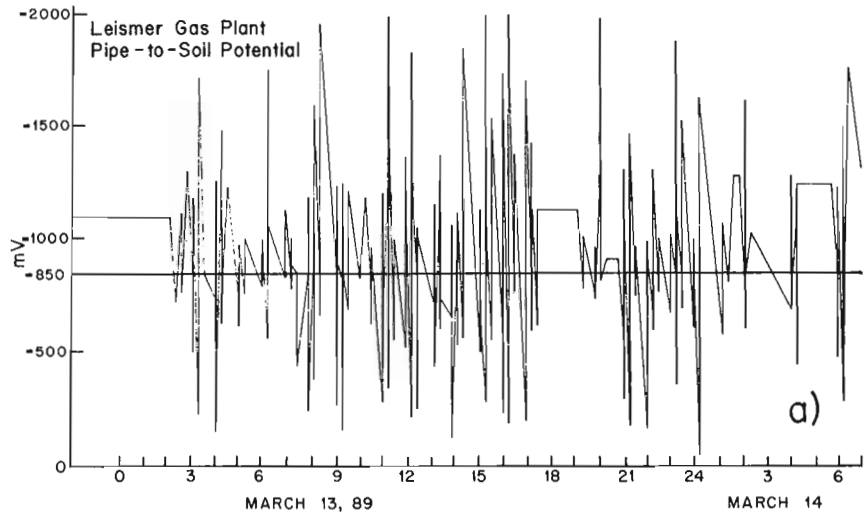

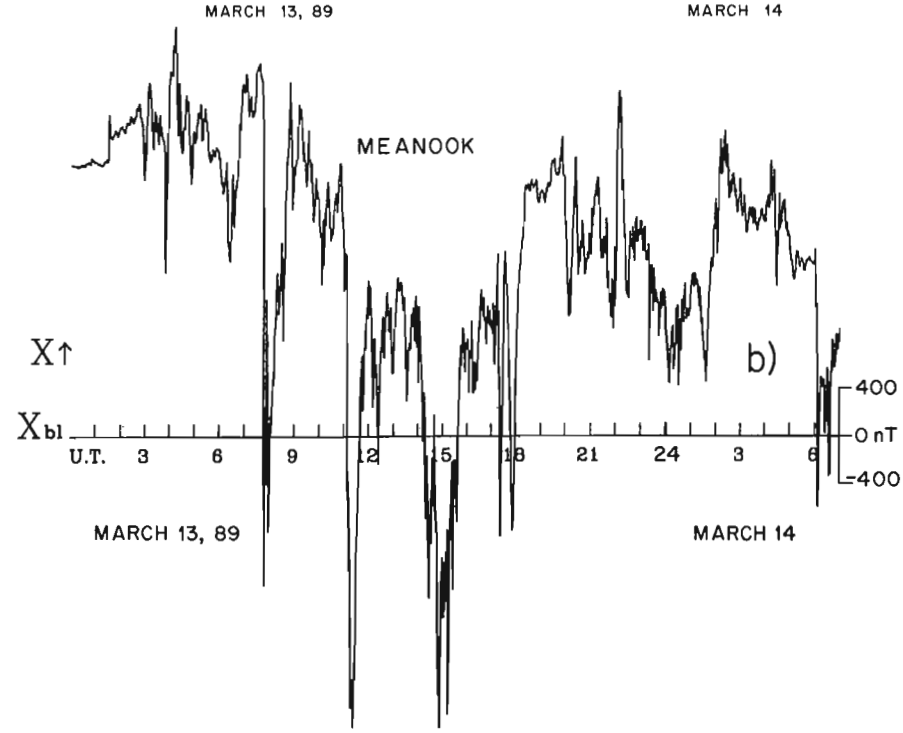

Figure 7. (a) Negative pipe-to-soil potential recorded at the Leismer Gas Plant; (b) Magnetic record of X component from the Meanook Magnetic Observatory, 13-14 March, 1989.

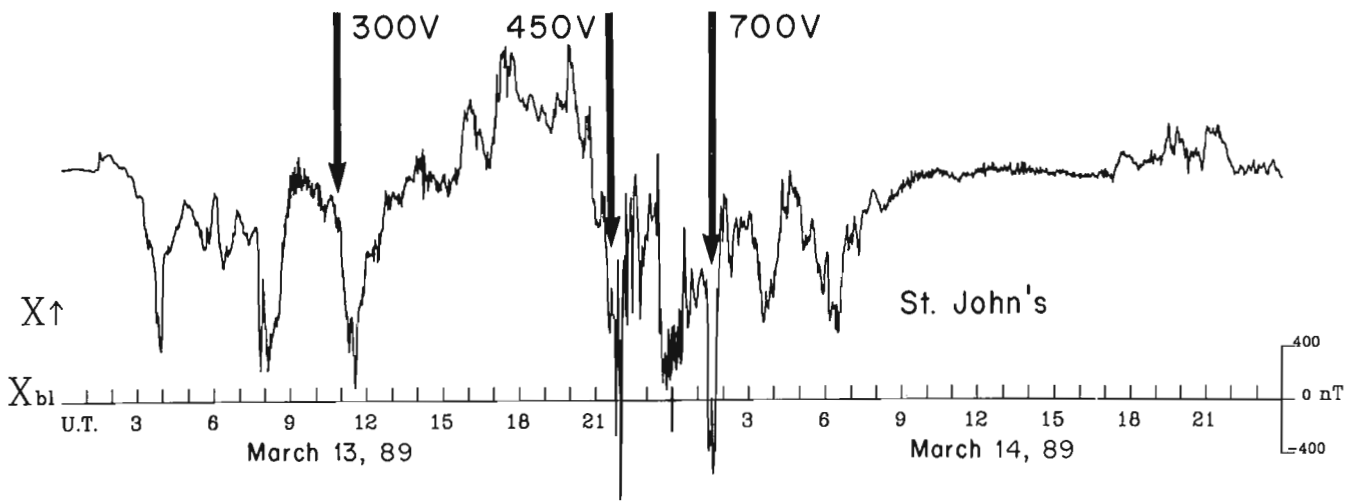

Figure 8. Variation of magnetic field at St. John's observatory and the peaks, marked by arrows, of voltage excursions measured on the fiber-optic transatlantic telecommunication cable during 13-14 March, 1989.

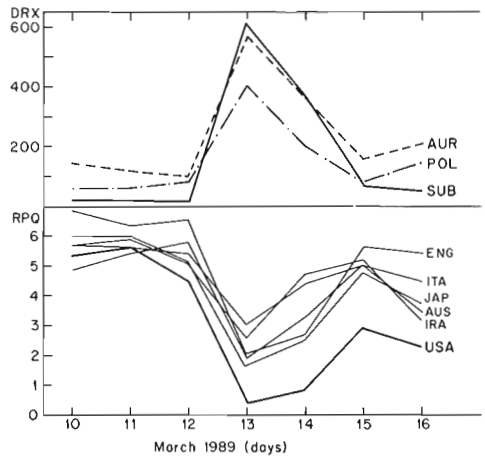

Figure 9. Geomagnetic indices DRX in subauroral (SUB), auroral (AUR), and polar cap (POL) zones, and radio propagation quality indices (RPQ) on circuit from West Germany to U.S.A., Iran, Australia, Japan, Italy, and England for the period 10-16 March, 1989.

in the Northeastern Power Coordinating Council, on the topic of establishing an enhanced magnetic forecasting service taking into consideration the needs of the utilities. Progress was being made toward an agreed goal of having the ARWC Ottawa system running on a seven day per week basis to be effective on 1 April, 1989. This included the daily production of the voice-message forecast (a service already in existence) and a computer-readable forecast (this latter to be accessed automatically by, among others, the electric power utilities). Several system elements, mainly software, had not been completed at the time of the mid-March disturbances, and so no forecaster was on duty during the weekend preceding the great storm. However, from the next weekend on, ARWC Ottawa has operated on a seven days per week basis. The March storm provided a considerable increase in the recognition of the importance of the Canadian magnetic forecasting and monitoring service for Canadian industry. The March storm has also triggered the ARWC Ottawa to establish new research tasks to respond to the needs of an enlarged user community.

CONCLUSION

This storm provided the scientific community with an exellent example of solar-terrestrial relationships, and of the importance of understanding these complicated processes and correlations. The impact of such natural phenomena on human enterprises stresses the necessity of close cooperation between research and industry.

ACKNOWLEDGMENTS

We would like to express our thanks to all contributors of information, records, and data, particularly to M.D. Wilson, R.W. Miller, and R.S. Shapka. We appeciate the constructive comments and suggestions from our colleagues during the preparation of this paper.

REFERENCES

Anderson, V.D., Thorson, Jr., J.M., and Miske, S.A.
1974: The effects of geomagnetic storms on electrical power systems; IEEE Transactions on Power Apparatus and Systems, v. PAS-93, no. 4, p. 1030-1044.

Campbell, W.H.
1986: An interpretation of induced electric currents in long pipelines caused by natural geomagnetic sources of the upper atmosphere; Surveys in Geophysics, v. 8, p. 239-259.

Campbell, W.H., Albertson, V.D., Boerner, V.M., Boteler, D.H., Goddard, W.R., Hruska, J., Irwing, S., and Kappenman, J.G.
1979: Geomagnetic applications — a working group report; Solar-Terrestrial Prediction Workshop Proceedings, v. 2, p. 133-136, NOAA.

Coffey, H. (editor)
1985: Solar-geophysical data, explanation of data reports, no. 489 (supplement); NOAA, Boulder, Colorado, U.S.A.
1989: Solar-geophysical data prompt reports no. 537—part 1; NOAA, Boulder, Colorado, U.S.A., 240.

Coles, R.L, Hruska, J., Thompson, K. and Miller, R.W.
1989: Effects of the magnetic storm of March 13-15, 1989 on power transmission in Canada; presented at the 6th Scientific Assembly of IAGA, Exeter, U.K.

Coles, R.L., Jansen van Beek, G., and Newitt, L.R.
1987: Annual report for magnetic observatories and repeat stations-1985; Geological Survey of Canada, Paper 86-25, Geomagnetic Series no. 31.

Commonwealth Seager Group
1987: Polarization decay on northern pipelines under telluric current influence; Phase II—IRAP-M 4830-18, Edmonton.

Haurwitz, M.W., S. Yoshida, and S.-I. Akasofu
1965: Interplanetary magnetic field asymmetries and their effects on polar cap absoption events and forbush decreases; Journal of Geophysical Research, v. 70, no. 13, p. 2977-2988.

Hruska, J. and Coles, R.L.
1987: A new type of magnetic activity forecast for high geomagnetic latitudes; Journal of Geomagnetism and Geoelectricity, v. 39, p. 521-534.

Lam, H.-L.
1987: Forecasts of geomagnetic activity in Canada by linear prediction filtering; Journal of Geomagnetism and Geoelectricity, v. 39, p. 534-542.

Lam, H.-L.
in press: A possible classification of Pc5 geomagnetic pulsation into two sub-groups (Pc5A and Pc5B) based on spectral structure; Journal of Geomagnetism and Geoelectricity.

Lam, H.-L. and Rostoker, G.
1978: The relationship of Pc5 micropulsation activity in the morning sector to the auroral westward electrojet; Planetary and Space Science, v. 26, p. 473-492.

Lanzerotti, L.J. and Gregori, G.
1986: Telluric currents: the natural environment and interactions with man-made systems; *in* The Earth's Electrical Environment, U.S. NRC Report.

Loomer, E.I. and Jansen van Beek, G.
1971: Magnetic substorms, December 5, 1968; Publications of the Earth Physics Branch, v. 41, no. 10.
1972: Polar magnetic substorms 03-06 UT, December 5, 1968; Publications of the Earth Physics Branch, v. 42, no. 4.

Miller, R.W.
1989: Geomagnetic activity and propagation conditions on a North Atlantic HF radio circuit; presented at the Solar-Terrestrial Predictions Workshop, Sydney, Australia.

Trigg, D.F. and Nandi, A.
1984: The automatic magnetic observatory system AMOS III; Earth Physics Branch, Geomagnetic Series, no. 27.

Watanabe, T. and Shier, R.M.
1982: Magnetic storm effects on power transmission systems; Geomagnetic Bulletin, no. 2-82, Earth Physics Branch, Ottawa.

Mining related seismic source mechanisms and ground vibrations

H.S. Hasegawa
Geophysics Division

Hasegawa, H.S., Mining related seismic source mechanisms and ground vibrations; in Current Research, Part A, Geological Survey of Canada, Paper 90-1A, p. 57-65, 1990.

Abstract

With ongoing volume convergence and the potential for increasing rates of volume extraction in Canadian hard-rock mines, it is becoming imperative to determine the exact nature of the source mechanism of larger mine-induced tremors. Potential modes of failure by non double-couple as well as the more familiar double-couple mechanisms, and their corresponding P- and S-wave radiation patterns, are presented and possible interactions between the various types discussed. Analysis of close-in records of seismograms, stress, strain, and tilt, in conjunction with evidence of damage to pillar supports and mine openings, should lead to a better understanding of the modes of failure and trigger mechanisms of the larger mine tremors. Thus a combined analysis should contribute toward the mitigation of the potential harmful effects and economic set backs due to some of the larger mine-induced tremors through adaptive mining methods.

Résumé

Avec une convergence des terrains continue et la possibilité d'une augmentation de la cadence d'extraction volumétrique dans les mines de roches dures canadiennes, il devient urgent de déterminer la nature exacte du mécanisme originel des grandes secousses provoquées par l'exploitation minière. Des modes potentiels de rupture dus aux mécanismes courants de couple-double et à d'autres mécanismes et leurs diagrammes de rayonnement correspondants des ondes P et S, sont présentés dans le présent rapport et des interactions possibles entre les divers types sont étudiées. Une analyse des données détaillées de sismogrammes, de contraintes, de déformations et de basculements, conjointement avec des données sur les dégâts subis par des piliers et les ouvertures de mines, devrait aboutir à une meilleure compréhension des modes de rupture et des mécanismes de déclenchement des grandes secousses provoquées par l'extraction minière. Ainsi, une analyse combinée devrait contribuer à l'atténuation des effets dangereux rendus possibles et des reculs économiques dus à certaines grandes secousses provoquées par l'extraction minière, grâce à l'emploi de méthodes d'extraction adaptatives.

INTRODUCTION

With the advent of mining techniques that can extract ore at ever-increasing rates and the cumulative, on-going volume convergence of mined-out regions, the potential for larger mine-induced tremors tends to increase (cf. McGarr, 1976; Wetmiller et al., 1989). Mine-induced tremors that cause damage are also referred to as rockbursts (Hedley and Wetmiller, 1985). Thus the need to understand the causative factors and the different mechanisms of mine-induced tremors is becoming more imperative.

For the case where the analysis of mining-related shocks is confined to teleseismic records, there are inherent drawbacks to determine the respective source mechanisms. The uncertainty in estimate of focal depth and epicentral coordinates tends to increase with increasing epicentral distance. Moreover, the high-frequency characteristics of the source spectrum are attenuated at these distances. In addition the diagnostic capability of differentiating between the various potential modes of mine-induced tremors tends to decrease, but this is not always the case. Therefore the need to analyze waveforms recorded near mines becomes urgent. The co-operation between federal government, industry, and Ontario has led to the installation of three-component digital seismograph arrays, which provide close-in waveforms for analyses.

The objectives of this paper are as follows: to describe the essential characteristics of "near-field" and "far-field" terms associated with a simple fault (double-couple) model; to discuss possible modes of failure, both double-couple and non- double-couple, within and adjacent to the mine excavation and the corresponding seismic radiation patterns; and to discuss potential interactions of mine-induced tremors, that is, how one mode of failure could trigger a subsequent type of failure in a nearby weakened or highly stressed region.

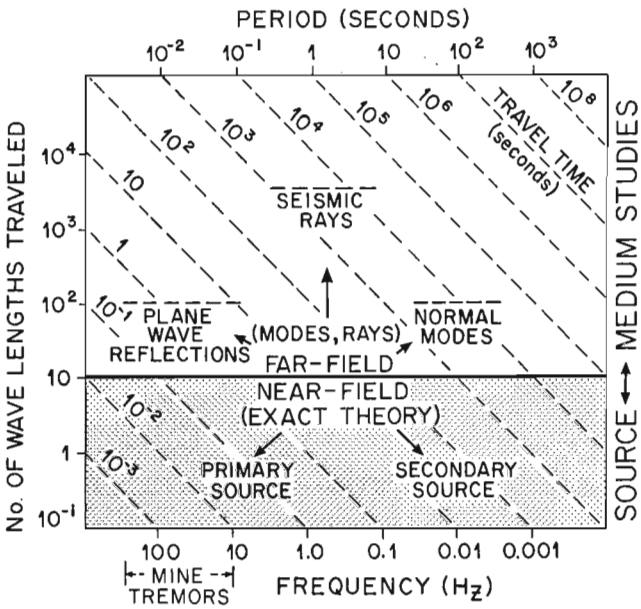

Figure 1. Generalized definition of near-field and far-field based on number of wavelengths traveled versus frequency or period and outline of general method for seismogram analysis.

NEAR-FIELD AND FAR-FIELD SEISMIC PHASES

A convenient generalization of the near-field and far-field (K. Aki, pers. comm., 1972) is shown in Figure 1. The high-frequency (greater than about 10 Hz) characteristics of the source can be derived only in the near-field. The longer-period characteristics of the source can be determined in the far-field from teleseismic records provided the attenuation and the geometric spreading factor are known. In the near-field of mine-induced strong ground vibrations, frequencies of the transient signal can range from a few Hz to more than a hundred Hz. There is coseismic deformation in the hypocentral and epicentral regions and, after postseismic recovery, in some cases a residual ground deformation that may be detectable, particularly for the larger, shallow events (e.g. dip-slip faulting). The epicentral distance range within which the exact (near- and far-field) theory must be used depends on the ratio of distance-to-fault length and is described in the next section.

Radiation from a simple fault model

A formulation of the total field generated by the rectangular, vertical strike-slip model shown in Figure 2a for the displacement component u_1 in the x_1-direction at time t and distance x is (Haskell, 1969):

$$[1]\quad u_1(x,t) = \left(\frac{\beta^2}{4\pi}\right)\int\int_s \Gamma_3\left(\sum_{i=1}^{5}\text{Term } i\right) d\epsilon_1\, d\epsilon_2$$

where:

$$\text{Term 1} = +\,6(5\Gamma_1^2 - 1)r^{-4} \times \int_{r/\alpha}^{r/\beta} D_1(\epsilon_1, \epsilon_2, t - t')t'dt'$$

$$\text{Term 2} = +\,2(6\Gamma_1^2 - 1)(\alpha r)^{-2} \times D_1\left(\epsilon_1, \epsilon_2, t - \frac{r}{\alpha}\right)$$

$$\text{Term 3} = -\,3(4\Gamma_1^2 - 1)(\beta r)^{-2} \times D_1\left(\epsilon_1, \epsilon_2, t - \frac{r}{\beta}\right)$$

$$\text{Term 4} = +\,2\Gamma_1^2(\alpha^3 r)^{-1}\dot{D}_1\left(\epsilon_1, \epsilon_2, t - \frac{r}{\alpha}\right)$$

$$\text{Term 5} = -\,(2\Gamma_1^2 - 1)(\beta^3 r)^{-1} \times \dot{D}_1\left(\epsilon_1, \epsilon_2, t - \frac{r}{\beta}\right)$$

and D_1 and $\dot{D}_1$ are the dislocation (slip) and time derivative of the slip vector, respectively; ϵ_1 and ϵ_2 are the coordinates of a rectangular element in a fault surface (s) of length L and width W; the direction cosine between the observer at distance r from the element and the respective axis is Γ_i (i=1,2,3); and the P-wave and S-wave velocity is α and β, respectively.

The near-field is represented by Terms 1, 2, and 3, and the far-field, by Terms 4 and 5. Term 1 has a fall-off with

distance that varies inversely as the fourth power of distance, Terms 2 and 3 as the second power of distance and Terms 4 and 5 as the first power of distance. Moreover, the near-field terms depend on the dislocation (D_1), whereas the far-field terms depend on the velocity of the dislocation ($\dot{D}_1$).

The transient ground motion curves associated with this vertical strike-slip model for the specific case of D_1 = 1 cm are shown in Figure 2b and for the coseismic slip in Figure 2c. With respect to the transient signal shown in Figure 2b and the residual displacement in Figure 2c, the near-field terms (1, 2, and 3) are significant for distances less than about a fault length and the far-field terms (4 and 5) start to dominate at greater distances. Figure 3 shows spectral amplitude density curves based on Term 4 (P-wave) for the fault dimensions shown. With respect to the displacement density curve, the low-frequency asymptote is proportional to seismic moment (M_o). The corner frequency f_3 is proportional to the ratio of rupture velocity (V_R) to fault length (L). The other corner frequencies f_1 and f_2 are related to stopping phases, and f_4 to attenuation (see bottom curve). A multiplication of the displacement spectra by angular frequency, Ω, generates a velocity density spectra. A further multiplication by Ω generates an acceleration density spectra, which corresponds to the Fourier transform of ground acceleration (FS). The attenuation (exponential term) depends on the quality factor Q and other terms that have been defined previously. At present there is a dichotomy concerning the causative factor of the high-frequency cut-off (f_{max}), which is not shown in Figure 3 because its exact value is uncertain; however, f_{max} is greater than f_4 (shown in lower graph in Fig. 3) and corresponds to the frequency where there is an abrupt fall-off in amplitude. The two postulates of f_{max} most frequently mentioned are source effects and attenuation (e.g. see Aki, 1987).

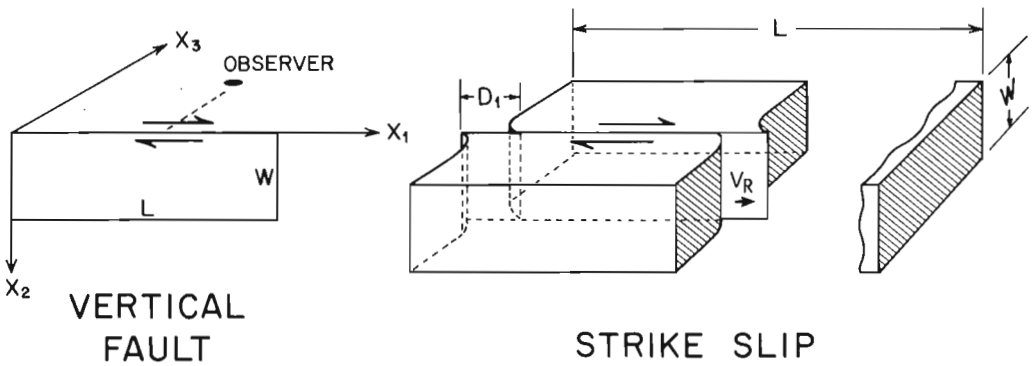

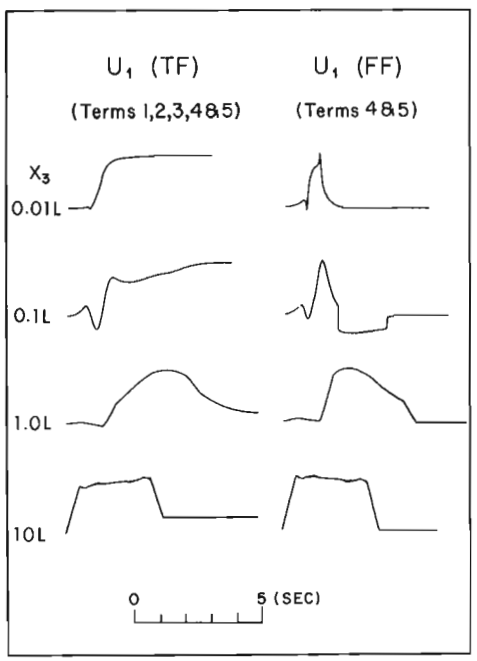

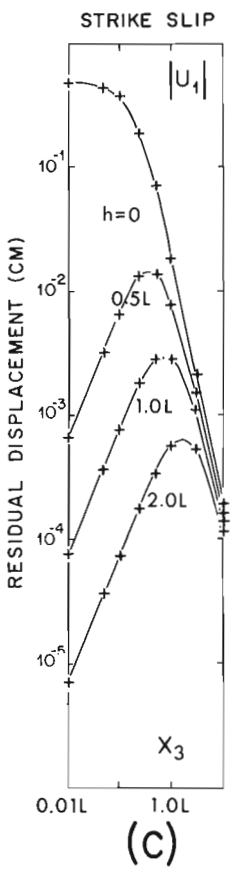

Figure 2. Part (a) shows vertical strike-slip model of length L, width W, dislocation D_1 and rupture velocity V_R. Part (b) shows displacement time history, u_1, using total field terms, TF, and far-field terms, FF, of Haskell (1969) for epicentral distances ranging from 0.01L to 10L. Part (c) shows coseismic ground displacement at various focal depths, h, based on closed formulation of Press (1965) (after Hasegawa, 1974, 1975).

A comparison of theoretical and actual FS spectra at a hypocentral distance of about 1.0L is shown in Figure 4 for the 1935 magnitude 6 Helena, Montana earthquake. For the relatively simple accelerogram shown in the inset, the correlation between the corresponding FS curve and the theoretical curve based on the far-field terms in the Haskell model is good. Thus records of mine tremors taken at epicentral distances greater than about a fault length are amenable to a comparable type of analysis (cf. Gibowicz et al., 1977; McGarr et al., 1981; Hinzen, 1982). As the epicentral distance decreases, the signal becomes progressively more like a ramp and less like a spike (see Fig. 2b) and the seismograph response will manifest this difference.

SCALING PARAMETERS OF EASTERN CANADA EARTHQUAKES

In addition to the b-value in the magnitude-recurrence relations (e.g. see Basham et al., 1982), another fundamental parameter that governs a basic scaling relation for Eastern Canada earthquakes is n, which appears as an exponent in the relation $M_o f_c^n \approx \delta\sigma$ where M_o is seismic moment, f_c is corner frequency and $\delta\sigma$ is stress drop. For Western North America (plate margin) earthquakes, n=3, which implies a constant $\delta\sigma$. For Eastern North America (mid-plate) earthquakes, some studies indicate n=3 also (Somerville et al., 1987), which implies that Western and Eastern North

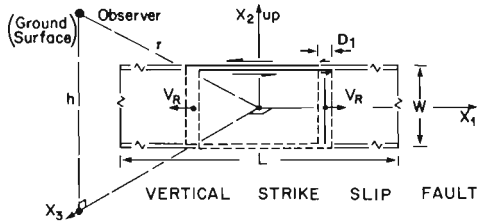

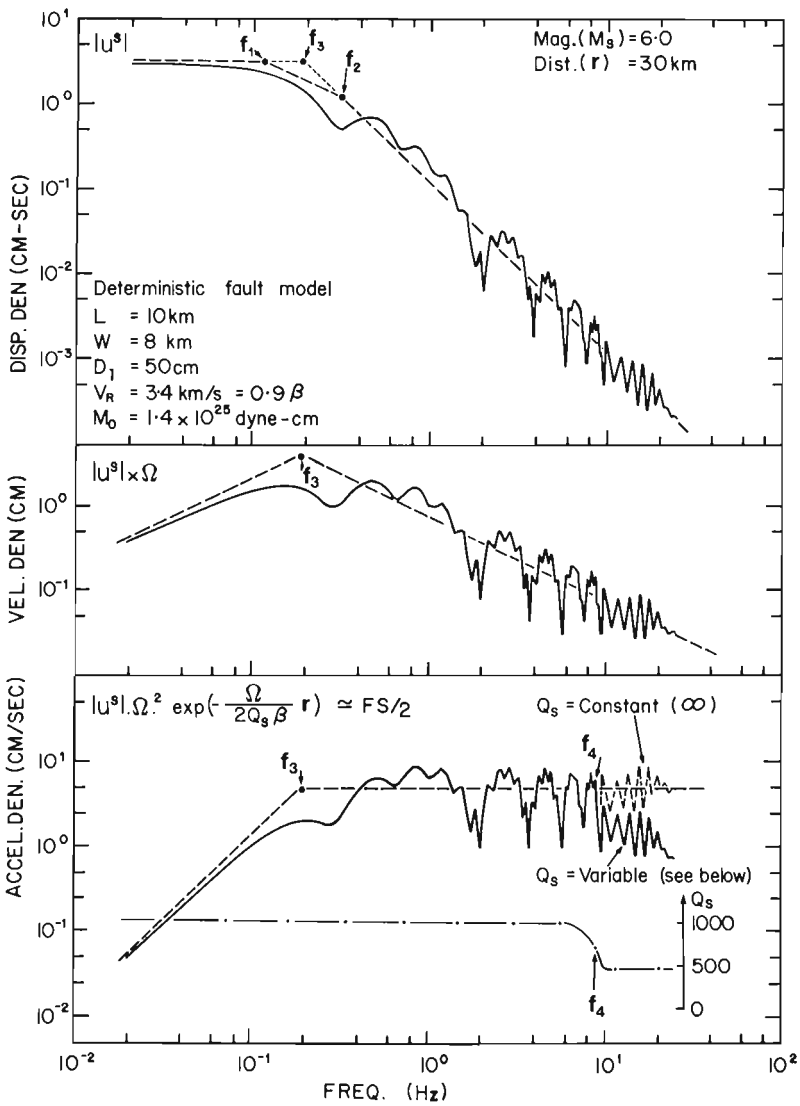

Figure 3. Top part shows model of vertical strike-slip fault with co-ordinate axes. Symbols are as described in Figure 2. Step-by-step development of corresponding displacement, velocity, and acceleration spectral amplitude density curves that are based on the far-field term (Term 4 in Eq. (1)) are shown. Formulation used to incorporate attenuation in bottom curve is described in text (from Hasegawa, 1974).

ican earthquakes obey a similar scaling law. However other studies indicate that n=4 (Nuttli, 1983), or n=3 1/2 (Hasegawa, 1983); these values indicate that $\delta\sigma$ increases with M_o, and consequently there is a basic difference between the scaling relation for Western and Eastern North American earthquakes. If n=3 for Eastern Canada mine-induced (double-couple) earthquakes, the stress drop of these earthquakes will tend to be constant, regardless of the size of the tremor. However if $4 \geq n > 3$, then the stress drop should increase with the size of the induced earthquake (cf. Hinzen, 1982). With respect to mining, stress drop has important implications because peak ground acceleration near the source is proportional to stress drop (e.g. see Brune, 1970).

EARTHQUAKE TRIGGER MECHANISMS

Figure 5 shows schematically, using the Coulomb-Mohr failure model, different potential ways in which mine-induced fault slip could be initiated. The basic premise is that there is a weakened fault with a low cohesive strength (s) such that the Coulomb failure line is close to the Mohr circle, as shown in Figure 5a. An increase in pore pressure (δP), either by injection of fluids (Healy et al., 1968) or in some special (perhaps rare) cases by an increase in the height of the water table, may be able to trigger fault slip as shown in Figure 5b. Where there exists a fault that connects a source of water to a mine opening, on-going volume closure could cause strain changes that cause partial separation of the fault, thereby creating a pathway (i.e. increase in permeability) for water inflow; as a consequence fault gouge could be created, resulting in a decrease in the friction angle ($\delta\Theta$) as shown in Figure 5c. On-going volume closure could also gradually weaken asperities in the fault, thereby causing a decrease in the effective cohesive strength (δs), as Figure 5d illustrates. Excavation decreases the effective vertical stress ($\delta\sigma_3$); in a thrust-fault environment the minimum principal stress, σ_3, is vertical and consequently this is a potential trigger mechanism as indicated by Figure 5e. Other possibilities are an increase in σ_1, and a simultaneous increase in σ_1 with a decrease in σ_3.

A comparison of the fault-plane solutions of natural earthquakes with mine-induced (double-couple) earthquakes in the same seismogenic region may indicate whether or not mine-induced stress and strain can actually dictate the mode of failure or merely act as a trigger mechanism for mine-induced earthquakes.

MECHANISMS FOR GENERATING MINE-INDUCED TREMORS

In addition to fault slip (double-couple) around the periphery of a mine opening, the potential exists for certain non-double-couple types of source mechanisms, several examples of which are shown in Figure 6. The main source of energy for these mechanisms is cumulative and on-going volume convergence. In some cases blasting could be a secondary contributor to, for example, cavity collapse in the footwall in the mine ceiling (Fig. 6a). Pillar bursts are a common occurrence in many mines (e.g. see Hedley and Wetmiller, 1985) and are simulated by a vertical dipole in Figure 6b. In some cases pillar bursts have coincided with an acceleration in the rate of volume convergence (Hedley et al., 1984). Since rocks are much weaker under tension than under compression, tensile faulting (Fig. 6c) could occur in a broad, mined-out region with a competent cap rock that is subjected to a considerable amount of flexure

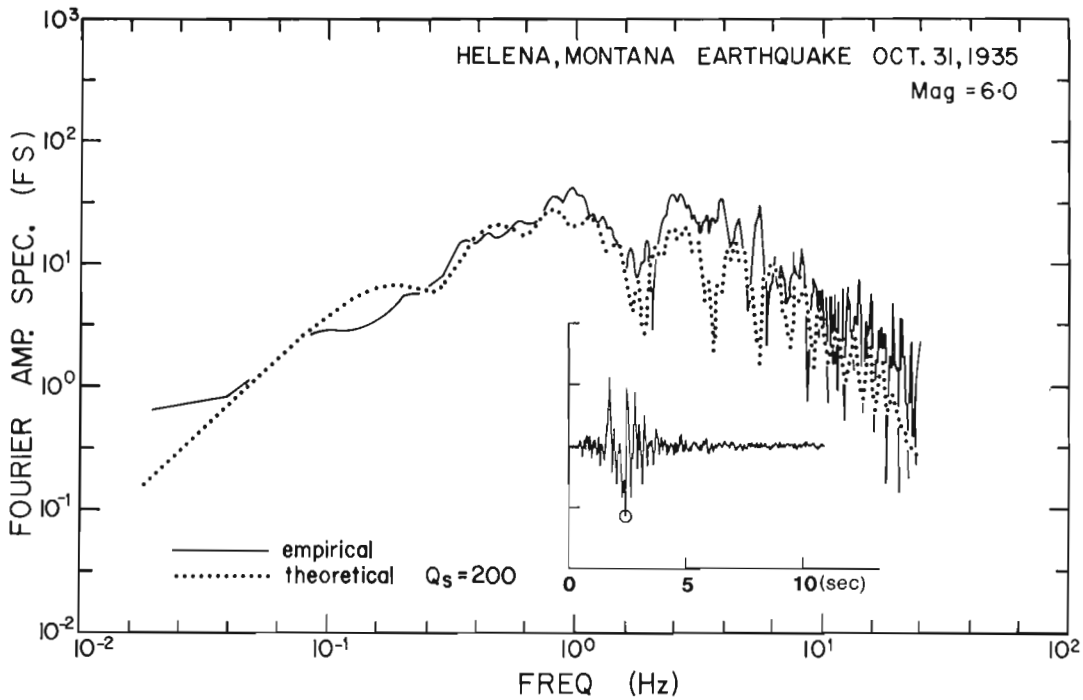

Figure 4. Comparison of actual acceleration amplitude density (FS) curve (from Brady et al., 1973) with theoretical curve calculated by technique illustrated in Figure 3. Distance is approximately a fault length (1L) from source. Inset shows actual accelerogram.

due to appreciable volume convergence. However, in most cases the design of mine excavation should be able to minimize this type of failure. When the advancing stope face encounters a fault, then faulting could be initiated as shown in Figure $6d_1$ (see Al-Saigh and Kusznir, 1987). In a predominantly thrust-fault seismotectonic environment such as Eastern Canada, the decrease in the vertical stress (usually σ_3) could trigger thrust faulting, as shown in Figure $6d_2$ (e.g. see Wetmiller et al., 1989). Microseismic and moderate tremors above potash mines in Saskatchewan may be the result of fault slip along the interface of the horizontal layering in the competent layering above the stope face being mined, as shown in Figure $6d_3$ (Gendzwill, 1983). The associated P-wave and S-wave radiation patterns (in a vertical plane) for the non- double-couple mechanisms are shown in Figures 6A, 6B, and 6C. By a suitable rotation of the radiation patterns and appropriate reversal of arrows in Figure 6D, the corresponding radiation patterns for the double-couple mechanisms in Figures $6d_1$, $6d_2$, and $6d_3$ can be generated. Data from a three-component seismograph array with an adequate azimuthal coverage can be used to provide information on the radiation pattern of P, SV, and SH phases, which contain diagnostic information on the mode of failure, that is type of source mechanism. (For details of the formulas for the radiation patterns shown in Fig. 6, the reader is referred to Hasegawa et al., 1989).

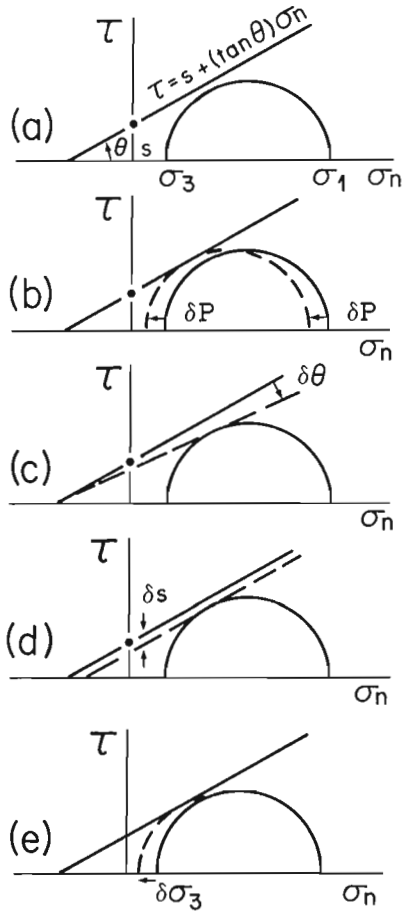

Figure 5. Trigger mechanisms for fault on verge of failure: Part (a) shows Coulomb-Mohr failure diagram for fault with low cohesive strength (s), coefficient of friction (tan Θ), maximum (σ_1), minimum (σ_3), and normal (σ_n) stress. Part (b) shows effect of increase in pore pressure (δP). Part (c) shows decrease in angle of friction (δΘ) as consequence of fault gouge. Part (d) shows decrease in cohesive strength (δs) of asperity that binds fault. Part (e) shows decrease in minimum principal stress ($\delta\sigma_3$) for thrust-fault environment as consequence of mine excavation.

Theoretical fomulations indicate significant differences in the body-waves and associated radiation patterns from an earthquake (double-couple) (see Eq. (1)) and from a confined explosion. For an underground explosion, that is a symmetrical point source (three orthogonal, equal-strength dipoles), the body wave radiation for displacement, $u_{sy}(\Omega,r)$ is (Haskell, 1967):

$$[2] \quad U_{sy}(\Omega,r) = \frac{P_o}{4\pi(\eta+2\mu)\alpha r}\left[\frac{1+24B}{[1+i(\Omega/k)]^4} - \frac{24B}{[1+i(\Omega/k)]^5}\right]$$

where

$$P_o = 4\pi(\eta+2\mu)\phi(\infty)$$

and the subscript sy stands for a symmetrical radiation pattern, Ω is angular frequency, k is wavenumber, r is distance from source, α is the P-wave velocity, i is the imaginary term, P_0 is the (symmetrical) dipole strength, η is the Lame parameter, μ is the shear modulus, $\phi(\infty)$ is the reduced displacement potential, which has comparable characteristics as Figure 2b for u_1(TF) at 0.01L quite often with an overshoot as shown in the subjacent curve, and B is an empirical constant. The minimum distance for r is the boundary between the inelastic zone (e.g. fractured) and the elastic zone; this boundary is a function of $\phi(\infty)$, which in turn is a function of the yield of the explosion. The displacement for an explosion (symmetrical point source) depends linearly on dipole strength (see Eq. (2)), whereas the displacement for an earthquake (double-couple) depends linearly on seismic moment. Provided a mine blast can, to a first-order approximation be simulated by a symmetrical point source, then the P-wave radiation pattern should be azimuthally symmetrical and any S-component observed would be due to conversion of P- to S- wave at boundaries, interfaces, or triggered faults. In actual practice the mine blasts are a succession of explosions, so that the associated radiation pattern is a superposition of that for a quasi-symmetrical point source with the appropriate time delays and migration of source. Since the above formulations were derived for underground nuclear explosions, caution must be exercized when scaling down to much smaller yields. Because the non- double-couple mechanisms (Fig. 6a, 6b and 6c) are accompanied by stress-strain changes in the surrounding rock mass, there exists the possibility of multiple seismic events. For example pillar bursts could trigger fault slip on suitably oriented nearby faults. Or the reverse situation could occur, that is fault slip near a mine opening could cause pillars to burst or generate rockfalls. Another possibility is that fault slip near a mine opening could manifest a non- double-couple component, which is due to the interaction of the ambient tectonic stress component with that induced by volumetric convergence and thus implies a volume change in addition to fault slip. A swarm type of activity would indicate a highly nonuniform or densely fractured

medium. A foreshock sequence followed by a main shock and aftershocks indicate a nonuniform medium. A single large main shock, with no foreshocks, indicates a uniform medium. According to Mogi's (1967) classification, the first sequence is of Type 3, the second Type 2, and the third Type 1. However, it should be emphasized that the various types of multiple seismic events discussed above are hypotheses that need to be tested.

RECURRENCE INTERVAL FOR SEISMIC SEQUENCES

The recurrence patterns for natural (large) earthquakes, based on a constant rate of strain build-up, is shown in Figures 7A, 7B, and 7C (from Shimazaki and Nakata, 1980). The periodic recurrence of earthquakes represented by Figure 7A is applicable to seismogenic regions with

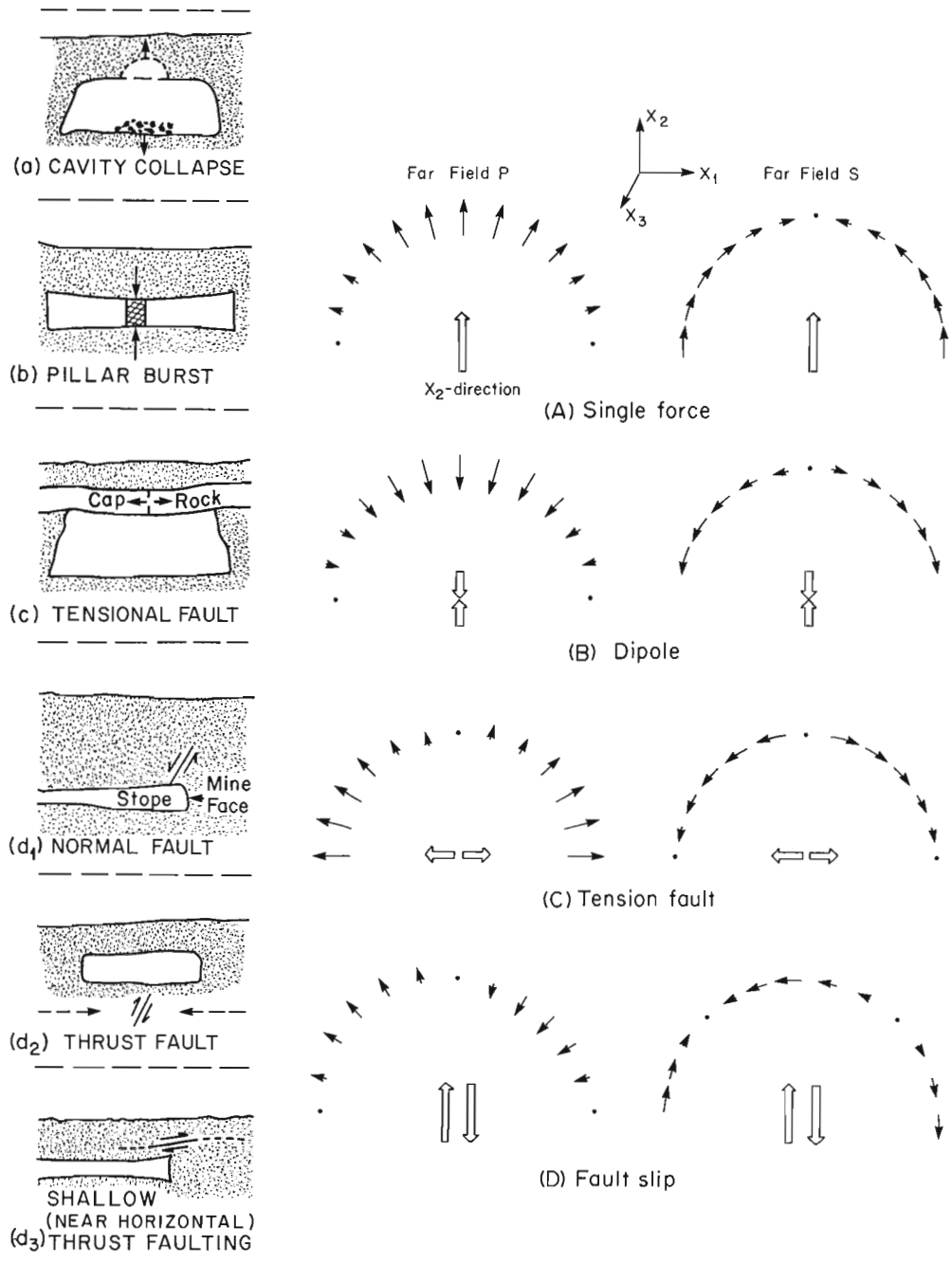

Figure 6. Different modes of rock failure around mines (left column) and associated P- and S-wave radiation pattern in vertical plane (two columns on right side) (after Hasegawa et al., 1989).

"characteristic" earthquakes (e.g. see Aki, 1984). The time-predictable model, Figure 7B, is applicable where the occurrence of the next large earthquake depends on the slip or magnitude of the preceding earthquake; this pattern seems to fit the earthquake sequence in certain areas of Japan (Shimazaki and Nakata, 1980). The slip-predictable model, for which the amount of slip of the next earthquake depends on the elapsed time since the previous large earthquake, is shown in Figure 7C. A model, whereby the strain rate increases dramatically for a relatively short time interval followed by a lengthy quiescent interval, such that the overall strain rate is constant, is shown for a mid-plate seismogenic environment in Figure 7D (from Wallace, 1987).

In addition to the pervasive tectonic strain rate, there are induced strain rates that depend on the various ways in which volumetric convergence can occur; Figures 7E to 7H show four examples. The maximum energy that can be released by an underground excavation is the product of the maximum stress σ_v, (see Fig. 7E) in the virgin rock around the excavation and the volume of excavation. Figure 7E shows the simplest case where convergence occurs without faulting and in the absence of any type of support in the cavity. For this case $W_R = W_I$, where W_R is the released strain energy and W_I is the stored strain energy and V_f is the maximum volumetric convergence; no seismic energy is released. Figure 7F shows the case where faulting occurs adjacent to the mine opening and $W_R > W_I$. Nearly all the energy difference, $W_R - W_I$, is converted into strain energy release by the fault slip (mine-induced earthquake) and a small percentage of this difference is released as seismic energy. Figure 7G shows the effect of a pillar under a stress of σ_s. When this pillar bursts, due to the increased load as a consequence of, for example, an accelerated volume closure rate, cumulative volume closure, or a combination of these two, the strain energy released is proportional to $\sigma_s \cdot V + \delta W_R$. Figure 7H shows how fill compaction absorbs energy W_F and effects a decrease in W_R by an amount δW_R, thus inhibiting mine tremors. (For details concerning the equations defining these parameters, the reader is referred to Jaeger and Cook, 1971). An understanding of mine tremors is facilitated by a joint analysis of the location and temporal sequence of the tremors, the radiation pattern of P, SV, and SH phases, strain gauges that measure volumetric convergence, and visual observation of mine damage.

DISCUSSION AND SUMMARY

Mine-induced tremors could depend on many factors and the potential exists for diversified failure mechanisms, that is non double-couple as well as the familiar double-couple source. Near-field terms could be important in some cases, especially near (within a fault length) the source of the mine tremor. One of the main trigger mechanisms of mine tremors is stress-strain changes due to cumulative and on-going volume convergence and the interaction of this induced stress field with the ambient plate tectonic stress field. Herget (1980) has documented in- situ stress measurements in mines in northern Ontario. On-going volume convergence can weaken the cohesive strength and frictional characteristics of faults around the mine opening as well as structures, such as pillar supports, within the mine opening. Water infiltration along faults for which the permeability is enhanced is also a possible trigger mechanism of fault slip. The pattern of mine-induced foreshock-mainshock-aftershock sequence could be diagnostic of the degree of

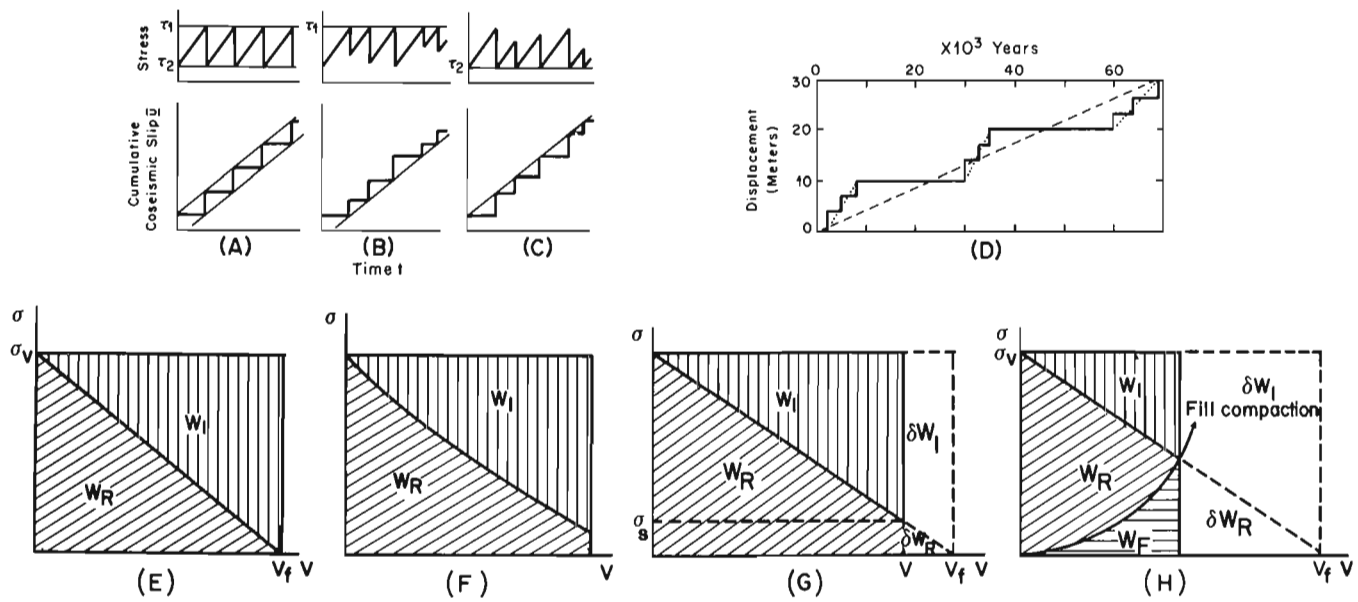

Figure 7. Coseismic slip patterns for uniform strain rate (A, B, and C) (from Shimazaki and Nakata, 1980) and quasi-uniform rate (D) (from Wallace, 1987). Bottom row of figures show how stored (W_I) and released (W_R) strain energy depends on volume convergence (V) for the following: (E) with no faulting or internal supports; (F) for case of fault slip; (G) for pillar support with load stress σ_s; and (H) for backfill, which absorbs energy W_F and decreases W_R and W_I by an amount δW_R and δW_I, respectively. Other symbols are as described in text (from Jaeger and Cook, 1971).

heterogeneity (e.g. fracture density) around the mine and the source type. A consideration of the above factors, and a determination of the actual modes of failure from new data now available from some mines should lead to a better understanding of the important causative factors and characteristics of mine-induced tremors. This information can then be used to mitigate the harmful effects and economic set backs posed by the larger mine-induced tremors.

ACKNOWLEDGMENTS

The author is grateful to the following for helpful comments: M.J. Berry, P.W. Basham, R.J. Wetmiller, G.G. Buchbinder, and R.J. North.

Much of the contents of this paper was presented at a workshop on "Seismic monitoring and analysis of mining induced events" held at CANMET'S Elliot Lake Laboratory on 20 September, 1989. Discussions with various members at the meeting have provided the author with a broader overview of mine-induced tremors.

REFERENCES

Aki, K.
1984: Asperities, barriers, characteristic earthquakes and strong motion prediction; Journal of Geophysical Research, v. 89, p. 5867-5872.
1987: Magnitude-frequency relation for small earthquakes: a clue to the origin of f_{max} of large earthquakes; Journal of Geophysical Research, v. 92, p. 1349-1355.

Al-Saigh, N.H. and Kusznir, N.J.
1987: Some observations on the influence of faults in mining-induced seismicity; Engineering Geology, v. 23, p. 277-289.

Basham, P.W., Weichert, D.H., Anglin, F.M., and Berry, M.J.
1982: New probabilistic strong seismic ground motion maps of Canada: a compilation of earthquake source zones, methods and results; Earth Physics Branch, Open File Number 82-33, 205 p.

Brady, A.G., Trifunac, M.D., and Hudson, D.E.
1973: Fourier amplitude spectra, v. IV; Earthquake Engineering Research Laboratory, California Institute of Technology, p. 73-100.

Brune, J.
1970: Tectonic stress and spectra of seismic shear waves from earthquakes; Journal of Geophysical Research, v. 75, p. 4997-5009.

Gendzwill, D.J.
1983: A theory for the source mechanism of the Cory Mine earthquakes; *in* Potash Technology, edited by R.M. McKercher, Pergamon Press, p. 197-202.

Gibowicz, S.J., Cichowicz, A., and Dybel, T.
1977: Seismic moment and source size of mining tremors in Upper Silesia, Poland; Acta Geophysica Polonica, XXV, p. 201-218.

Hasegawa, H.S.
1974: Theoretical synthesis and analysis of strong motion spectra of earthquakes; Canadian Journal of Earth Sciences, v. 11, p. 278-297.
1975: Seismic ground motion and residual deformation near a vertical fault; Canadian Journal of Earth Sciences, v. 12, p. 523-538.
1983: Lg spectra of local earthquakes recorded by the Eastern Canada Telemetered Network and spectral scaling; Bulletin of the Seismological Society of America, v. 73, p. 1041-1061.

Hasegawa, H.S., Wetmiller, R.J., and Gendzwill, D.J.
1989: Induced seismicity in mines in Canada — an overview; PAGEOPH, v. 129, p. 423-453.

Haskell, N.A.
1967: Analytic approximation for the elastic radiation from a contained underground explosion; Journal of Geophysical Research, v. 72, p. 2583-2587.
1969: Elastic displacements in the near-field of a propagating fault; Bulletin of the Seismological Society of America, v. 59, p. 865-908.

Healy, J.H., Rubey, W.W., Griggs, D.T., and Raleigh, C.B.
1968: The Denver earthquakes - disposal of waste fluids by injection into a deep well has triggered earthquakes near Denver, Colorado; Science, v. 161, p. 1301-1310.

Hedley, D.G.F. and Wetmiller, R.J.
1985: Rockbursts in Ontario mines during 1984; Mineral Research Program SP-85-5, Canada Centre for Mineral and Energy Technology, Energy, Mines and Resources, Canada, 36 p.

Hedley, D.G.F., Roxburgh, R.W., and Muppalaneni, S.N.
1984: A case history of rockbursts at Elliot Lake; 2nd International Conference on the Stability in Underground Mines, Lexington, Kentucky.

Herget, G.
1980: Regional stresses in the Canadian Shield; *in* Proceedings of the 13th Canadian Rock Mechanics Symposium, CANMET, Energy, Mines and Resources, Canada, Division Report MRP/MRL 80-8 (OP), p. 9-16.

Hinzen, K.-G.
1982: Source parameters of mine tremors in the eastern part of the Ruhr-District (West-Germany); Journal of Geophysics, v. 51, p. 105-112.

Jaeger, J.C. and Cook, N.G.W.
1971: Fundamentals of Rock Mechanics; Chapman and Halls Ltd., London, 515 p.

McGarr, A.
1976: Seismic moments and volume changes; Journal of Geophysical Research, v. 81, p. 1487-1494.

McGarr, A., Green, R.W.E., and Spottiswoode, S.M.
1981: Strong ground motion of mine tremors: some implications for near-source ground motion parameters; Bulletin of the Seismological Society of America, v. 71, p. 295-319.

Mogi, K.
1967: Earthquakes and fractures; Tectonophysics, v. 5, p. 35-55.

Nuttli, O.W.
1983: Average seismic source-parameter relations for mid-plate earthquakes; Bulletin of the Seismological Society of America, v. 73, p. 519-535.

Press, F.
1965: Displacements, strains and tilts at teleseismic distances; Journal of Geophysical Research, v. 70, p. 2395-2412.

Shimazaki, K. and Nakata, T.
1980: Time-predictable recurrence model for large earthquakes; Geophysical Research Letters, v. 7, p. 279-282.

Somerville, P.G., McLaren, J.P., LeFevre, L.V., Burger, R.W., and Helmberger, D.V.
1987: Comparison of source scaling relations of eastern and western North American earthquakes; Bulletin of the Seismological Society of America, v. 77, p. 322-346.

Wallace, R.E.
1987: Grouping and migration of surface faulting and variations in slip rates on faults in the Great Basin Province; Bulletin of the Seismological Society of America, v. 77, p. 868-876.

Wetmiller, R.J., Plouffe, M., Cajka, M.G., and Hasegawa, H.S.
1989: Natural and mining-related seismic activity in northern Ontario; *in* Current Research, Part C, Geological Survey of Canada, Paper 89-1C, p. 353-361.

Southeastern Canadian Earthquake Activity, 01 January, 1988 to 30 September, 1989

Janet Drysdale
Geophysics Division

Drysdale, J., Southeastern Canadian Earthquake Activity, 01 January, 1988 to 30 September, 1989; in Current Research, Part A, Geological Survey of Canada, Paper 90-1A, p. 67-71, 1990.

Abstract

From 01 January, 1988 to 30 September, 1989, 550 earthquakes in southeastern Canada were located and 29 were reported felt. Fifty-five earthquakes had magnitude 3.0 or greater. The spatial pattern of activity was generally similar to that of previous years, but many unusual earthquakes occurred, making this period of earthquake activity one of the most notable in recent memory. The largest earthquake in 53 years in eastern North America occurred on 25 November, 1988 about 35 km south of Chicoutimi, Québec. This magnitude 6 earthquake, known as the Saguenay earthquake, was preceded by a magnitude 4.7 foreshock on 23 November, 1988 and had minor aftershock activity. Other notable earthquakes were an unprecedented magnitude 4.3 earthquake doublet in the Charlevoix-Kamouraska seismic zone on 9 and 11 March, 1989; an offshore swarm on the Laurentian Slope, which started on 2 February, 1989 with a magnitude 4.5 earthquake; a magnitude 5.7 earthquake in Ungava Bay, Québec, on 16 March, 1989; and a magnitude 5.3 earthquake in the Labrador Sea on 14 March, 1989.

Résumé

Du 1er janvier 1988 au 30 septembre 1989, on a localisé dans le sud-est du Canada 550 séismes, dont 29 ont été ressentis. Cinquente-cinq d'entre eux avaient une magnitude d'au moins 3. La configuration spatiale des activités ressemblait en général à celle des années précédentes, mais il y a eu de nombreux séismes exceptionnels, rendant ainsi cette période d'activité sismique une des plus remarquable de mémoire d'homme. Le plus grand séisme qui s'est produit en 53 ans dans l'est de l'Amérique du Nord a eu lieu le 25 novembre 1988 à 35 km environ au sud de Chicoutimi (Québec). Le séisme de magnitude 6, connu sous le nom de séisme du Saguenay, a été précédé par une secousse prémonitoire de magnitude 4,7 le 23 novembre 1988, et a eu des répliques peu importantes. Voici les autres séismes importants: un doublet de séismes de magnitude 4,3 sans précédent survenu dans la zone sismique de Charlevoix et Kamouraska les 9 et 11 mars 1989; un essaim de séismes de magnitude 4,5, au large des côtes sur le talus continental Laurentien, qui a commencé le 2 février 1989; un séisme, de magnitude 5,7, qui a eu lieu dans la baie d'Ungava (Québec) le 16 mars 1989; et un séisme, de magnitude 5,3, qui s'est produit dans la mer du Labrador le 14 mars 1989.

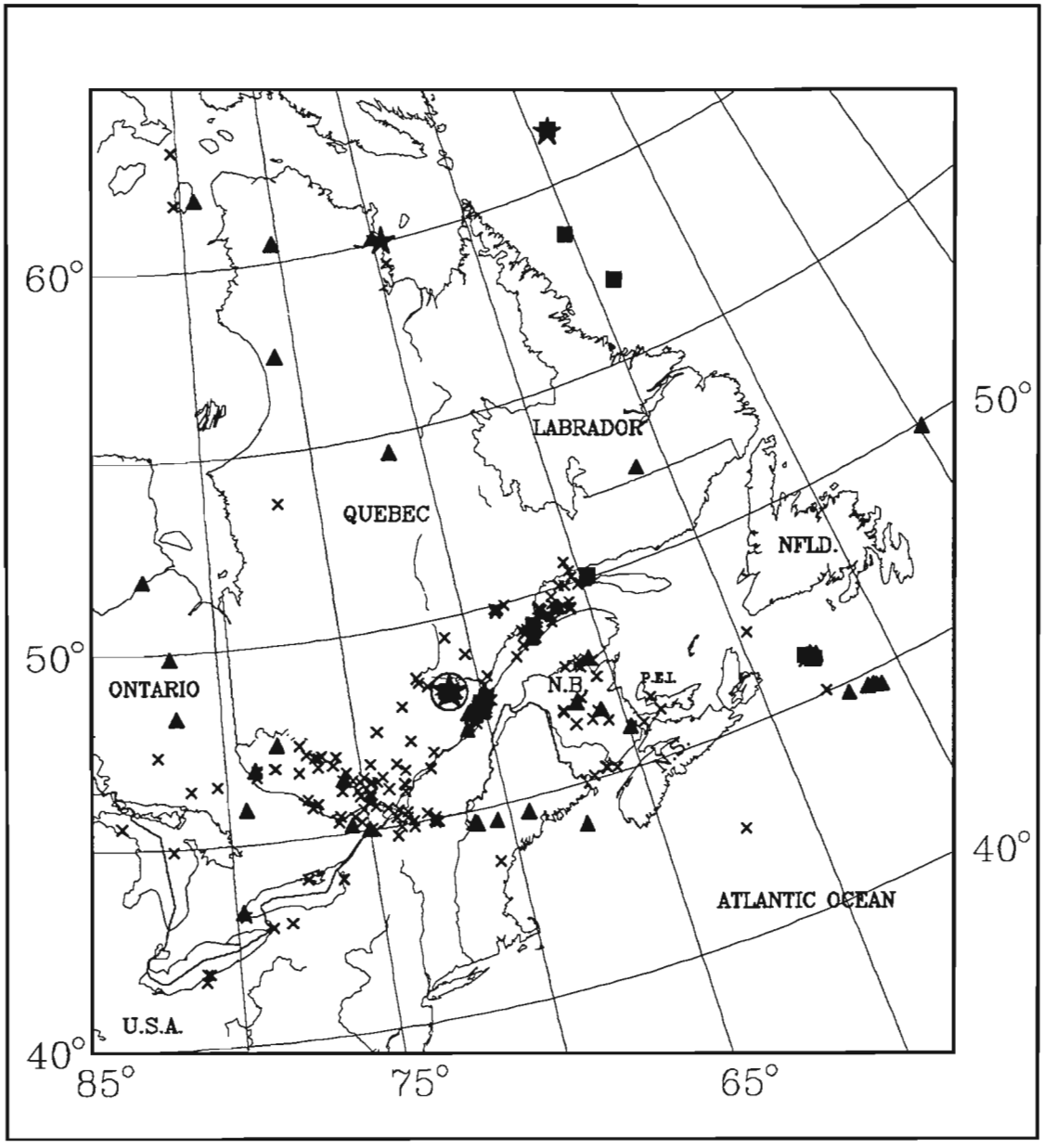

DEFINITIONS

M<3 ×
M≧3 ▲
M≧4 ■
M≧5 ★
M≧6 ⍟

Figure 1. Earthquake epicentres in eastern Canada and adjacent regions of the United States, 01 January, 1988 to 30 September, 1989. All magnitudes are shown.

INTRODUCTION

This report is a continuation of the reports on seismic activity in Canada published in last year's Current Research (Drysdale et al., 1989; Horner and Kolinsky, 1989) and is a summary of activity in southeastern Canada. During the 21-month period from 01 January, 1988 to 30 September, 1989, 550 earthquakes in southeastern Canada were analyzed for location and magnitude (Fig. 1). Fifty-five earthquakes had magnitude 3.0 or greater, the largest being the magnitude 6.0 Saguenay, Québec earthquake on 25 November, 1988. Twenty-nine earthquakes were reported felt in southeastern Canada. Figure 1 shows that, aside from the Saguenay earthquake, the spatial pattern of activity continued to be similar to that of previous years, occurring primarily in the recognized seismic zones of West Québec; Charlevoix, Québec; Lower St. Lawrence, Québec; Miramichi, New Brunswick; and the Laurentian Slope. However, as discussed below, the temporal pattern seemed somewhat unusual.

Several notable earthquakes were recorded during the report period.

A magnitude 4.7 earthquake occurred on 23 November, 1988 at 04:11 EST near 48.13°N, 71.20°W in the Laurentide Fauna Reserve of Québec. It was strongly felt in the Chicoutimi area and was felt significantly in Québec City. Many people in Montréal and a few in Ottawa also reported feeling this foreshock. The earthquake occurred in an area with no previous significant seismic activity. The Geophysics Division (GD) dispatched a field team to the epicentral area that day to conduct an aftershock survey. They had recorders set up at three sites close to the epicentre of the event by the following afternoon. This earthquake turned out to be a foreshock to a much larger event.

Sixty-two hours after the foreshock, on 25 November, 1988, at 19:46 EST, the magnitude 6.0 Saguenay earthquake took place. Its epicentre was only a few kilometres

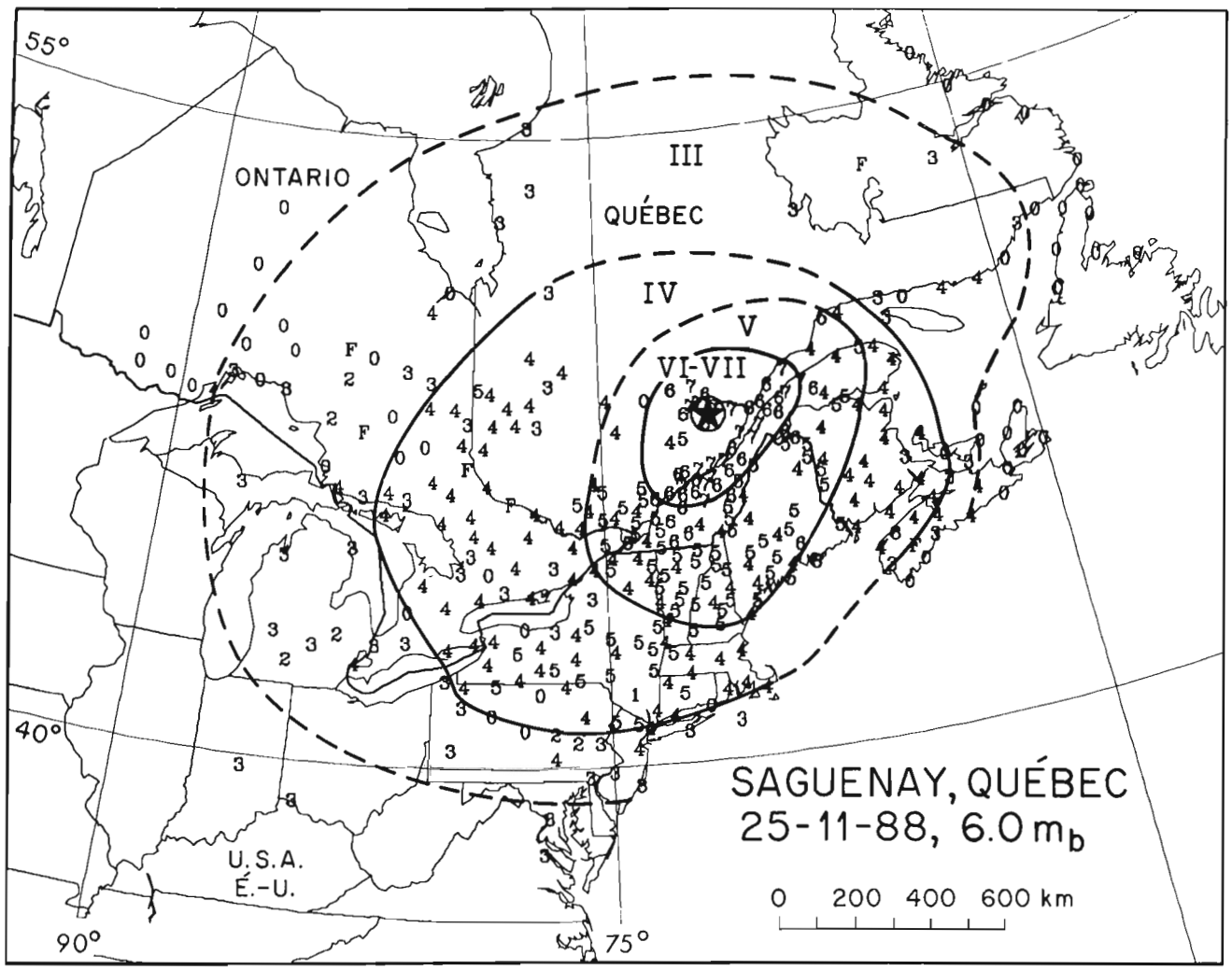

Figure 2. Intensity distribution for the 25 November, 1988 Saguenay, Québec, earthquake. Only 350 of the 2924 data points have been plotted for clarity, but all were used to contour (from a paper in preparation by author).

from that of the foreshock and within ten kilometres of the portable recorders deployed by the GD field crew. The local recorders allowed the depth of the start of the rupture to be calculated accurately and confirmed that the event occurred unusually deep in the crust at a depth of 29 km. No seismic activity prior to the mainshock with magnitude greater than 1.0 had been detected by the portable field recorders. The GD sent additional equipment and personnel to the area following the mainshock. As of 30 September, 1989, 85 aftershocks, only 2 of which were greater than magnitude 3.0, have been located using two stations installed following the mainshock by the GSC and four field stations operated by the University of Québec at Chicoutimi. Aftershock depths range from 15 to 30 km with the majority near 25 km.

The Saguenay earthquake was felt with maximum intensity VII in the Chicoutimi- Jonquière-La Baie area, was felt strongly by most people within 500 km, felt by many within 1000 km, and was perceptible by some people in special circumstances beyond 1000 km. The earthquake was felt south to Washington, D.C., north to Poste-de-la-Baleine, east to Goose Bay and Halifax, and west to Thunder Bay and Illinois. The total felt area exceeds 3 million km^2. The GD sent over 2000 questionnaires to rural postmasters in Québec, Ontario, the Maritime provinces, and Newfoundland in order to determine the intensity distribution of the earthquake. The Canadian data have been combined with similar data collected by the National Earthquake Information Center in the United States to produce an intensity distribution map as shown in Figure 2 (paper in preparation by author). Further information about this sequence of earthquakes is summarized by Lamontagne et al. (1990).

Two magnitude 4.3 events in the Charlevoix-Kamouraska zone on 9 and 11 March, 1989 had very similar relative times and waveforms on all the Charlevoix Local Telemetered Network (CLTN) stations. The hypocentre of this doublet lies under the St. Lawrence River at a depth of 10 km at the northeastern end of the seismic zone in the same area where the last large earthquake, magnitude 6.7, occurred on 01 March, 1925. Earthquake doublets of any size in the Charlevoix-Kamouraska seismic zone have been extremely rare since detailed monitoring began in the zone in 1977. A doublet of magnitude 4.0 or larger has probably not occurred in this seismic zone at any time since 1925 (Wetmiller and Adams, 1990).

The January-March 1989 period included one of the most unusual flurries of seismic activity experienced in eastern Canada in recent years. Starting with the Saguenay earthquake on 25 November, 1988 and continuing for approximately four months, exceptional earthquakes occurred in the Saguenay region, the Lower St. Lawrence valley, the Laurentian Channel, the Charlevoix region, the Labrador Sea, the Ungava Bay region, and the Labrador margin. These regions are widely separate and no obvious relationship could be seen among activities in the different regions. These earthquakes, except for those in the Labrador Sea and Labrador margin, were strongly felt in their epicentral area and resulted in numerous media inquiries and much public interest. The sequence of these events starting with the Saguenay earthquake at day 0 is shown in Table 1.

Table 1. Significant eastern Canadian earthquakes following the Saguenay earthquake.

#	Area	Mag.	Days After	Comments
1	Saguenay	6.0	0	largest in eastern Canada in 53 years
2	Lower St. Lawrence	4.3	36	largest locally in 20 years
3	Atlantic Margin	4.5	68	largest locally in 15 years
4	Lower St. Lawrence	4.1	76	
5	Charlevoix-Kamouraska	4.3	103	largest locally in 10 years
6	Charlevoix-Kamouraska	4.3	105	repeated event
7	Labrador Sea	5.3	108	largest locally in 20 years
8	Ungava	5.7	110	largest locally in 30-50 years
9	Labrador Margin	4.1	120	

Offshore seismicity was dominated by a swarm of earthquakes in the Laurentian Channel during 1989, which started with a magnitude 4.5 event on 02 February, 1989. In total there were 21 events recorded above magnitude 2.5. Most recently there was a magnitude 4.7 earthquake on 21 August, 1989. The swarm occurred in a hitherto aseismic region of the Laurentian Channel.

Another significant event, possibly another member of the flurry noted above, occurred near Sundridge, Ontario on 13 February, 1989 at 17:52 EST. It had magnitude 3.5 and was felt with maximum intensity IV by local residents. The event took place in an area of historically low seismicity in central Ontario, beyond the western boundary of the West Québec Seismic Zone, and was the largest event in the area in at least 44 years. Even more unusual, it was preceded by a magnitude 2.2 foreshock at 17:34 EST and followed by a magnitude 2.6 aftershock at 18:08 EST the same day.

In the Maritimes, two earthquakes were located in areas of previous low level and sporadic activity. The first, magnitude 3.8, occurred on 28 January, 1988 in the Bay of Chaleur, between Québec and New Brunswick, and the second, magnitude 3.6, took place on 24 April, 1988 near Moncton, New Brunswick. Both were felt locally. An additional six earthquakes, all with magnitude less than 3.0, were located near the Bay of Chaleur during the report period. There is a good possibility the two small events located on Prince Edward Island are blasts, but no blasting source could be confirmed.

On 9 September, 1988 the first earthquake ever located in Prince Edward County on the northeastern shore of Lake Ontario was recorded. It was only magnitude 2.2, but is considered significant because of the lack of previous seismic activity and the fact that the area had been selected in 1986 as one of three study areas for the multiagency enhanced neotectonic investigations in eastern Canada (MAGNEC). The event was thoroughly investigated by the GD and no source of blasting could be identified to explain it.

On 5 August, 1989 a magnitude 3.2 earthquake was located at the western end of Lake Ontario near Hamilton, Ontario. This tremor was felt in Hamilton, Oakville, and Mississauga, Ontario. The previous earthquake from the western Lake Ontario region took place on 23 July, 1987 and had a similar magnitude of 3.4.

All waveform and calculated data are kept in a relational data base on the Geophysics Division computer network. Specific information about earthquakes in Canada is available upon request to the Geophysics Division.

REFERENCES

Drysdale, J.A., Lamontagne, M., and Horner, R.B.
1989: Canadian earthquakes, January 1987 to September 1988; *in* Current Research, Part F, Geological Survey of Canada, Paper 89-1F, p. 31-36.

Horner, R.B. and Kolinsky, R.
1989: Earthquakes in western Canada from January 1987 to September 1988; *in* Current Research, Part E, Geological Survey of Canada, Paper 89-1E, p. 269-273.

Lamontagne, M., Wetmiller, R.J., and DuBerger, R.
1990: Some results from the 25 November, 1988 Saguenay, Québec earthquake; *in* Current Research, Part B, Geological Survey of Canada, Paper 90-1B.

Wetmiller, R.J. and Adams, J.
1990: An earthquake doublet in the Charlevoix seismic zone; *in* Current Research, Part B, Geological Survey of Canada, Paper 90-1B.

National gravity survey program, 1989-90

D.B. Hearty and R.A. Gibb
Geophysics Division

Hearty, D.B. and Gibb, R.A., National gravity survey program, 1989-90; in Current Research, Part A, Geological Survey of Canada, Paper 90-1A, p. 73-77, 1990.

Abstract

In 1989, six gravity surveys were completed under the national gravity survey program: four were reconnaissance surveys located in the high Arctic, in central British Columbia in the Great Lakes, and in the Strait of Georgia; two were local surveys over targets in southern British Columbia and Newfoundland. More than 9500 new gravity stations were added to the National Gravity Database as a result of these surveys.

Résumé

En 1989, on a effectué six levés gravimétriques dans le cadre du Programme national de levés gravimétriques; quatre d'entre eux, de type reconnaissance, se trouvaient dans le haut Arctique, dans la partie centrale de la Colombie-Britannique, dans les Grands Lacs et dans le détroit de Georgia, deux étaient des levés locaux effectués sur des cibles situées dans la partie sud de la Colombie-Britannique et à Terre-Neuve. Plus de 9500 nouvelles stations gravimétriques ont été ajoutées au Répertoire national des données gravimétriques à la suite de ces levés.

INTRODUCTION

Completion of the regional gravity survey of Canada's landmass and offshore areas by the year 2005 is a major objective of the GSC's gravity program (Gibb and Thomas, 1976). Major areas that remain to be surveyed include parts of the Cordillera of northern British Columbia and the Yukon Territory, parts of the Arctic Islands and Arctic Channels, and parts of the Arctic Ocean (Fig. 1) These regions all pose special problems with respect to horizontal and vertical positioning of gravity stations and logistic difficulties of terrain, ice, and climate.

Gravity surveys completed in 1989-90 are numbereed 1 to 6 in Figure 1 and are summarized below. Figure 2 is an index showing the location of GSC open File gravity maps.

PEEL SOUND AND BARROW STRAIT (AREA 1, FIG. 1)

A gravity and bathymetry survey of Peel Sound and Barrow Strait was completed by the Geophysics Division during March and April 1989 in co-operation with the Canadian Hydrographic Service (CHS), Department of Fisheries and Oceans, and with logistic support from the Polar Continental Shelf Project (PCSP). Approximately 1025 gravity and 6000 bathymetry stations were established on the ice at 6 to 10 km grid spacing. Syledis navigation with transmitters located at first order Geodetic control points was used for horizontal positioning and through-the-ice acoustic sounders were used for vertical positioning. The data are available in digital form and as a computer generated Open File gravity map.

LAKE HURON AND GEORGIAN BAY (AREA 2, FIG. 1)

A dynamic gravity and bathymetry survey of Lake Huron and Georgian Bay was completed in May 1989 by the Geophysics Division in support of the Great Lakes International Multidisciplinary Program on Crustal Evolution (GLIMPCE). This survey was conducted in co-operation with the United States Geological Survey (Woods Hole), the Canadian Hydrographic Service (Central Region) and the Department of Fisheries and Oceans, Canada Centre for Inland Waters. More than 5600 line kilometres were steamed aboard the CSS Limnos on predominantlty east-west lines at 18 km spacing. In addition, gravity and bathymetry observations were collected along previously established seismic profiles lines in Lake Huron, Georgian Bay, and Lake Michigan. Loran C was the primary source of navigation supplemented with differential Global Positioning System (GPS) positioning for four hour periods each day. Approximately 7200 new gravity stations, at one-minute intervals along the ship's track, have been added to the National Gravity Database. A separate experiment was conducted to evaluate and compare the GPS in translocation mode using the portable Trimble Pathfinder units and the high precision Texas Instruments 4100 units with a monitor station at Tobermory, Ontario. These data are currently under analysis and a paper should be available for release in early 1990.

CENTRAL BRITISH COLUMBIA (AREA 3, FIG. 1)

A regional gravity survey in north-central British Columbia was completed in the summer of 1989 by the Geophysics Division in co-operation with the Pacific Geoscience Centre and the Geodetic Survey of Canada. The survey covered all or part of nine 1:250 000 NTS map sheets and approximately 850 gravity stations were established at 10 to 12 km intervals. All gravity observations were collected using LaCoste and Romberg model G gravity meters and horizontal (latitude and longitude) and vertical (elevations) positioning were established using the Litton Inertial Survey System (ISS/LASS II)

SOUTHERN BRITISH COLUMBIA (AREA 4, FIG. 1)

A gravity survey along Lithoprobe seismic lines and along profiles across intrusives in the Kamloops area was completed in July 1989 by the Geophysics Division in response to a request from the Continental Geoscience Division. More than 200 new gravity stations were established using portable GPS receivers to supplement conventional methods — NTS maps and altimeters — for determining horizontal and vertical positioning.

NEWFOUNDLAND (AREA 5, FIG. 1)

A gravity survey along Lithoprobe seismic lines was completed in September 1989 by the Geophysics Division in western Newfoundland in response to a request from the Continental Geoscience Division. Approximately 500 gravity observations were established along five seismic profiles at 2 km intervals. Horizontal and vertical positioning was supplied by a private contractor using traditional survey methodologies. The loan of a four-wheel drive vehicle from Newfoundland Department of Mines contributed to a successful survey at significantly reduced cost. In addition, 39 gravity measurements were made in the Cow Head area of Gros Morne Provincial Park in support of a research agreement with Memorial University. All data will be available in digital form from the National Gravity Database in early 1990.

STRAIT OF GEORGIA (AREA 6, FIG. 1)

A dynamic gravity survey was conducted by the Pacific Geoscience Centre in co-operation with the Geophysics Division and the United States Geological Survey (Menlo Park) in late October in the Strait of Georgia aboard the CSS Tully. This international multiparameter survey provided a 3 km grid of gravity, bathymetry, magnetics and 3.5 kHz shallow sub-bottom seismic profiles along 4240 km of ship's track during a 10 day period. Navigation for the survey was supplied by a satellite-based positioning system called STARFIX, which was used for the first time on a gravity cruise for horizontal positioning.

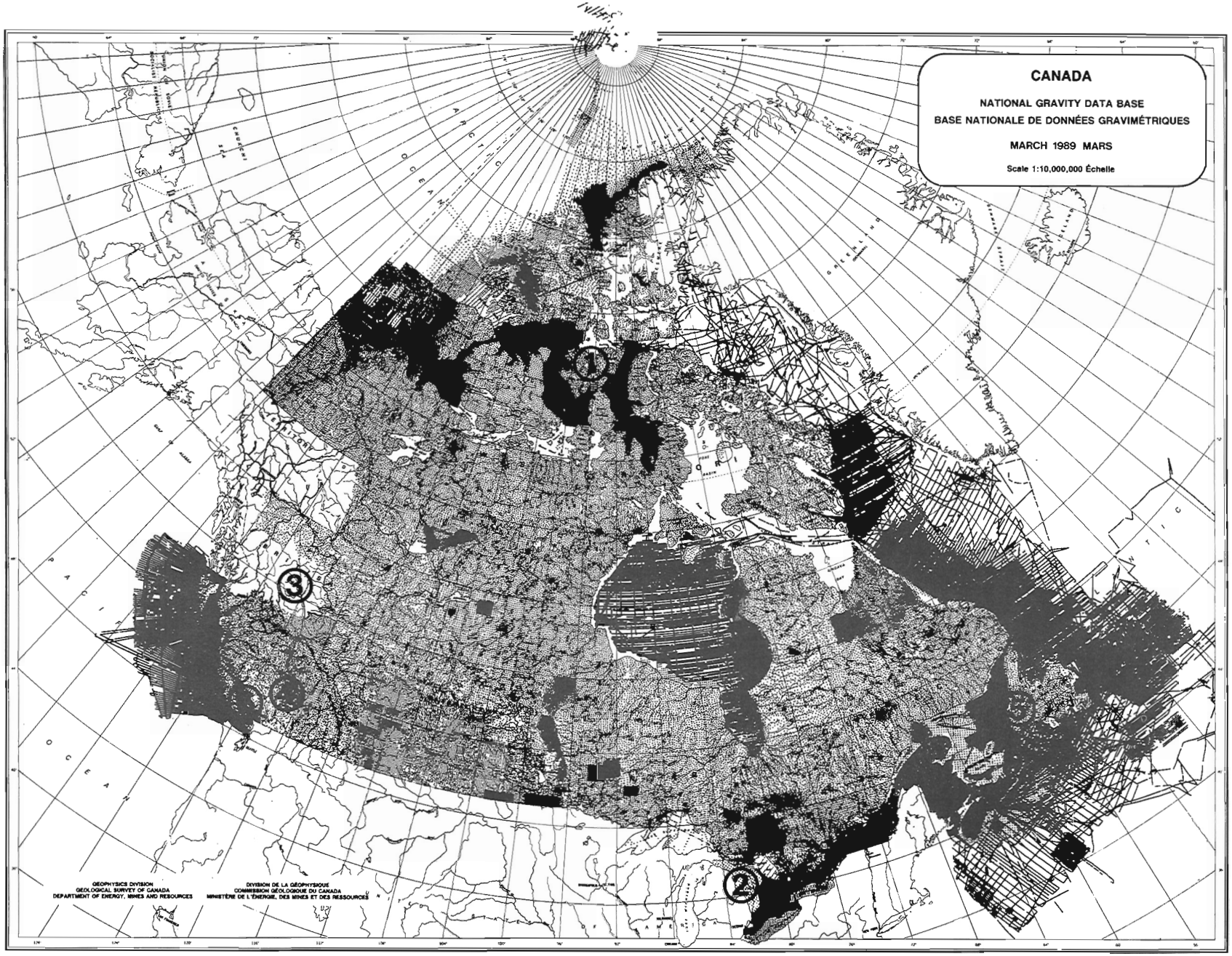

Figure 1. Distribution of gravity stations in Canada. Numbers refer to surveys completed in 1989-90.

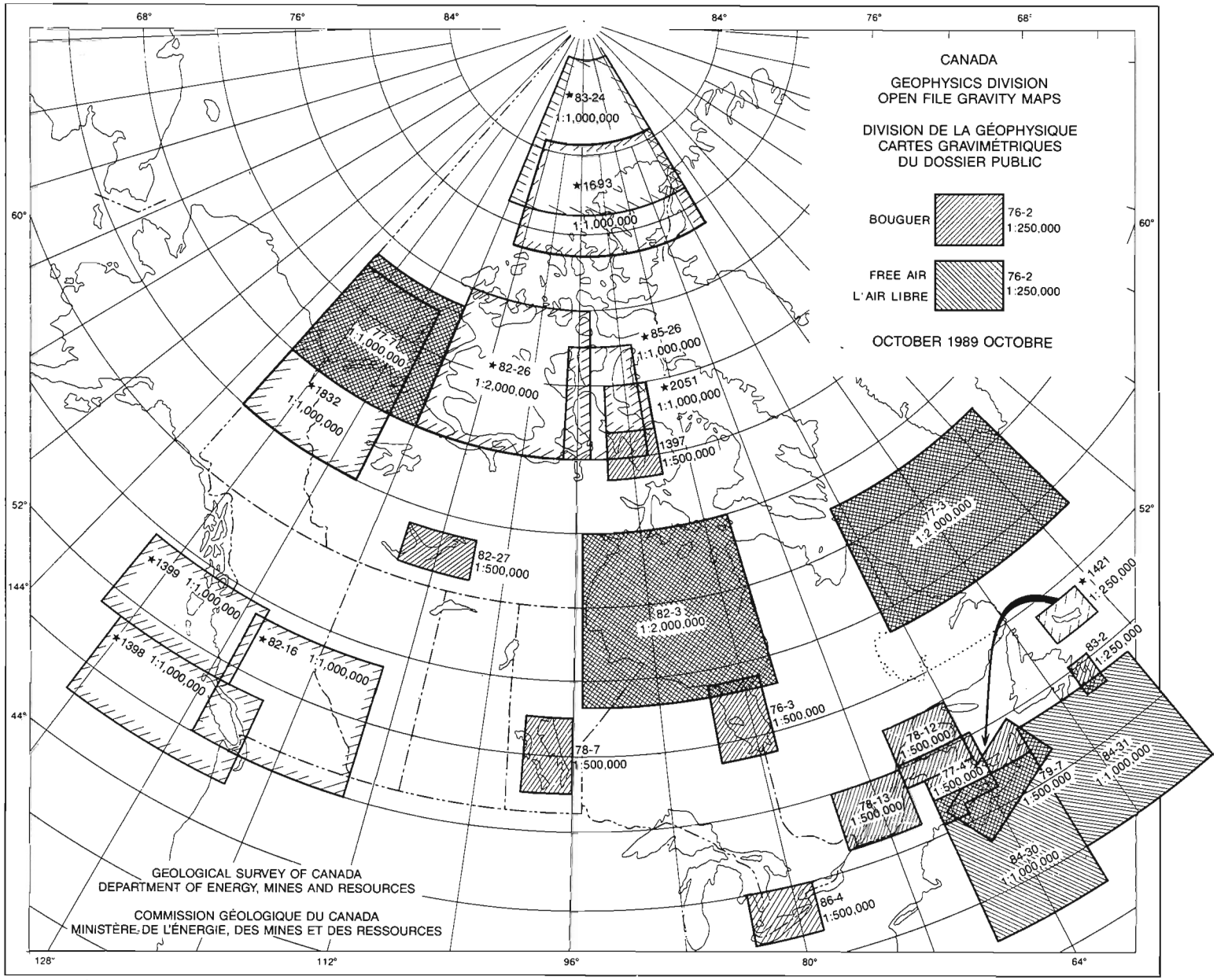

★ BOUGUER ON LAND — FREE AIR OFFSHORE
★ BOUGUER SUR LE CONTINENT — AIR LIBRE AU LARGE

Figure 2. Index to open file gravity maps

GRAVITY STANDARDS

Absolute gravity measurements were made at three primary sites in Churchill, Kuujjuarapik (Great Whale River) and Schefferville and at two corresponding sites at each location. Data will be used as datum control for the readjustment of the Canadian Gravity Standardization Net 1980 (CGSN80) and in support of postglacial crustal rebound and secular change studies.

The Canadian Absolute Gravity Site (CAGS) established just north of Ottawa in 1987 is maintained on a continuous basis to provide a national absolute gravity reference value. Research into the effects of environmental influences such as rainfall, air pressure, etc. on the absolute gravity instrumentation is in progress.

GRAVITY DATABASE

All GSC gravity data are maintained in the National Gravity Database of the Geophysical Data Centre (McConnell, 1976). It currently contains in excess of 600 000 data points. A variety of services and gravity data products are available to users both inside and outside the GSC. The major products include anomaly and control station data in the form of plots, tapes, or listings; digital terrain data; open file-, manuscript-, and Versatec-type maps; contour overlays; derived maps; gridded gravity values; calibration line data; earth tide values; and computer software.

Approximately 13 000 gravity observations from five surveys completed under the National Gravity Mapping Program or contributed by other agencies were added to the digital holdings of the National Gravity Database. In excess of 500 requests for gravity information or derived products were processed in the Geophysical Data Centre. More than 300 maps were generated to user specifications on the Versatec electrostatic colour plotter or the Calcomp monochrome plotter.

A new gravity database using "ORACLE" has been designed, developed, implemented, and tested on the VAX 8700 to replace the current production database under SYSTEM 2000 on the CYBER 730. The new database is currently being loaded and is expected to be in production by 31 March, 1990.

GRAVITY MAP PRODUCTION

A gravimetric geoid map for Canada with explanatory marginal notes was printed at a scale of 1:10 000 000 in the Geophysical Atlas Series. Several other maps including the vertical gradient of Bouguer anomalies are in preparation.

Ten (10) free air and Bouguer Anomaly maps in the National Earth Science Series (NESS) (scale 1:1 000 000) corresponding to five map areas in the east coast offshore were printed and are available through the publications office.

Two Open File gravity maps were produced: GSC Open File 1832 Gravity Anomaly Field: Northern Yukon, Northern District of Mackenzie and Beaufort Sea (1:2 000 000); GSC Open file 2051 Gravity Anomaly Field:Committee Bay (1:1 000 000).

A free air gravity map (scale 1:2 000 000) was printed as a contribution to the Labrador Shelf Basin Atlas, the first in the series of East Coast Basin atlases, being published by the Atlantic Geoscience Centre, and prototypes were produced for the Scotian Shelf, Grand Banks, and Gulf of St. Lawrence atlases. Optronics screens were produced for the Bouguer Anomaly map of Venezuela which was published in Venezuela at a scale of 1:2 000 000 under a cooperative project with V. Graterol of Universad Simon Bolivar, Caracas.

REFERENCES

Gibb, R.A. and Thomas, M.D.
1976: Gravity mapping in Canada; *in* Geophysics in the Americas, edited by J.G. Tanner and M.R. Dence, Publications of the Earth Physics Branch, Ottawa, v. 46, no. 3, p. 48-57.

McConnell, R.K.
1976: The Management of the Canadian national gravity data base; *in* Geophysics in the Americas, edited by J.G. Tanner and M.R. Dence, Publications of the Earth Physics Branch, Ottawa, v. 46, no. 3, p. 107-112.

Application of statistical analyses (dendograph and correspondence analysis) in the geological sciences

Marcel Labonté and Fariborz Goodarzi
Institute of Sedimentary and Petroleum Geology, Calgary

Labonté, M. and Goodarzi, F., Application of statistical analyses (dendograph and correspondence analysis) in the geological sciences; in Current Research, Part A, Geological Survey of Canada, Paper 90-1A, p.79-84, 1990.

Abstract

Different applications of the correspondence analysis and dendograph methods are shown. Both methods lead to the grouping of samples, and the analysis of the groups leads to the causes for this grouping. There usually is a physicochemical reason associated with each presentation. These methods synthesize only a part of all the information presented and produce a "picture", which may be used for geological interpretation.

Résumé

Les auteurs présentent différentes applications de la méthode de l'analyse par correspondance et de la méthode des dendrogrammes. Ces deux méthodes mènent au regroupement d'échantillons et l'analyse des groupes mène aux causes de ces regroupements. Il existe en général une raison physico-chimique associée à chaque présentation. Ces méthodes font la synthèse uniquement d'une partie de toutes les données présentées et produisent une « image » qui peut servir à l'interprétation géologique.

INTRODUCTION

The processing of data from a large number of samples in geological sciences is greatly facilitated by using statistical methods. Comparative studies based on element and maceral contents, Rock-Eval parameters, and organic geochemical parameters (Goodarzi et al., 1985, 1987; Barker et al., 1988; Kalkreuth et al., 1989), are reviewed summarily here.

Labonté and Goodarzi (1985, 1987) described the dendograph and correspondence analysis techniques for processing data from fossil fuels, particularly with respect to trace elements in coal.

Description of methods

The properties of the correlation coefficient have been described by Labonté and Goodarzi (1987). The "Pearson Product Moment Correlation Coefficient" is a measure of the linear relationship between two observed random variables X and Y. Consequently, the many variables in a multivariable situation must be analyzed in pairs. This results in a correlation matrix that is a concise representation of the linear relationships contained in the values of a data set, and measures the similarities between objects.

This similarity matrix (correlation matrix) is provided in the program (CORRMAT/PROB) by Jones and Facer (1982). This program has been modified to produce an output compatible with the dendograph program.

The use of the dendograph has centreed on its ability to resolve geological problems from an input of seemingly complex and multivariate data. This is achieved through computing similarity coefficients like the correlation coefficient and then producing a classification of these objects with the use of the dendograph method.

The dendograph method and its use were described by McCammon and Wenninger (1970). Modifications to this program have been described by Labonté (1989).

Correspondence analysis offers the possibility of computing and interpreting another kind of similarity coefficient than the correlation coefficient described above. The concept utilized here involves the chi-square distance, and the computation of similarities proceeds equally through the analysis of pairs. The chi-square distance concept is better understood through its use (Lebart et al., 1984). A comprehensive discussion of this method has been published by David et al. (1977). Correspondence analysis can resolve geological problems in a manner similar to the dendograph, but its application is based on different considerations. When using it in the field of geochemistry, for example, one must first understand the chemistries of the elements studied and then proceed to analyze these chemical elements into coherent groups (Mellinger, 1984).

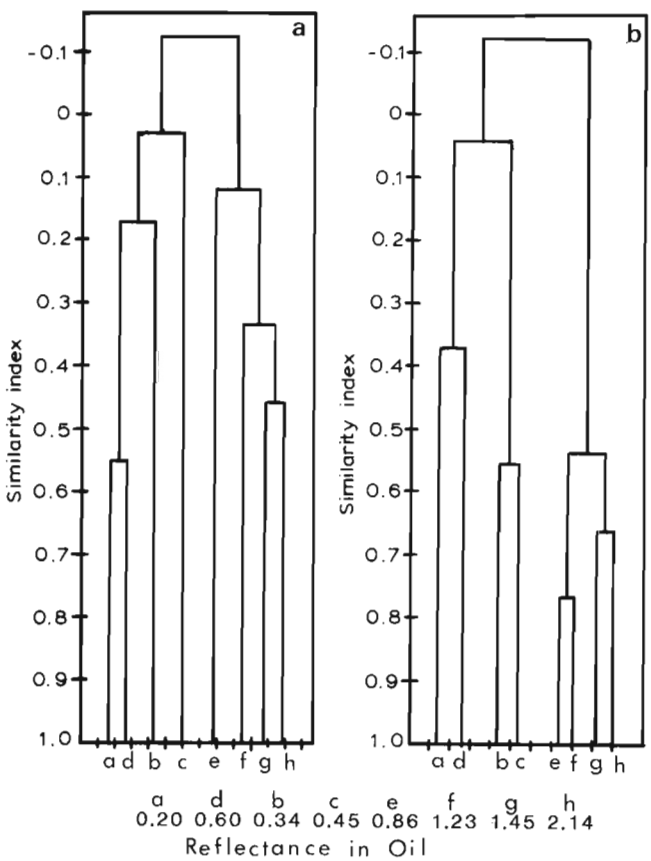

Figure 1. Dendograph showing the similarity index between coals a) based on the trace elements in coal, and b) based on the trace elements in coal ashes. Lignite-subbituminous, a-d; bituminous-semianthracite, e-f. (Redrawn after Goodarzi et al., 1985.)

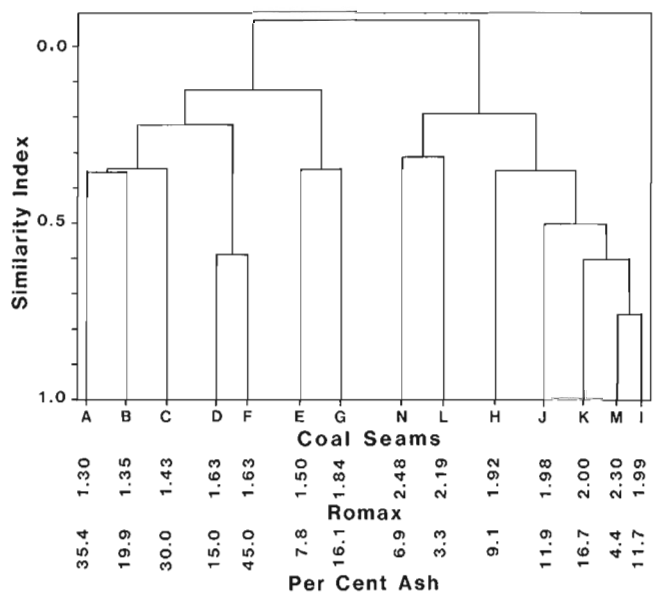

Figure 2. Dendograph showing the similarity indexes among the coal samples from Mount Allan, Alberta, based on the elements in ashes; the reflectance and ash content of the samples are also shown. (After Goodarzi and Cameron, 1987.)

APPLICATION OF METHODS

The dendograph

The dendograph method has been used extensively to compare the similarities between the elemental concentrations in suites of coal samples (Fig. 1) and also to show the similarities within a suite of coals (Fig. 2). Both Figures 1 and 2 show a grouping of coals, based on trace element data, that seem to reflect a clustering by rank, and age. In Figure 1 coals of different age, rank, and geographic origin are separated into two groups: one composed of lignites and subbituminous coals of Late Cretaceous and Tertiary age from the western Canadian plains; the other including Late Jurassic coals of bituminous to anthracitic rank from the Rocky Mountains. Figure 2 shows a more restricted population of samples from one locality and of one age, but again the clustering appears to be rank-related. One major subpopulation comprises mostly medium volatile and some low volatile bituminous coals, whereas the rank of coals in the other group is mainly semianthracite. The relationship between rank and trace element is not resolved here, and

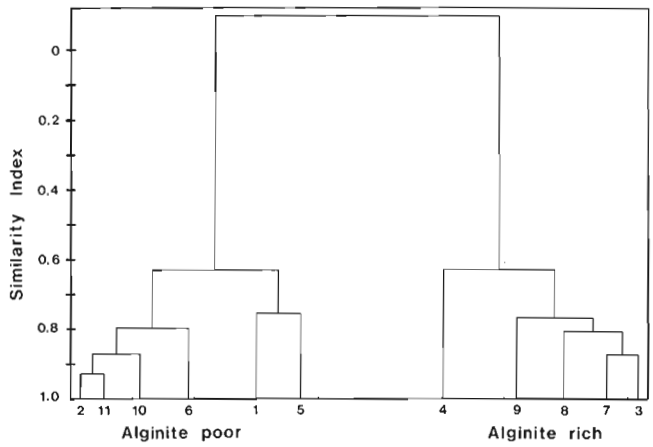

Figure 3. Dendograph showing the similarity indexes between the oil shales from Grinnell Peninsula, Emma Fjord Formation, Arctic Archipelago, based on a comparison of all variables — chemical, petrographic, and boron content. (After Goodarzi et al., 1987.)

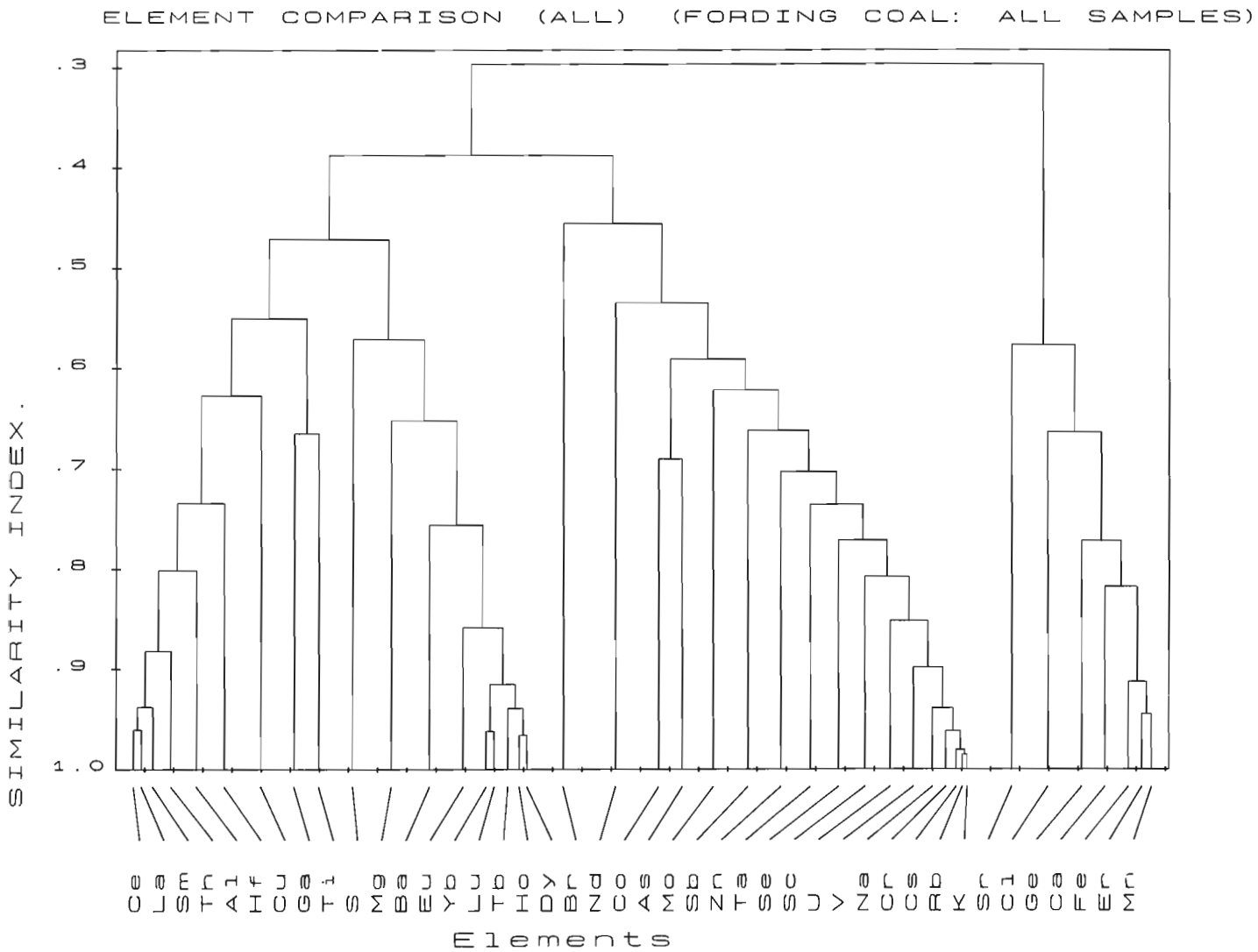

Figure 4. Similarity indexes between the elements in Fording coals, British Columbia. (After Goodarzi, 1988.)

this may be due to a physical phenomenon that led to the inclusion of trace elements in the coals. Nevertheless, this separation of coals by rank can be useful in the geological sciences, and this type of relationship requires more study.

The dendograph technique is also useful in the classification of oil shales. Figure 3 shows oil shales from the Lower Carboniferous Emma Fjord Formation in the Canadian Arctic Archipelago. These oil shales are grouped according to the environment of deposition (Goodarzi et al., 1987).

The dendograph method can be used to show the similarities between the elemental concentrations in a suite of samples. The grouping of elements in the samples is often informative. For example, elements like Al, Ti, K, and the REEs (rare earth elements) are usually grouped together, indicating the presence of aluminosilicates (or clay minerals). Even within this grouping one subgroup is evident (Fig. 4), where K, Rb, and Cs are grouped adjacently. The high similarity between these three elements is due to the property of dispersal elements assigned to Rb and Cs with regards to the element K (Mason and Moore, 1982) (Fig. 4).

In the classification scheme of the dendograph method, the dispersal element property supersedes the fact that these elements are related to aluminosilicate mineral phases.

Correspondence analysis

Correspondence analysis has been used to classify groundwater samples based on their geochemistry (Barker et al., 1988). Different parameters usually associated with the contamination of groundwater by landfill leachates were analyzed, and correspondence analysis was used to resolve the impact of pollutants into the aquifer table from a landfill site over a long period of time. A difficulty here is that inorganic and organic substances already present in the ground tend to produce similar dissolved species as those that can emanate from a landfill site. Consequently, it was not possible to identify dissolved species in the water that came only from the landfill, and the samples projected onto the plans produced by the correspondence analysis method were assigned to two categories.

One category comprised samples that delineated an area designated as the impacted area and the other, samples that delineated the nonimpacted area (Fig. 5). The term "impacted" means that there is a sufficiently large and coherent effect present in all trace organics (and some other pertinent parameters) to justify assigning a pollution effect to some samples. Another feature of correspondence analysis is the possibility of posting simultaneously on the same projection plan the samples and the variables. The adjacency of these elements can often be utilized with advantage, albeit the wording must be indirect because of the mathematical artifice at its source. The proximity of one type of trace organic variable to a sample will mean that comparatively, there is more of that trace organic in this sample than in the other samples. Note that the one-ring aromatic compounds are grouped very closely (O-Xylene, P-Xylene, etc.) and that samples located close to these "impacted" samples had a high leachate impact. The closeness of boron to these aromatic hydrocarbons is interesting, as B is an anion commonly found in landfill leachates at high concentration.

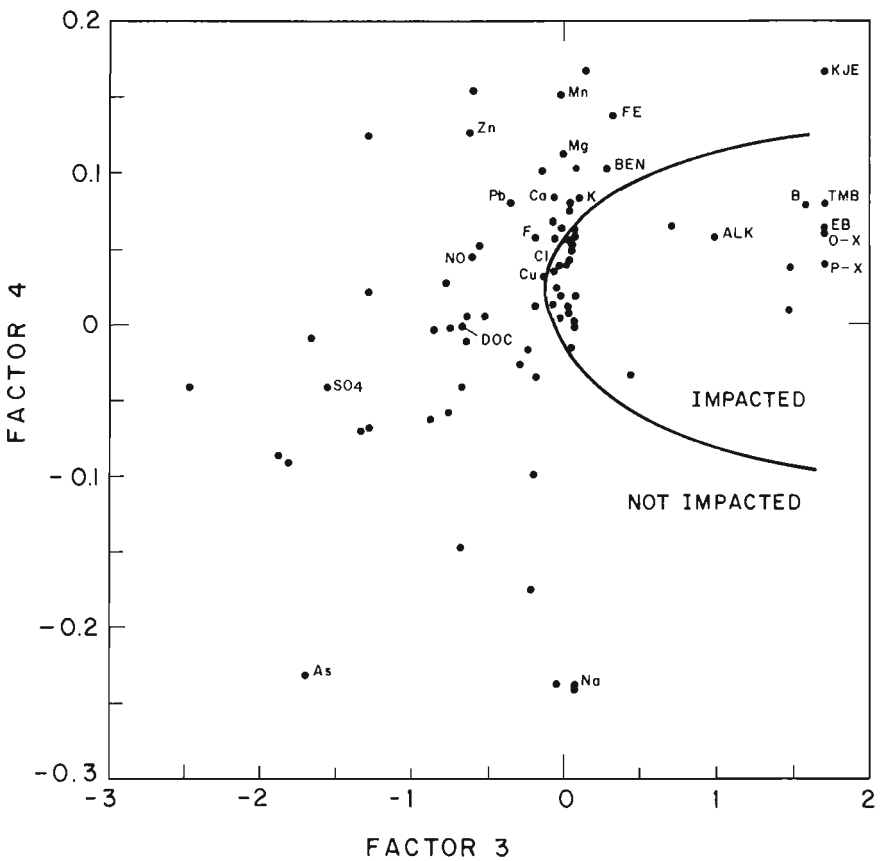

Figure 5. Grouping of groundwater and chemical parameters based on correspondence analysis. B, boron; BEN, benzene; ALK, alkalinity; O-X, O-xylene; P-X, P-xylene; KJE, kjeldahl N; NO, nitric oxide; DOC, dissolved organic carbon; TMB, trimethylbenzene; EB, ethylbenzene; and other chemical element ionic abundances easily identifiable by their chemical element symbolic names. (Redrawn after Barker et al., 1988.)

Boron also has affinities for clays and can even migrate inside clay lattices (Nicholls, 1968). The nature of the plans produced by correspondence analysis are, however, only at the "qualitative" level and do not allow for quantification of pollutant effects.

Correspondence analysis based upon data obtained from a petrographic analysis of coals was used to determine their environment of deposition (Kalkreuth et al., 1989). In this analysis, the axes of the projection plan are given an identity by considering the absolute contributions. These are used to evaluate which samples or variables contribute the most to each axis. The proximity of certain variables to certain factor axes is the reason these axes become associated with some effects. In this case, the first axis is associated with the rank of these coals and the second axis is associated with the type of detrital material encountered. These results were used to formulate a model of subsidence of coal-forming peat bogs. (Fig. 6).

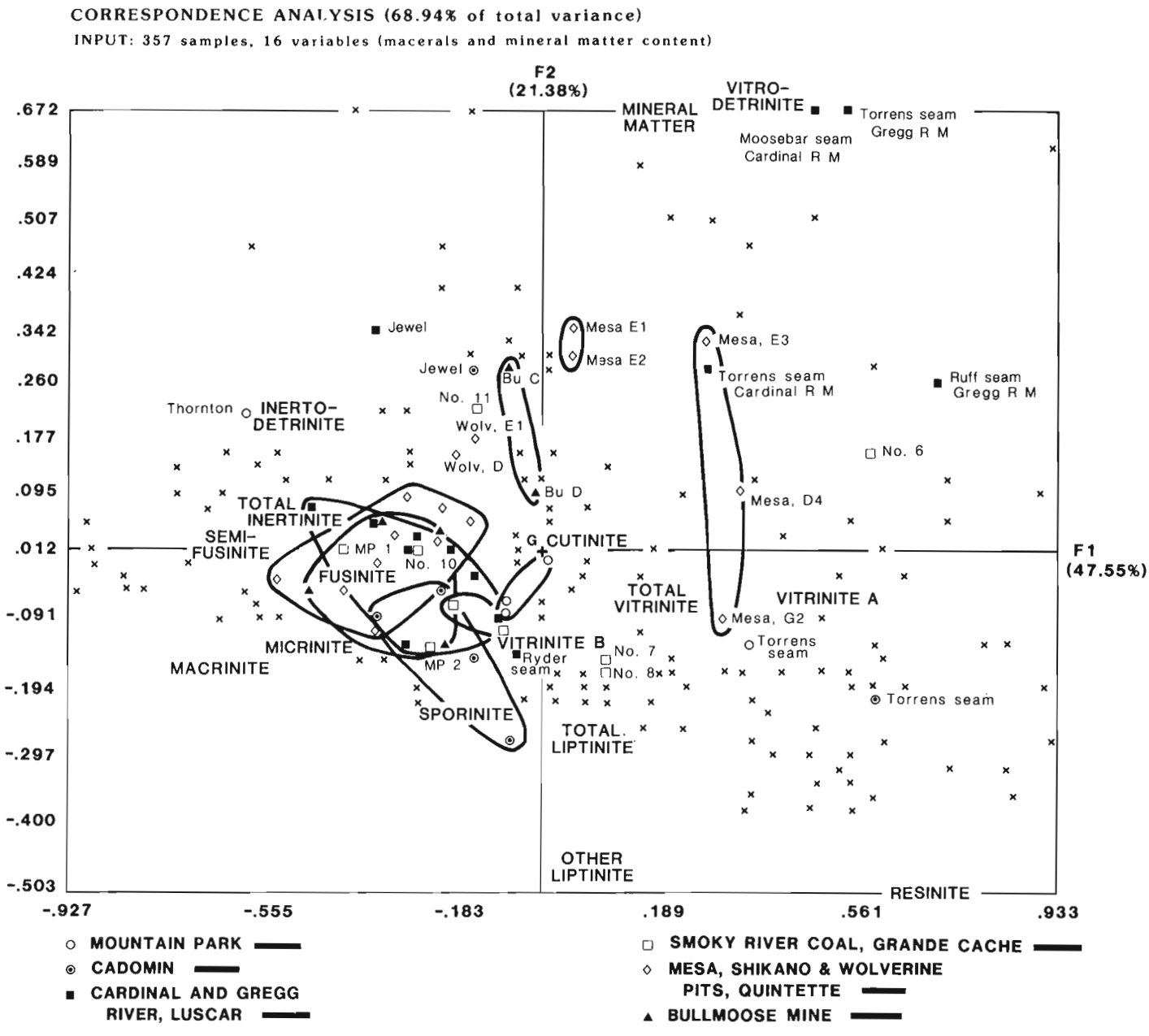

Figure 6. Projection plan from correspondence analysis of a data set containing data from coals formed during the Early Cretaceous. The positions of the different macerals relative to the different localities help toward the elaboration of a geological model. (After Kalkreuth et al., 1989.)

Oil shales can be classified (Fig. 7) using correspondence analysis to show the samples that were deposited under similar environmental conditions. The input data consisted of Rock-Eval parameters, petrology, and boron content (Goodarzi et al., 1987). Based on correspondence analysis, three groups can be identified: Group 1, consisting of only one sample (1); Group 2, consisting of samples 2, 5, 6, 10, and 11; and Group 3, comprising samples 3, 4, 7, 8, and 9. Group 1 is coal, Group 2 contains oxygen-rich oil shales, and Group 3 is made up of hydrogen-rich shales. Thus, correspondence analysis has clearly delineated three different suites of material, each with special significance in terms of depositional environment.

CONCLUSIONS

The dendograph method and correspondence analysis are important tools in the interpretation of a large information database. This interpretation can be used for the formulation of geological models and will serve to corroborate the concepts that may already have been elaborated by other means. The classification of samples afforded by these two methods may have important implications about the environment of deposition of the materials studied. In order to achieve this, however, some physicochemical phenomenon may have to be recognized and alluded to. These two methods are thus an instrument of geological reasoning and become an interface between the geologist and the digital information gathered for geological research.

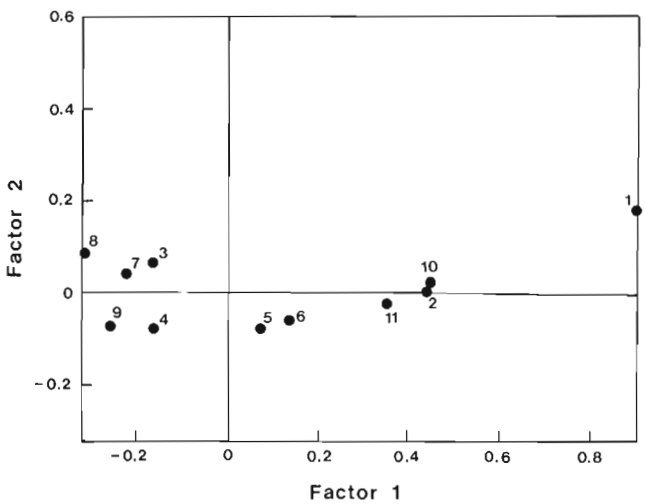

Figure 7. Correspondence analysis projection plan showing similar grouping of the oil shales and coals from the Grinnell Peninsula, Emma Fjord Formation, Arctic Archipelago. Coal: 1; oxygen-rich oil shales: 2, 5, 6, 10, and 11; hydrogen-rich oil shales: 3, 4, 7, 8, and 9. (After Goodarzi et al., 1987.)

REFERENCES

Barker, J.F., Barbash, J.E., and Labonté, M.
1988: Groundwater contamination at a landfill sited on fractured carbonate and shale; Journal of Contaminant Hydrogeology, v. 3, p. 1-25.

David, M., Dagbert, M., and Beauchemin, Y.
1977: Statistical analysis in geology: correspondence analysis method; Quarterly of the Colorado School of Mines, v. 72, January 1977, no. 1.

Goodarzi, F.
1988: Elemental distribution in coal seams at the Fording Coal Mine, British Columbia; Chemical Geology, v. 68, p. 129-154.

Goodarzi, F. and Cameron, A.R.
1987: Distribution of major, minor and trace elements in coals of Kootenay group, Mount Allan, Alberta; Canadian Mineralogist, v. 25, p. 555-565.

Goodarzi, F., Davis, G.R., Nassichuck, W.W., and Snowdon, L.R.
1987: Organic petrology and Rock-Eval analysis of the Lower Carboniferous Emma Fjord Formation in the Sverdrup Basin, Canadian Archipelago; Marine and Petroleum Geology, v. 4, p. 132-145.

Goodarzi, F., Foscolos, A.E., and Cameron, A.R.
1985: Mineral matter and elemental concentration in selected western Canadian Coals; Fuel, v. 64, p. 1599-1605.

Jones, B.G. and Facer, R.A.
1982: CORRMAT/PROB, a program to create and test a correlation coefficient matrix from data with missing values; Computers and Geosciences, v. 8, no. 2, p. 191-198.

Kalkreuth, W., Leckie, D.A., and Labonté, M.
1989: Gates Formation (Lower Cretaceous) coals in Western Canada: a sedimentological and petrographical study; Contributions to Canadian Coal Geosciences, Paper 89-9, p. 14-25.

Labonté, M.
1989: Description of computer methods and computer programs for correspondence analysis and use of dendograph analysis as means of coal data processing; Contributions to Canadian Coal Geosciences, Paper 89-8, p. 156-162.

Labonté, M. and Goodarzi, F.
1985: Use of the dendograph for data processing in fuel science; Fuel, v. 64, p. 1177-1178.
1987: The relation between dendographs and Pearson product-moment correlation coefficients; *in* Current Research, Part A, Geological Survey of Canada, Paper 87-1A, p. 353-356.

Lebart, L., Morineau, A., and Warwick, K. M.
1984: Multivariate Descriptive Statistical Analysis. Correspondence Analysis and Related Techniques for Large Matrices; John Wiley & Sons, 231 p.

Mason, B. and Moore, C.B.
1982: Principles of Geochemistry; John Wiley & Sons, 344 p.

McCammon, R. and Wenninger, G.
1970: The dendograph; Computer Contribution 48, State Geological Survey, The University of Kansas, 28 p.

Mellinger, M.
1984: Correspondence analysis in the study of lithogeochemical data: general strategy and the usefulness of various data-coding schemes; Journal of Geochemical Exploration, v. 21, p. 455-469.

Nicholls, C.D.
1968: The geochemistry of coal-bearing strata; *in* Coal and Coal-Bearing Strata, edited by D. Murchison and T.S. Westoll, Oliver and Boyd, Edinburgh.

AUTHOR INDEX

Geological Survey of Canada, Paper 90-1, Current Research is published as six parts, listed below, that can be purchased separately.

Recherches en cours, une publication de la Commission géologique du Canada, Étude 90-1, est publiée en huit parties, énumérées ci-dessous ; chaque partie est vendue séparément.

Part A, National and general programs
Partie A, Programmes nationaux et généraux

Part B, Eastern and Atlantic Canada
Partie B, Est et région atlantique du Canada

Part C, Canadian Shield
Partie C, Bouclier canadien

Part D, Interior Plaines and Arctic Canada
Partie D, Plaines intérieures et région arctique du Canada

Part E, Cordillera and Pacific Margin
Partie E, Cordillère et marge du Pacifique

Part F, Frontier Geoscience Program, Cordilleran and offshore basins, British Columbia
Partie F, Programme géoscientifique des régions pionnières, bassins de la Cordillère et extracôtiers, Colombie-Britannique